

Electronic Supplementary Information (ESI)

Dinuclear tricarbonylrhenium(I) complexes: Impact of regioisomerism on the photoluminescence properties

Stephen Le Garrec, David Martins-Bessa, Mariusz Wolff, Béatrice Delavaux-Nicot, Sonia Mallet-Ladeira, Charles-Louis Serpentine, Eric Benoist, Florence Bedos-Belval, and Suzanne Fery-Forgues

Synthesis and characterization

Abbreviations	3
Figure S1. ¹ H NMR spectrum of 2-octyl-5-(pyridin-2-yl)-1,3,4-oxadiazole (1) in CDCl ₃	4
Figure S2. ¹³ C NMR spectrum of 2-octyl-5-(pyridin-2-yl)-1,3,4-oxadiazole (1) in CDCl ₃	5
Figure S3. HSQC and HMBC NMR spectra of 2-octyl-5-(pyridin-2-yl)-1,3,4-oxadiazole (1) in CDCl ₃	6
Figure S4. ¹ H NMR spectrum of ligand L-Phe in acetone- <i>d</i> ₆	7
Figure S5. ¹³ C NMR spectrum of ligand L-Phe in acetone- <i>d</i> ₆	8
Figure S6. HSQC and HMBC NMR spectra of ligand L-Phe in acetone- <i>d</i> ₆	9
Figure S7. ¹ H NMR spectrum of ligand L-paraPhe in acetone- <i>d</i> ₆	10
Figure S8. ¹³ C NMR spectrum of ligand L-paraPhe in acetone- <i>d</i> ₆	11
Figure S9. HSQC and HMBC NMR spectra of ligand L-paraPhe in acetone- <i>d</i> ₆	12
Figure S10. ¹ H NMR spectrum of ligand L-metaPhe in acetone- <i>d</i> ₆	13
Figure S11. ¹³ C NMR spectrum of ligand L-metaPhe in acetone- <i>d</i> ₆	14
Figure S12. HSQC and HMBC NMR spectra of ligand L-metaPhe in acetone- <i>d</i> ₆	15
Figure S13. ¹ H NMR spectrum of complex Mono-Re-Phe in acetone- <i>d</i> ₆	16
Figure S14. ¹³ C NMR spectrum of complex Mono-Re-Phe in acetone- <i>d</i> ₆	17
Figure S15. HSQC and HMBC NMR spectra of complex Mono-Re-Phe in acetone- <i>d</i> ₆	18
Figure S16. ¹ H NMR spectrum of complex Bi-Re-paraPhe in acetone- <i>d</i> ₆	19
Figure S17. ¹³ C NMR spectrum of complex Bi-Re-paraPhe in acetone- <i>d</i> ₆	20
Figure S18. HSQC and HMBC NMR spectra of complex Bi-Re-paraPhe in acetone- <i>d</i> ₆	21
Figure S19. ¹ H NMR spectrum of complex Bi-Re-metaPhe in acetone- <i>d</i> ₆	22
Figure S20. ¹³ C NMR spectrum of complex Bi-Re-metaPhe in acetone- <i>d</i> ₆	23
Figure S21. HSQC and HMBC NMR spectra of complex Bi-Re-metaPhe in acetone- <i>d</i> ₆	24
Figure S22. ATR FT-IR spectra of microcrystalline powders of complexes Mono-Re-Phe and Bi-Re-metaPhe	25
Figure S23. ATR FT-IR spectra of the microcrystalline powder of complex Bi-Re-metaPhe	26

Crystallographic data

Table S1. Selected bond lengths for Mono-Re-Phe , Bi-Re-metaPhe , L-paraPhe and L-metaPhe	26
Table S2. Selected angles for complexes Mono-Re-Phe , Bi-Re-metaPhe , and ligands L-paraPhe and L-metaPhe	27
Comment S1. Crystal lattice of Re-Phe	28
Figure S24. Centrosymmetric dimers of Re-Phe and intermolecular interactions	28
Figure S25. Dimers of Re-Phe connected <i>via</i> intermolecular interactions into looped chains	28
Figure S26. Dimers of Re-Phe linked by intermolecular stacking interactions into stair chain	29
Figure S27. Neighboring molecules of Re-Phe connected <i>via</i> intermolecular interactions into a zig-zag chain	29
Figure S28. Crystal cell of complex Mono-Re-Phe	30
Figure S29. Centrosymmetric dimers of Mono-Re-Phe and intermolecular interactions	30
Figure S30. Crystal cell of Bi-Re-metaPhe , dimers and molecular view perpendicular to the central phenyl ring	31
Figure S31. Intermolecular and intramolecular interactions in Bi-Re-metaPhe	31
Table S3. Octahedral distortion parameters of complexes Re-Phe , Mono-Re-Phe and Bi-Re-meta-Phe	31

Table S4. Experimental and DFT-optimized octahedral distortion parameters in the singlet (S_0 , S_1 excited) and triplet (T_1 , excited) states of complexes Re-Phe , Mono-Re-Phe and Bi-Re-meta-Phe	32
Table S5. Geometrical parameters for short contacts in Re-Phe , Mono-Re-Phe and Bi-Re-metaPhe	32
Table S6. Geometrical parameters for C–H··· π interactions in Re-Phe , Mono-Re-Phe and Bi-Re-metaPhe	33
Table S7. Geometrical parameters for π ··· π interactions detected in structure of Re-Phe	33
Comment S2. Hirshfeld surfaces (HS) analysis of Re-Phe , Mono-Re-Phe and Bi-Re-metaPhe	33
Figure S32. 2D FP for overall interactions and individual interactions in crystal packing of Re-Phe	34
Figure S33. 2D FP for overall interactions and individual interactions in crystal packing of Mono-Re-Phe	35
Figure S34. 2D FP for overall interactions and individual interactions in crystal packing of Bi-Re-metaPhe	36

Calculations

Table S8. Selected calculated bond lengths and angles in the ground (S_0), first singlet excited (S_1) and first triplet excited (T_1) states for Re-Phe , together with the experimental data	37
Table S9. Selected calculated bond lengths and angles in the ground (S_0) first singlet excited (S_1) and first triplet excited (T_1) states for Mono-Re-Phe , together with the experimental data	38
Table S10. Selected calculated bond lengths and angles in the ground (S_0) first singlet excited (S_1) and first triplet excited (T_1) states for Bi-Re-metaPhe , together with the experimental data	39
Table S11. Selected calculated bond lengths and angles in the ground (S_0) first singlet excited (S_1) and first triplet excited (T_1) states for Bi-Re-paraPhe	40
Table S12. Calculated torsion angle value between pyta and R for the ground (S_0), first singlet excited (S_1) and first triplet excited state (T_1) of the four complexes, and obtained from crystallographic data	41
Table S13. The frontier molecular orbital compositions (%) and energy levels for Re-Phe (in DCM)	41
Table S14. The frontier molecular orbital compositions (%) and energy levels for Mono-Re-Phe (in DCM)	41
Table S15. The frontier molecular orbital compositions (%) and energy levels for Bi-Re-metaPhe (in DCM)	42
Table S16. The frontier molecular orbital compositions (%) and energy levels for Bi-Re-paraPhe (in DCM)	42
Table S17. The main electronic transitions for Re-Phe (in DCM)	43
Table S18. The main electronic transitions for Mono-Re-Phe (in DCM)	43
Table S19. The main electronic transitions for Bi-Re-metaPhe (in DCM)	44
Table S20. The main electronic transitions for Bi-Re-paraPhe (in DCM)	44
Table S21. Excitation energies and oscillator strengths of the four complexes (in DCM)	45
Table S22. Phosphorescence emission energies of the four complexes	45
Table S23. Natural population analysis of the orbitals of the central atom in the four complexes	46
Table S24. Atomic charges from the Natural Population Analysis (NPA) for the four complexes	46
Table S25. Absolute electronegativity, absolute hardness, dipole moment, electrophilicity index and global softness of the four complexes	47
Figure S35. The isodensity plots of the frontier molecular orbitals of Re-Phe (in DCM)	48
Figure S36. The isodensity plots of the frontier molecular orbitals of Mono-Re-Phe (in DCM)	49
Figure S37. The isodensity plots of the frontier molecular orbitals of Bi-Re-metaPhe (in DCM)	50
Figure S38. The isodensity plots of the frontier molecular orbitals of Bi-Re-paraPhe (in DCM)	53
Figure S39. Spin density distribution for the lowest triplet state T_1 of the four complexes	56
Figure S40. Molecular Electrostatic Potential (MEP) of the four complexes	57
Figure S41. The experimental and simulated FT-IR and UV-Vis absorption spectra of Re-Phe (in DCM)	58

Electrochemistry

Table S26. Experimental electrochemical data used, and calculated values of the energy gaps (E_g) for complexes Mono-Re-Phe , Bi-Re-paraPhe , and Bi-Re-metaPhe .	59
Comment S3. Evaluation of the electrochemical energy gap values (E_g^{el}) for the Re complexes	59
Figure S42. OSWVs: anodic and cathodic scans of complex Mono-Re-Phe	60
Figure S43. Cyclic voltammograms of complex Mono-Re-Phe , and of its first oxidation and reduction processes	60
Figure S44. Cyclic voltammograms of the first oxidation process of complex Mono-Re-Phe at 1, 10, and 50 V/s, and of its first reduction process at 1, 10, and 50 V/s	60
Figure S45. OSWVs: anodic and cathodic scans of complex Bi-Re-paraPhe	61
Figure S46. Cyclic voltammograms of complex Bi-Re-paraPhe , and of its first oxidation and reduction processes	61

Figure S47. Cyclic voltammograms of the first oxidation process of complex Bi-Re-paraPhe at 1, 5, 10, and 50 V/s, and of its first reduction process at 1, 2, 5, 10, and 50 V/s	61
Figure S48. OSWVs: anodic scans of complex Bi-Re-paraPhe at different frequencies (20/50/100/200/500/1000) with amplitude 20 mV and step potential 5 mV	61
Figure S49. OSWVs: anodic and cathodic scans of complex Bi-Re-metaPhe	62
Figure S50. Cyclic voltammograms of complex Bi-Re-metaPhe , its first oxidation and reduction processes at 5, 10, 50 V/s, and its first reduction potential 0.1, 0.5, 1 V/s	62
Figure S51. OSWVs: anodic and cathodic scans of complex Bi-Re-paraPhe vs. Bi-Re-metaPhe	62
Figure S52. OSWVs: anodic scans of ligands L-Phe , L-paraPhe and L-metaPhe and of the corresponding electrochemical medium without the ligand	63
Figure S53. Cyclic voltammograms of ligands L-Phe , L-paraPhe and L-metaPhe and of the corresponding electrochemical medium without the ligand	63

Spectroscopy

Figure S54. Emission decays of Mono-Re-Phe , Bi-Re-paraPhe , and Bi-Re-metaPhe in DCM solutions	64
Figure S55. Emission decays of Mono-Re-Phe and Bi-Re-paraPhe as powders	65
Figure S56. Emission decays of Bi-Re-metaPhe as pristine and ground powders	66
Figure S57. Powder XRD patterns of the pristine, ground and THF-fumed powders of bimetallic complexes	66

Calculations - Annex

Table S27. Cartesian coordinates of Re-Phe in S_0 (in DCM)	67
Table S28. Cartesian coordinates of Re-Phe in S_1 (in DCM)	67
Table S29. Cartesian coordinates of Re-Phe in T_1 (in DCM)	68
Table S30. Cartesian coordinates of Mono-Re-Phe in S_0 (in DCM)	68
Table S31. Cartesian coordinates of Mono-Re-Phe in S_1 (in DCM)	69
Table S32. Cartesian coordinates of Mono-Re-Phe in T_1 (in DCM)	69
Table S33. Cartesian coordinates of Bi-Re-metaPhe in S_0 (in DCM)	70
Table S34. Cartesian coordinates of Bi-Re-metaPhe in S_1 (in DCM)	71
Table S35. Cartesian coordinates of Bi-Re-metaPhe in T_1 (in DCM)	72
Table S36. Cartesian coordinates of Bi-Re-paraPhe in S_0 (in DCM)	73
Table S37. Cartesian coordinates of Bi-Re-paraPhe in S_1 (in DCM)	74
Table S38. Cartesian coordinates of Bi-Re-paraPhe in T_1 (in DCM)	75

Synthesis and characterization

Abbreviations

DIPEA: *N,N*-Diisopropylethylamine

HATU: *O*-(7-aza-1*H*-benzotriazol-1-yl)-*N,N,N',N'*-tetramethyluronium hexafluorophosphate

p-TsCl: *p*-Toluenesulfonyl chloride

p-TsOH: *p*-Toluenesulfonic acid

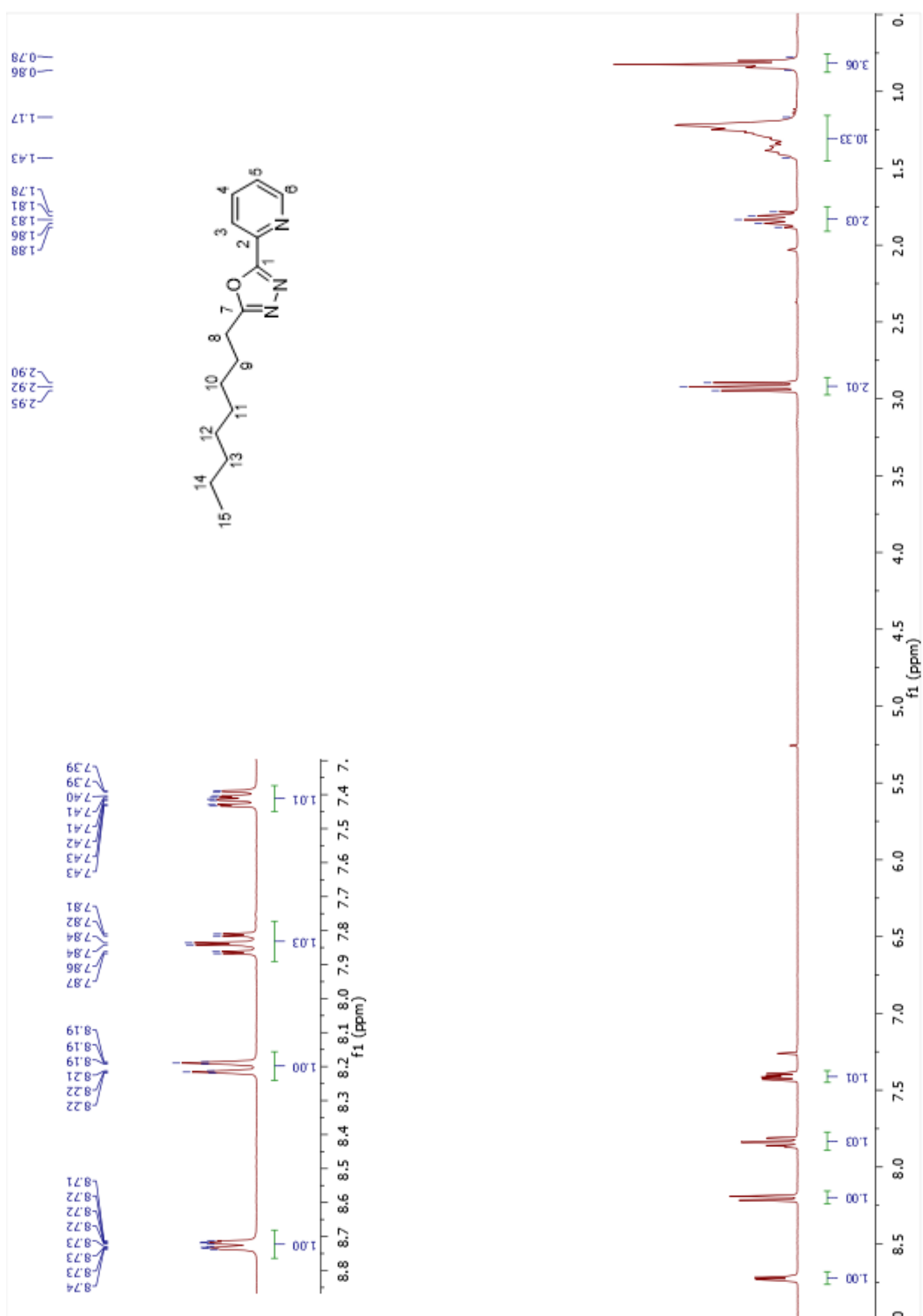


Figure S1. ¹H NMR spectrum of 2-octyl-5-(pyridin-2-yl)-1,3,4-oxadiazole (1) in CDCl₃ at 25°C (300 MHz).

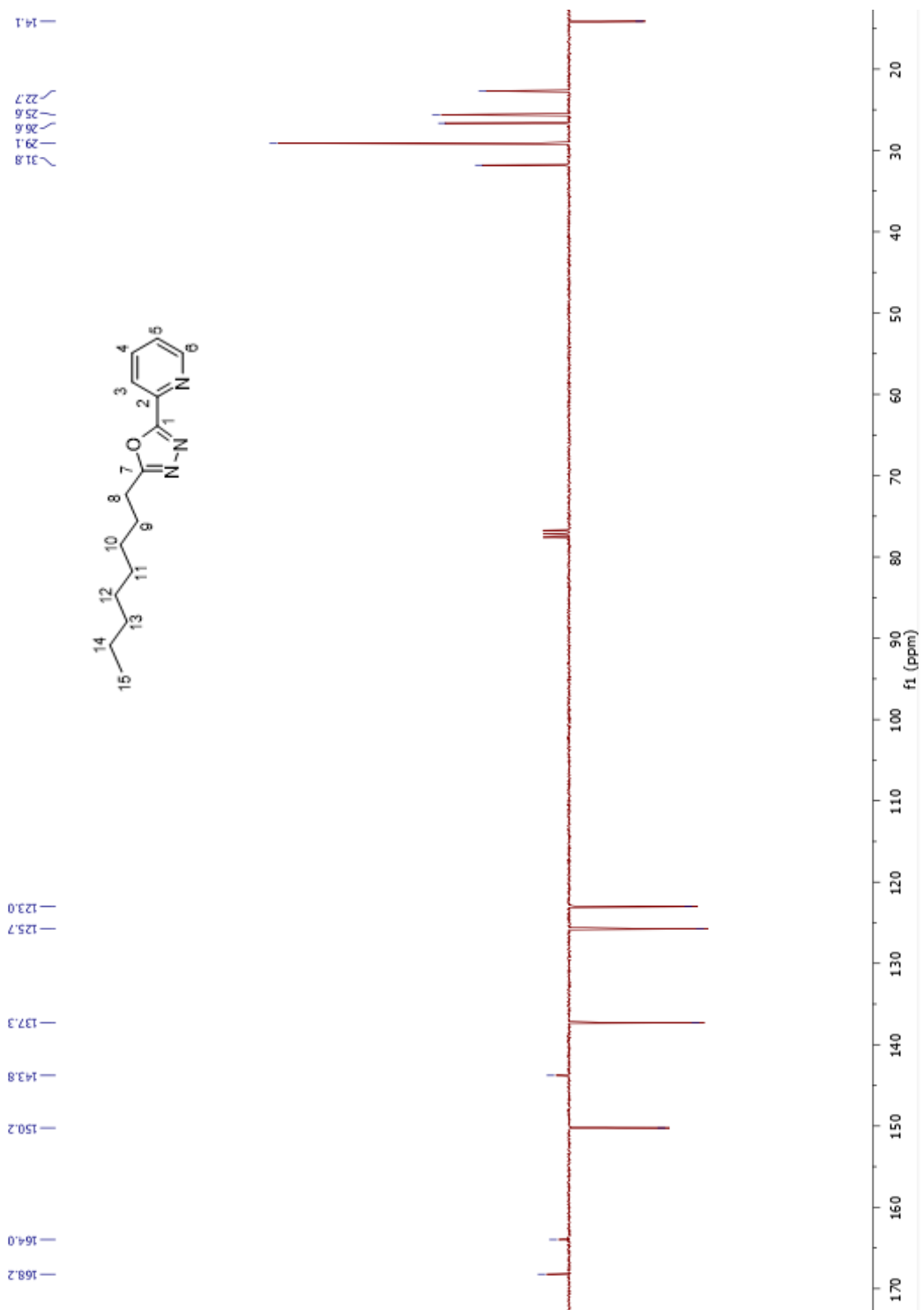


Figure S2. ¹³C NMR spectrum of 2-octyl-5-(pyridin-2-yl)-1,3,4-oxadiazole (1) in CDCl₃ at 25°C (300 MHz).

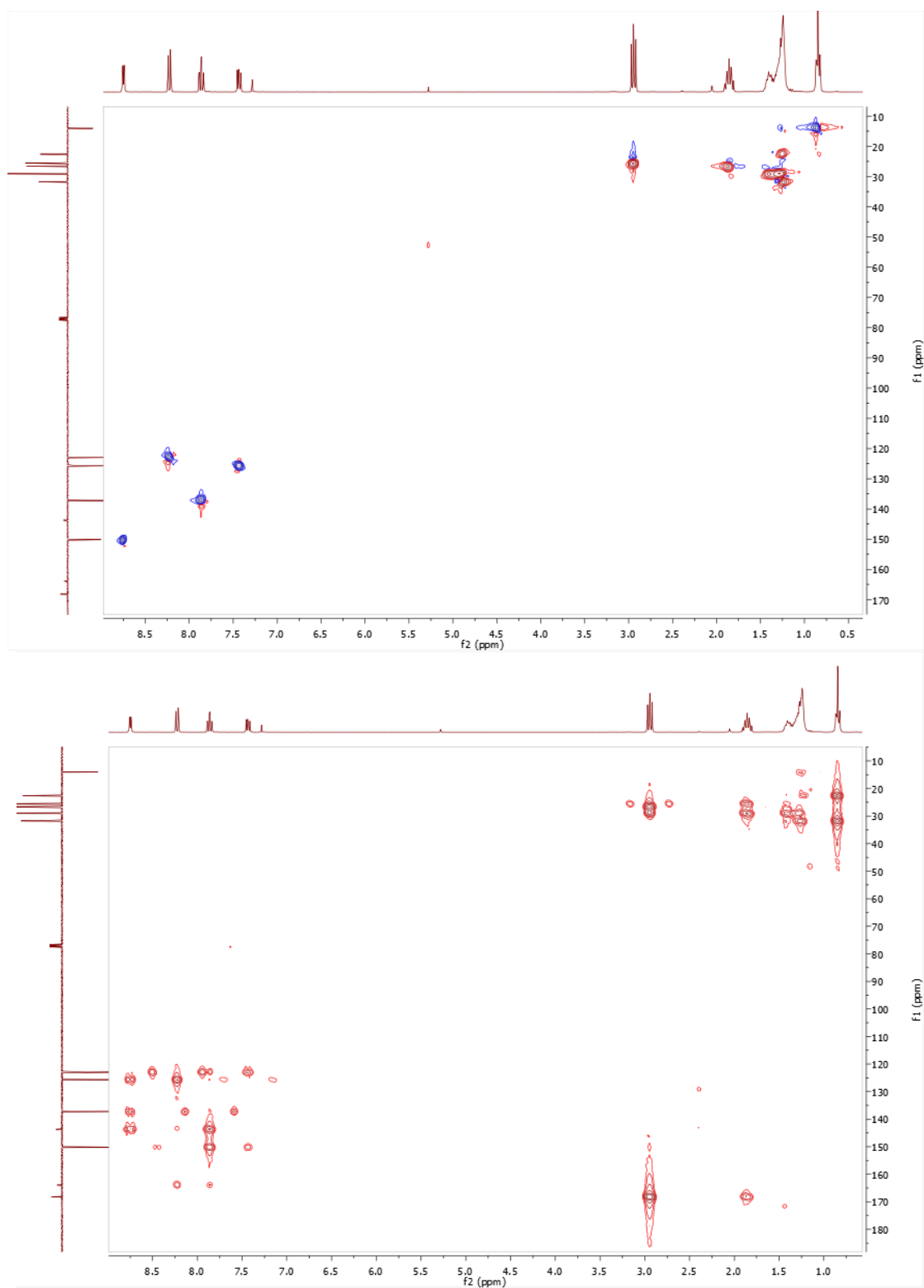


Figure S3. HSQC (top) and HMBC (bottom) NMR spectra of 2-octyl-5-(pyridin-2-yl) 1,3,4-oxadiazole (**1**) in CDCl₃ at 25°C (300 MHz).

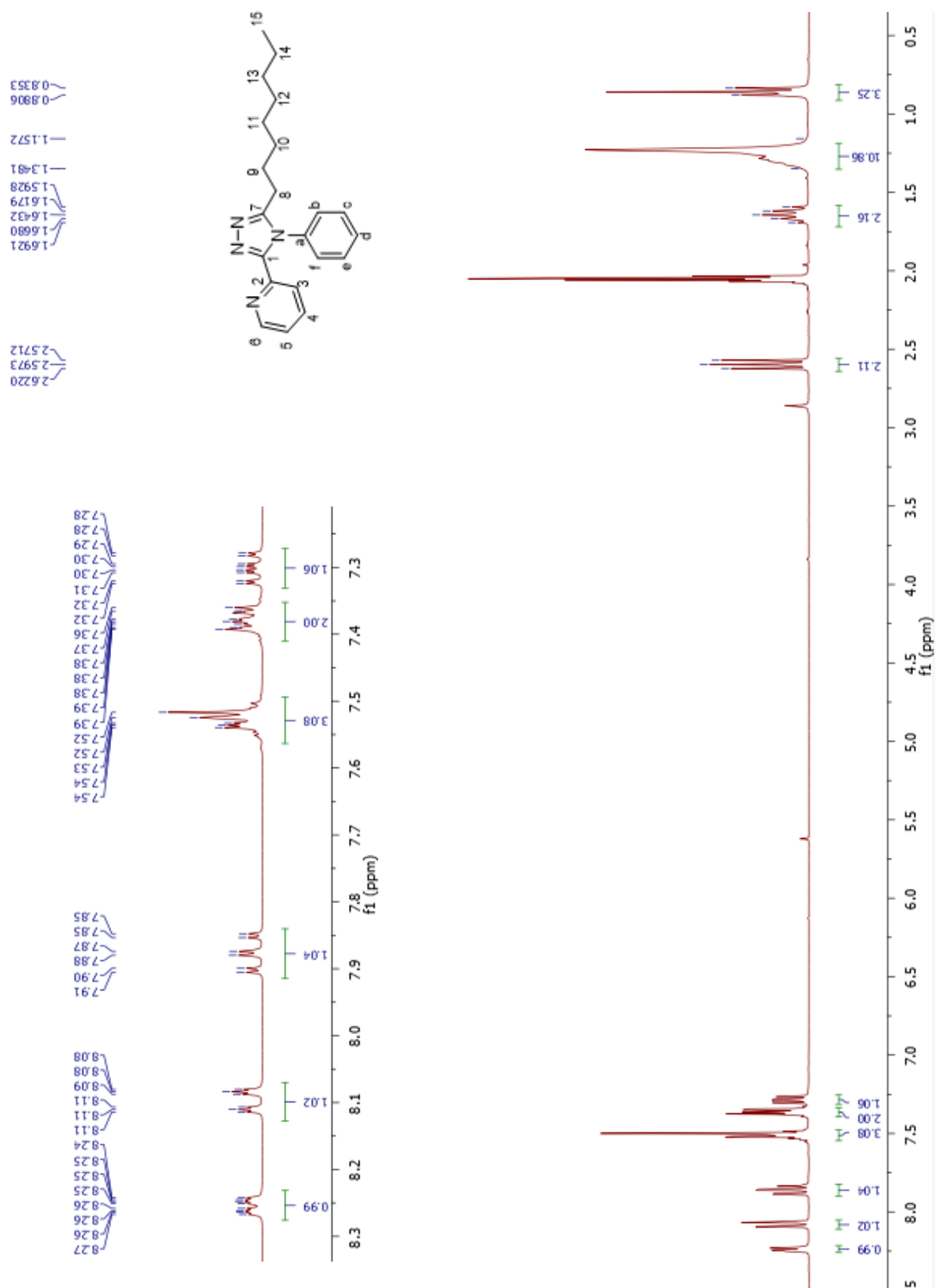


Figure S4. ¹H NMR spectrum of ligand L-Phe in acetone-d₆ at 25°C (300 MHz).

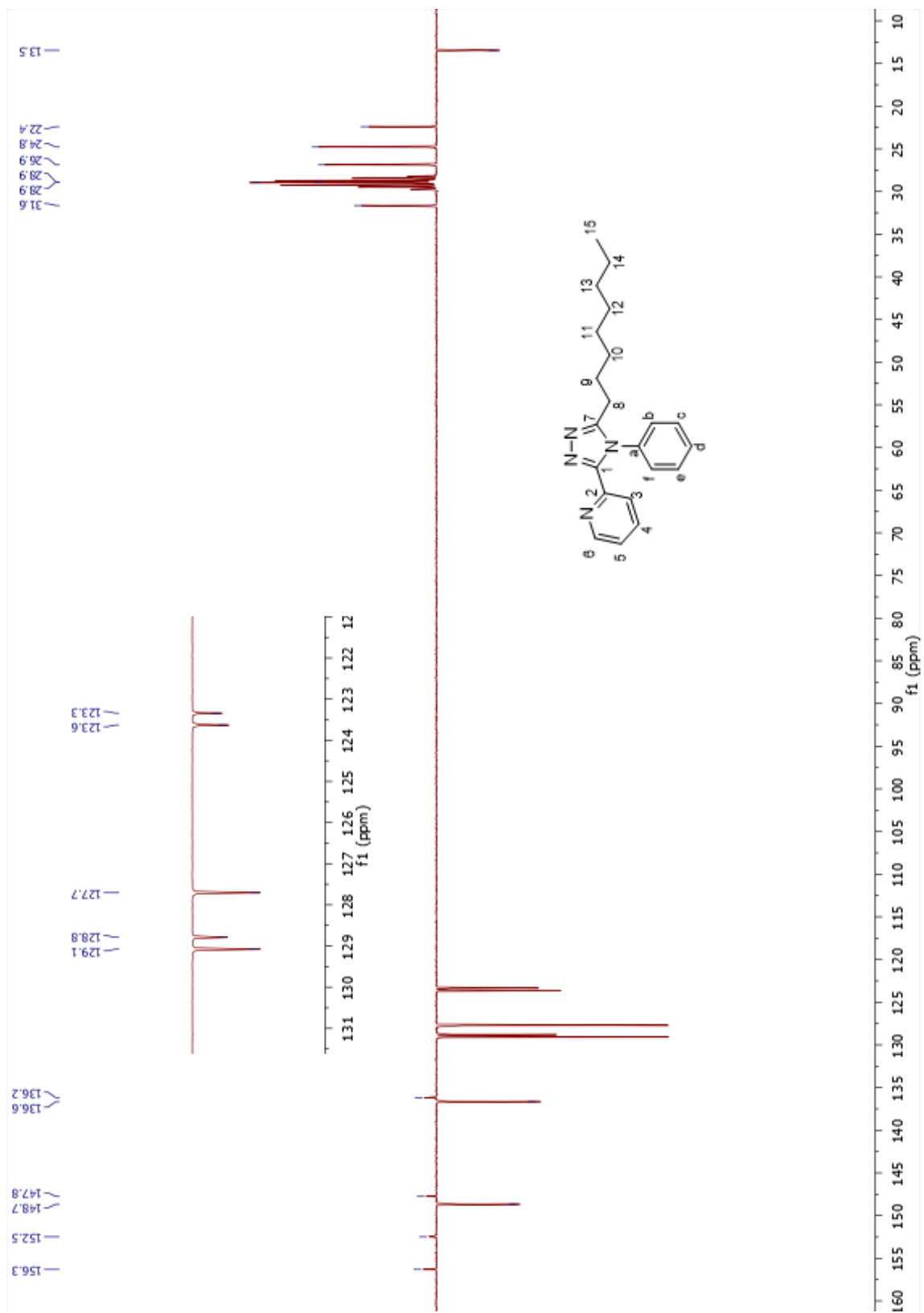


Figure S5. ^{13}C NMR spectrum of ligand L-Phe in acetone- d_6 at 25°C (300 MHz).

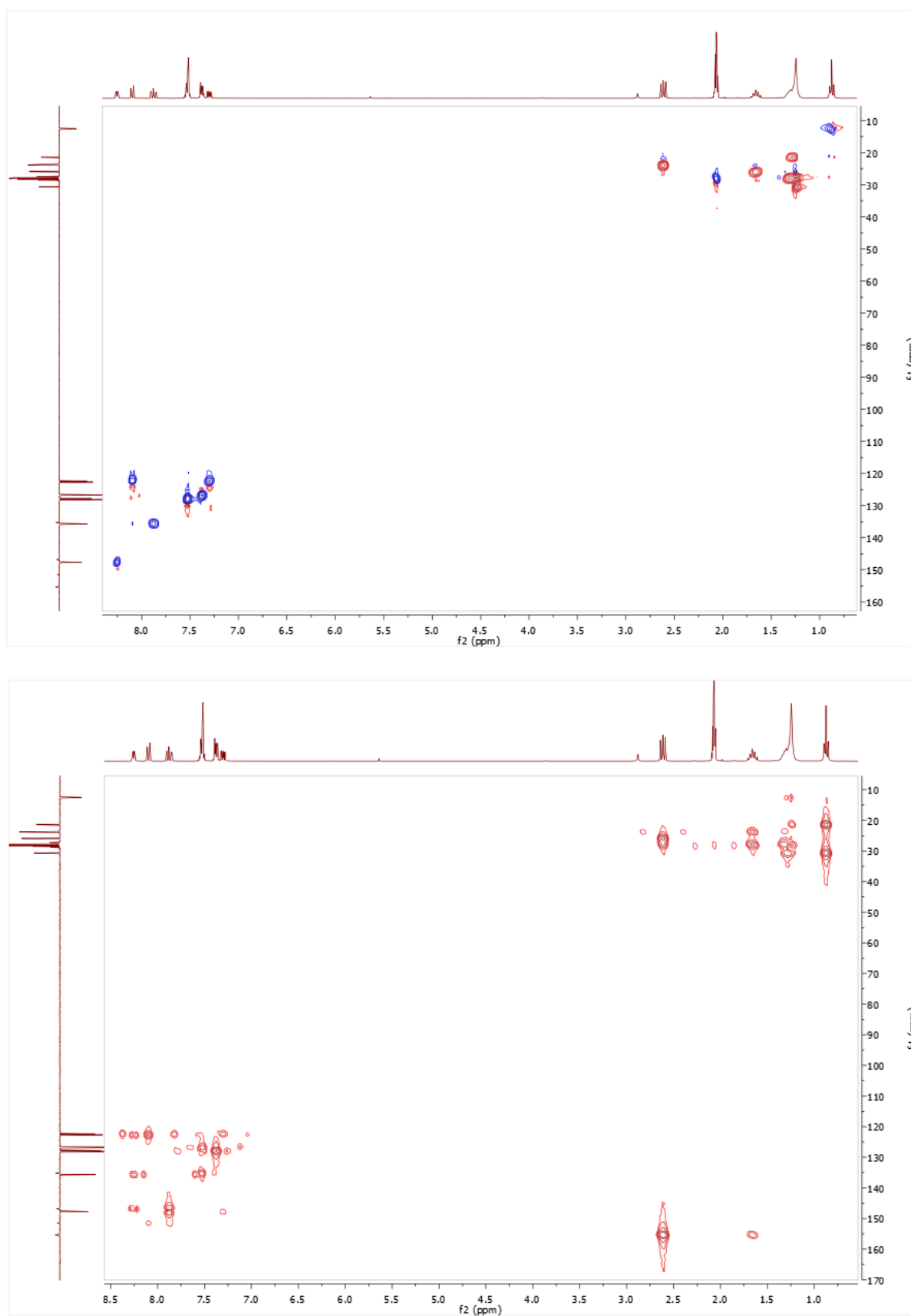


Figure S6. HSQC (top) and HMBC (bottom) NMR spectra of ligand **L-Phe** in acetone- d_6 at 25°C.

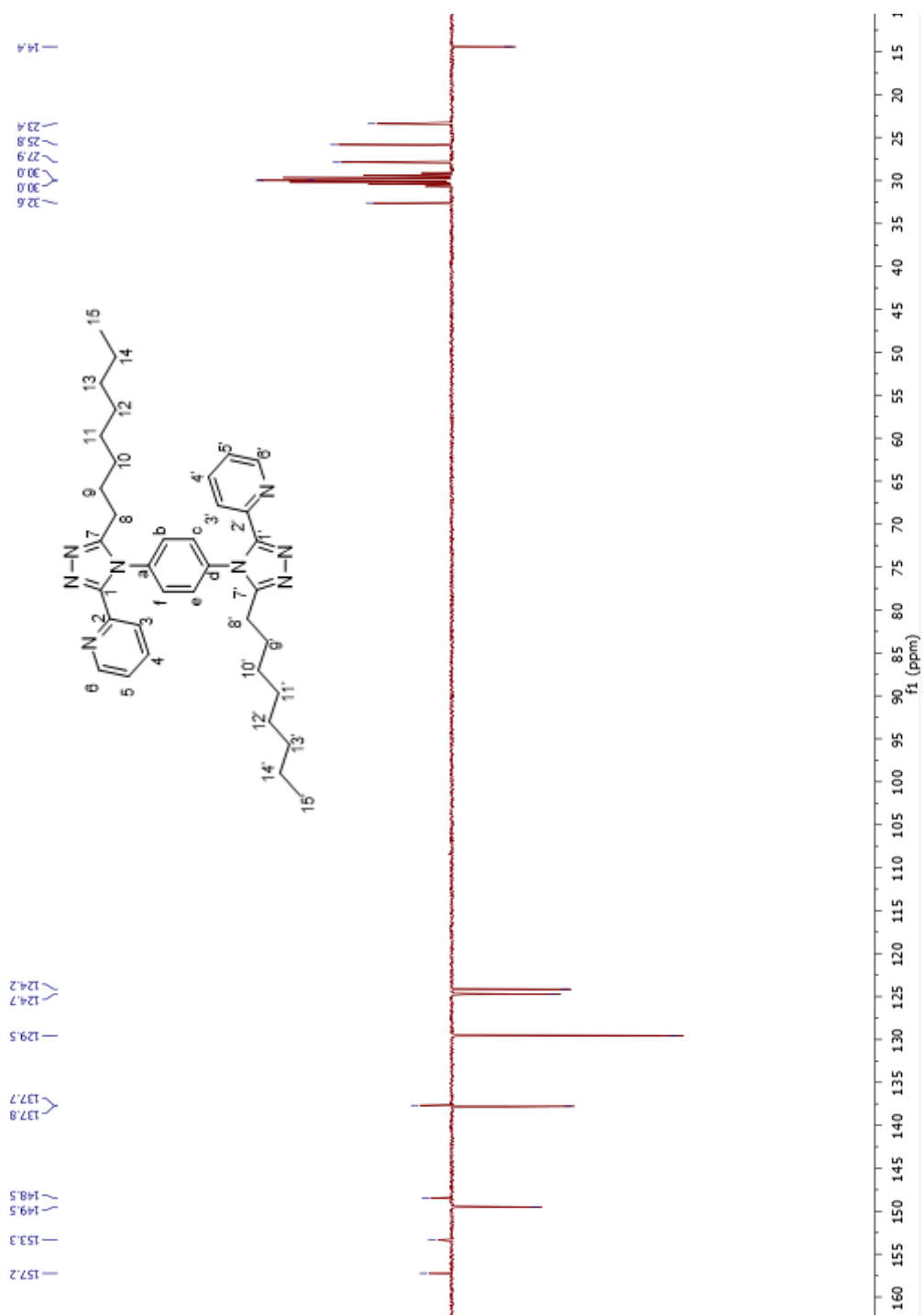


Figure S8. ^{13}C NMR spectrum of ligand **L-paraPhe** in $\text{acetone-}d_6$ at 25°C (300 MHz).

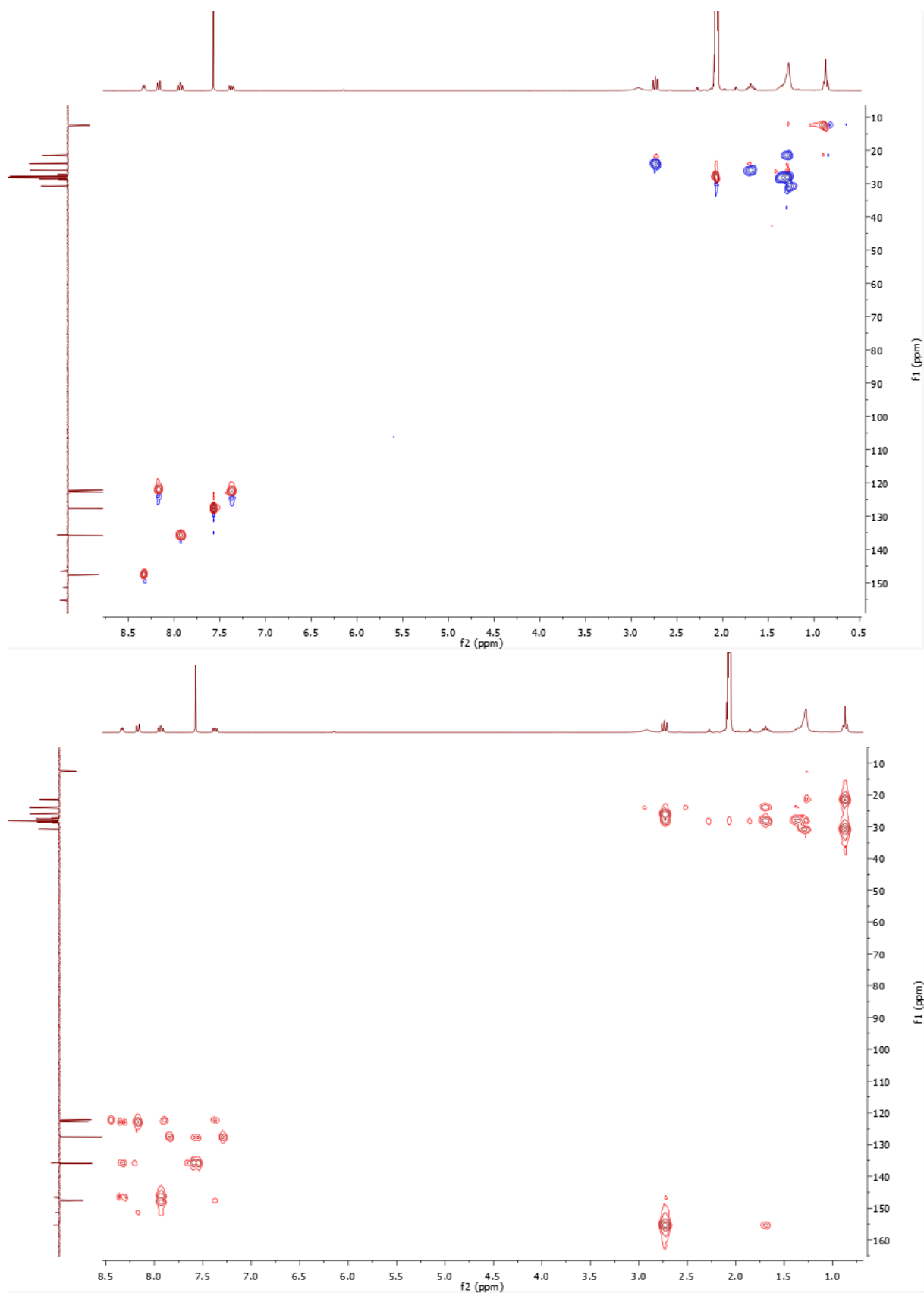


Figure S9. HSQC (top) and HMBC (bottom) NMR spectra of ligand *L-paraPhe* in acetone-*d*₆ at 25°C (300MHz).

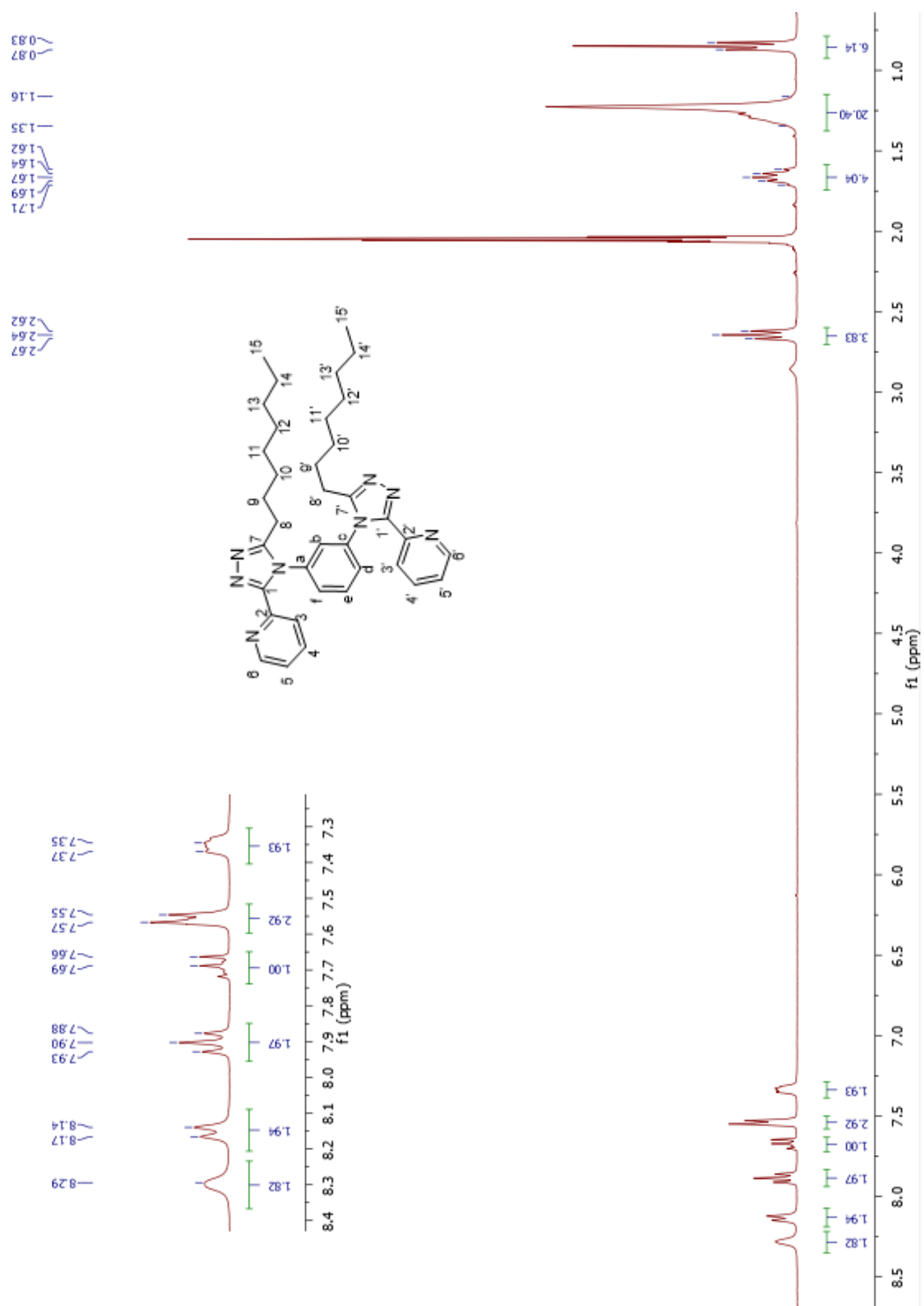


Figure S10. ^1H NMR spectrum of ligand **L-metaPhe** in $\text{acetone-}d_6$ at 25°C (300 MHz).

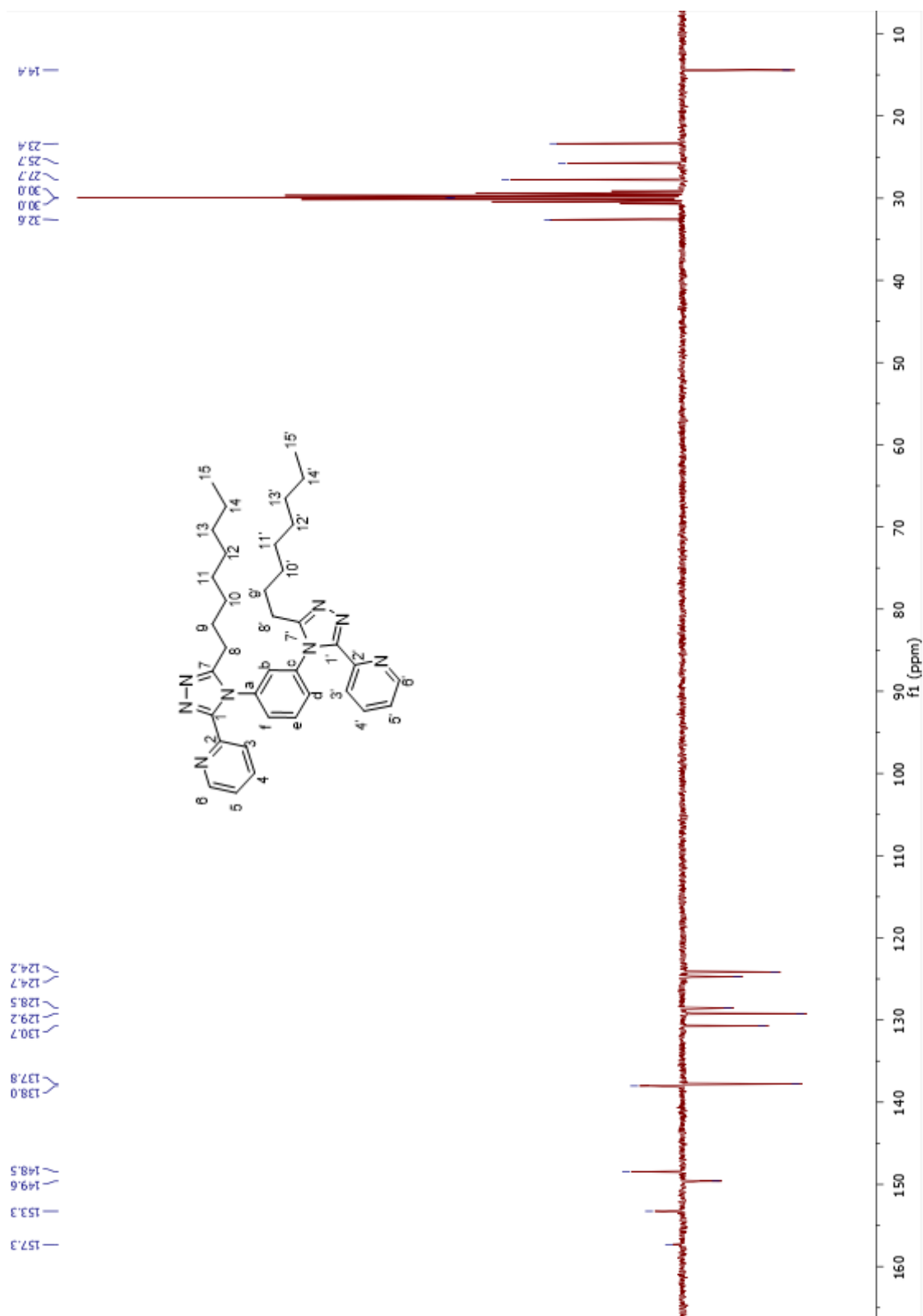


Figure S11. ^{13}C NMR spectrum of ligand *L*-metaPhe in acetone- d_6 at 25°C (300 MHz).

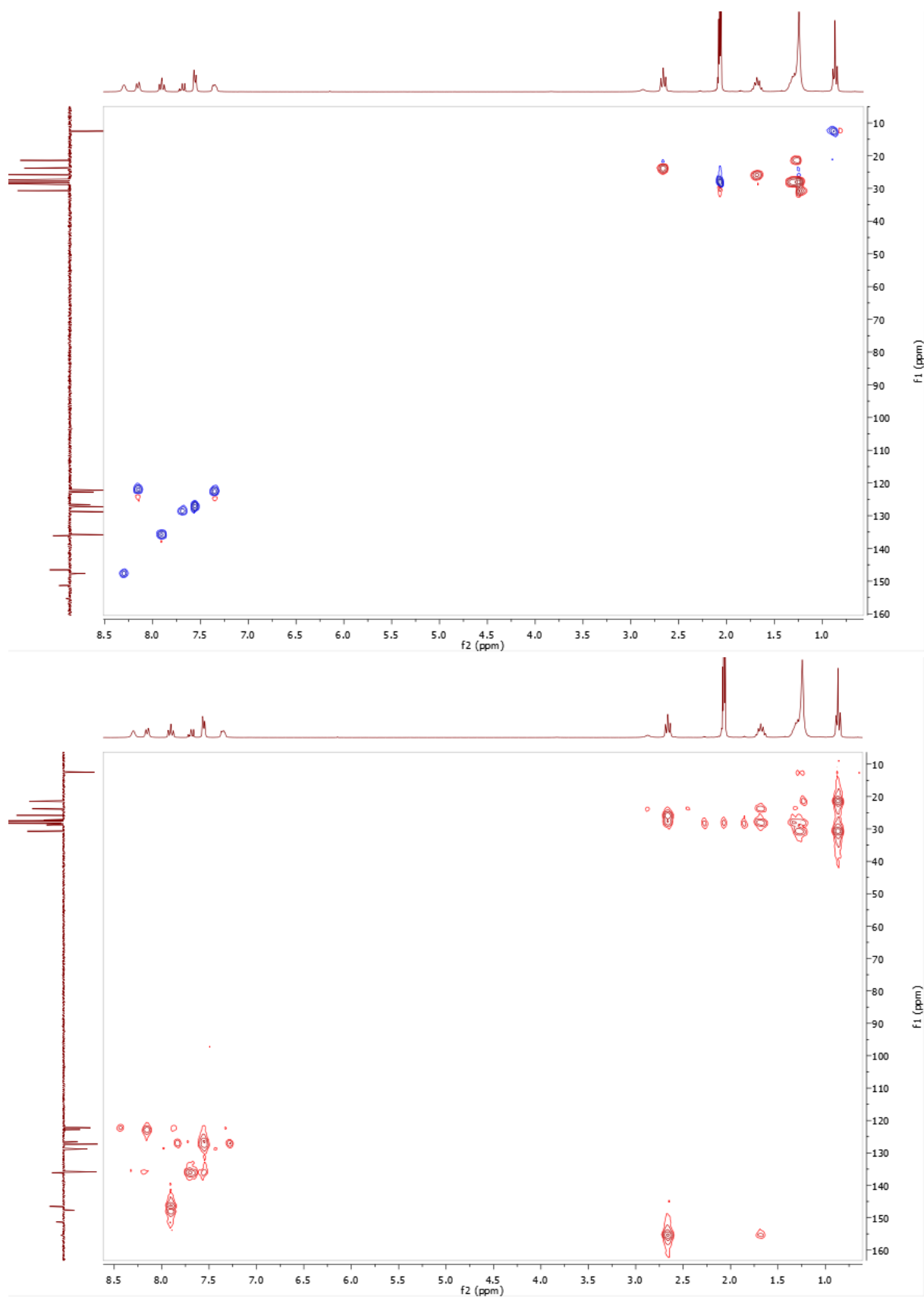


Figure S12. HSQC (top) and HMBC (bottom) NMR spectra of ligand *L*-metaPhe in acetone-*d*₆ at 25°C (300MHz).

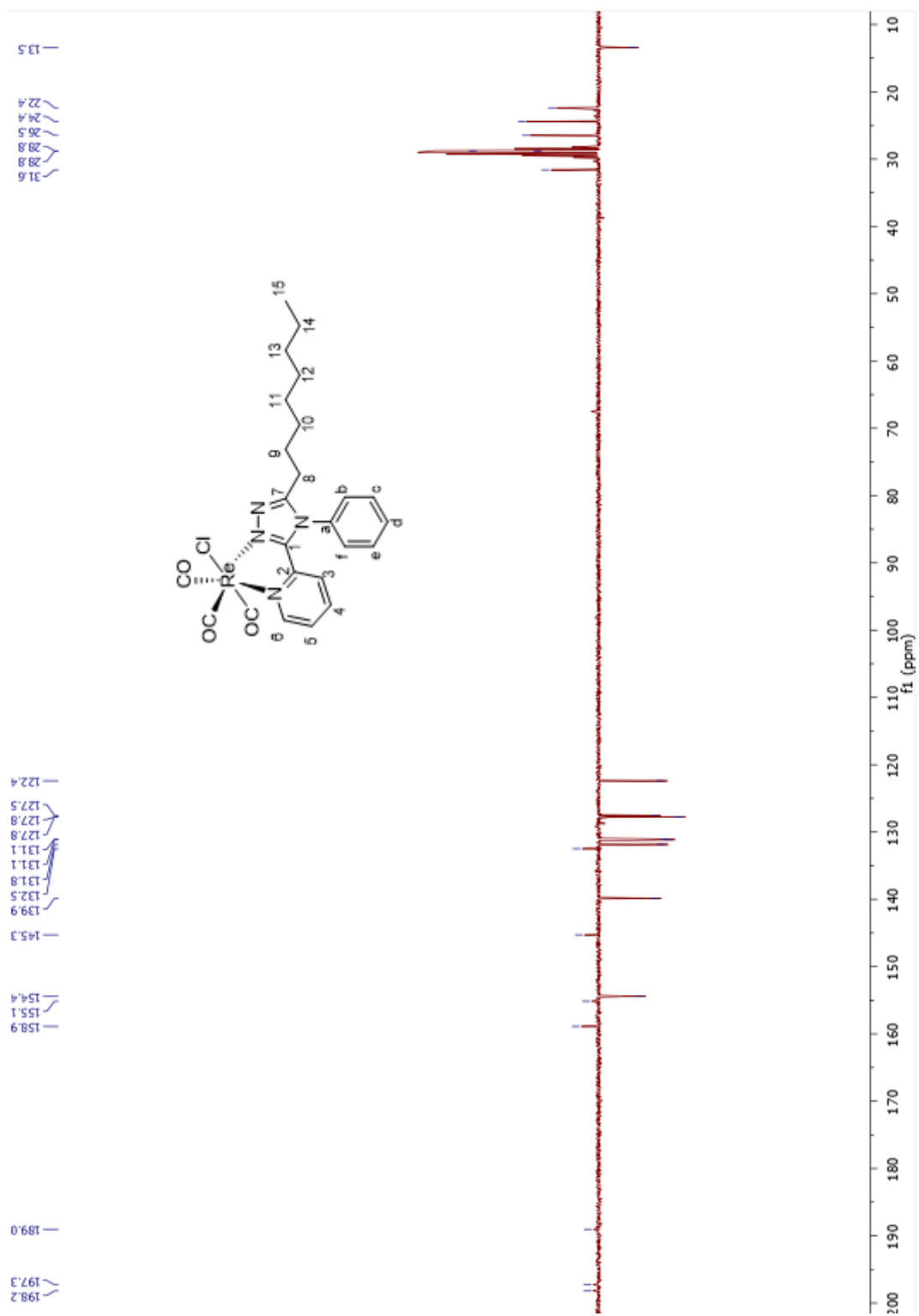


Figure S14. ^{13}C NMR spectrum of complex **Mono-Re-Phe** in acetone- d_6 at 25°C (300 MHz).

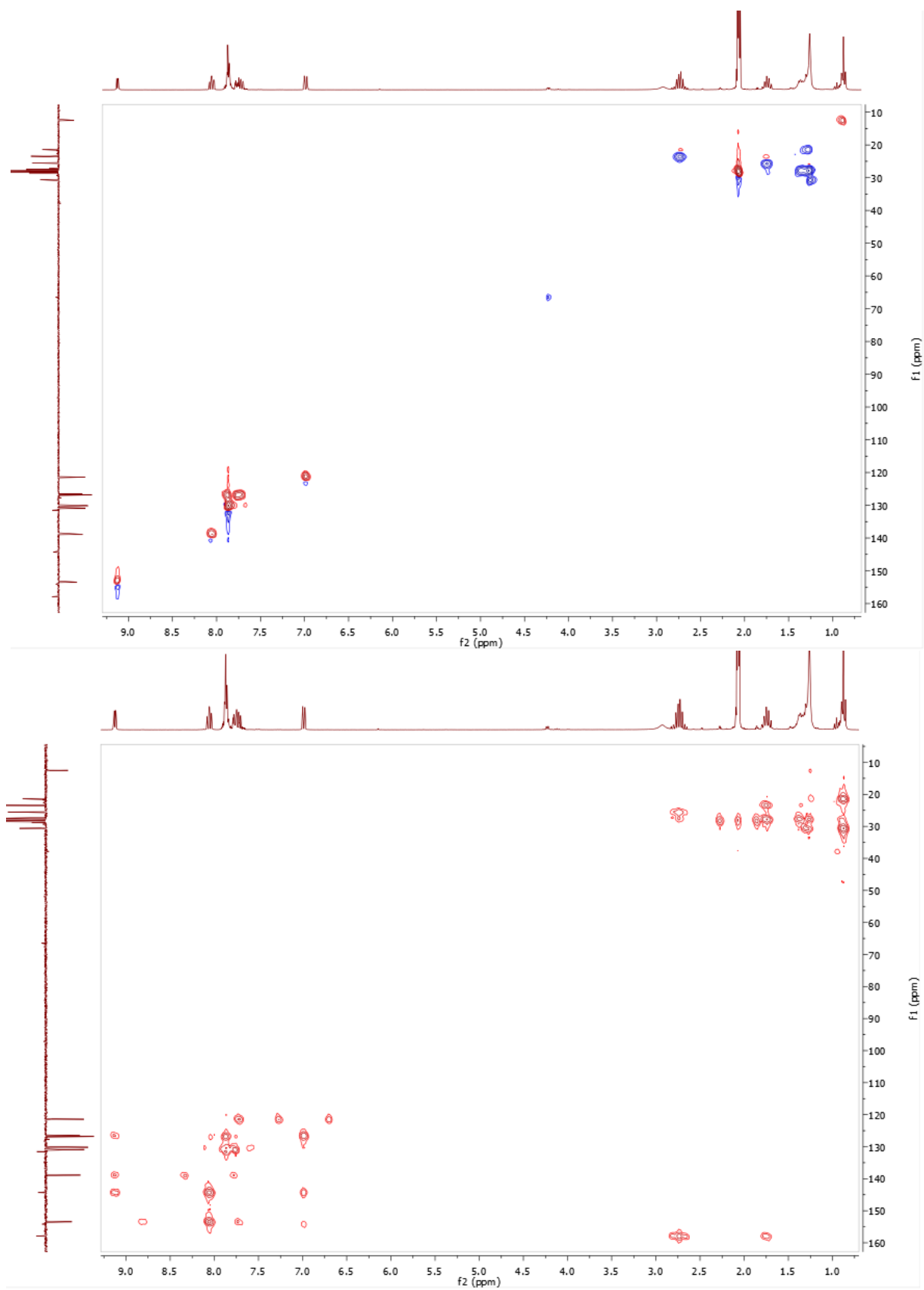


Figure S15. HSQC (top) and HMBC (bottom) NMR spectra of complex **Mono-Re-Phe** in acetone- d_6 at 25°C (300MHz)

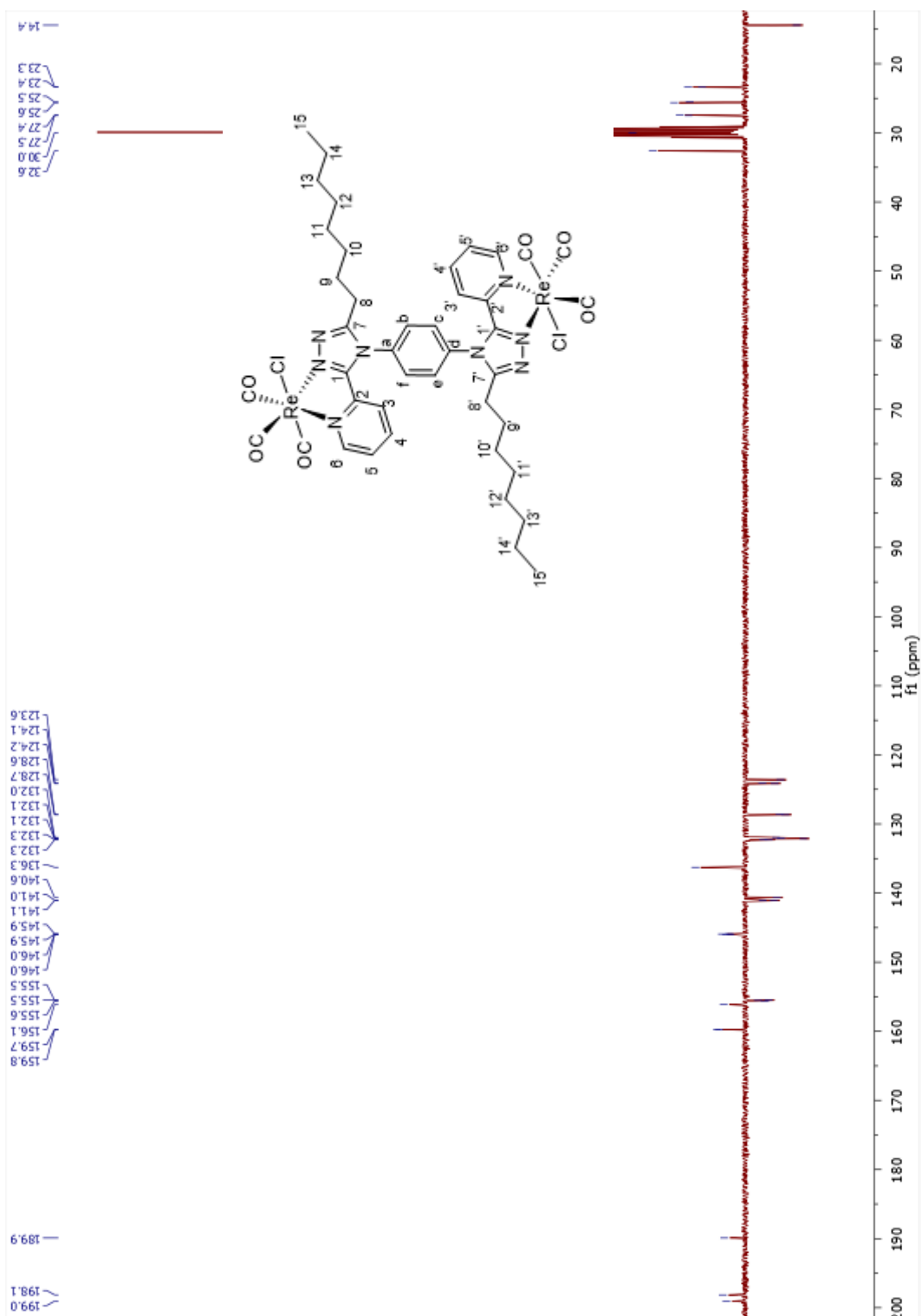


Figure S17. ^{13}C NMR spectrum of complex **Bi-Re-paraPhe** in $\text{acetone-}d_6$ at 25°C (300 MHz).

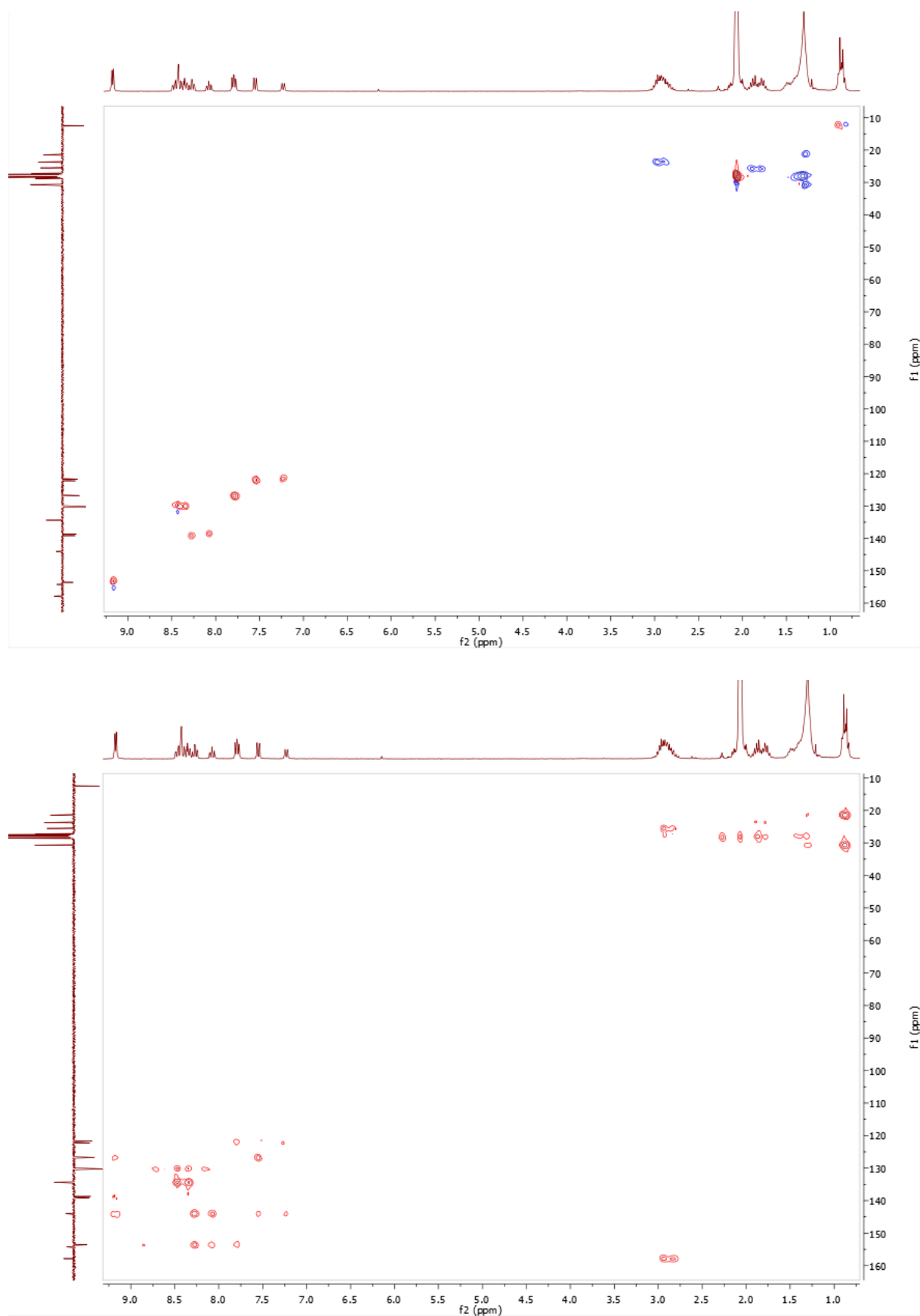


Figure S18. HSQC (top) and HMBC (bottom) NMR spectra of complex **Bi-Re-paraPhe** in acetone- d_6 at 25°C (300 MHz).

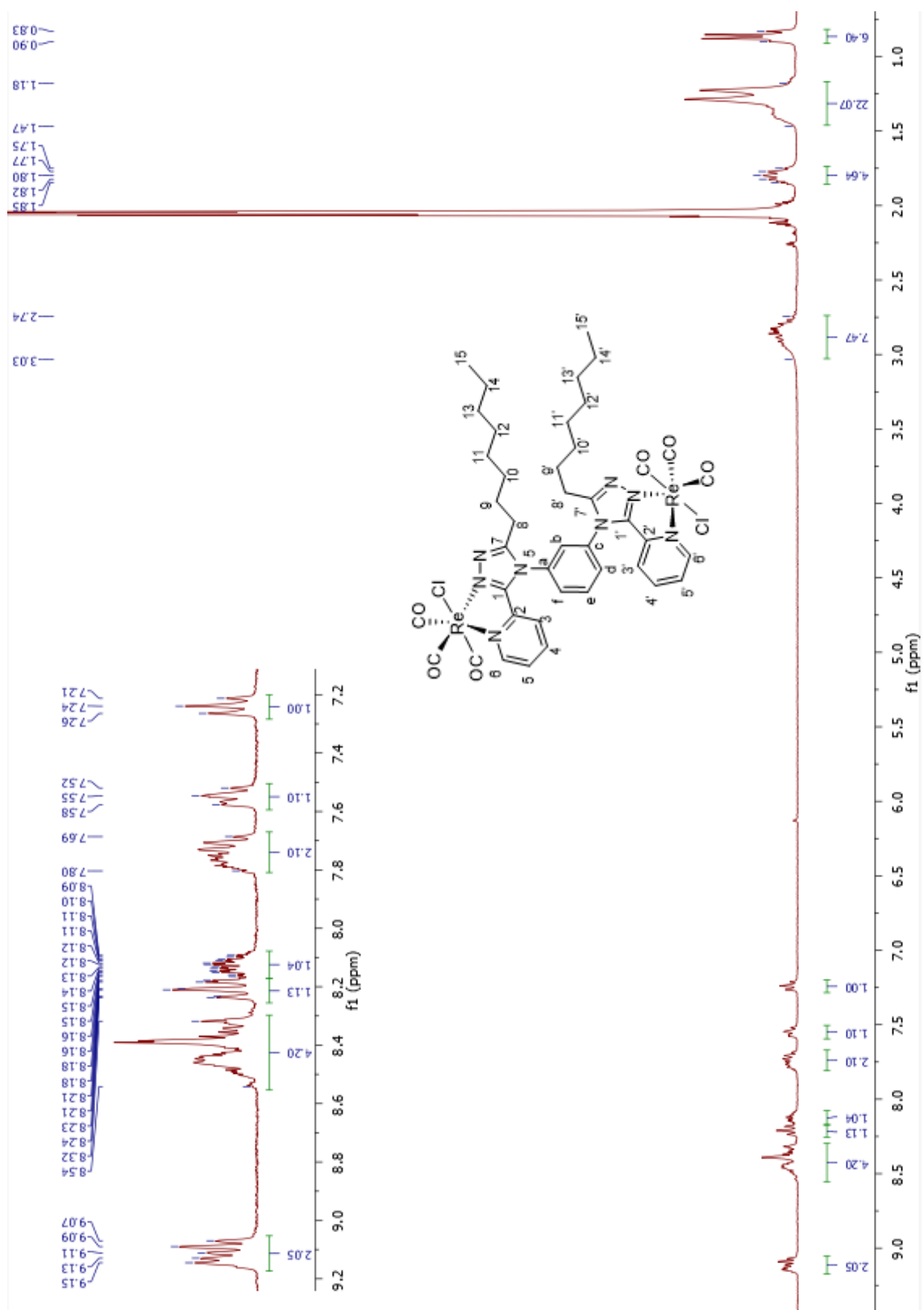


Figure S19. ¹H NMR spectrum of complex **Bi-Re-metaPhe** in acetone-*d*₆ at 25°C (300 MHz).

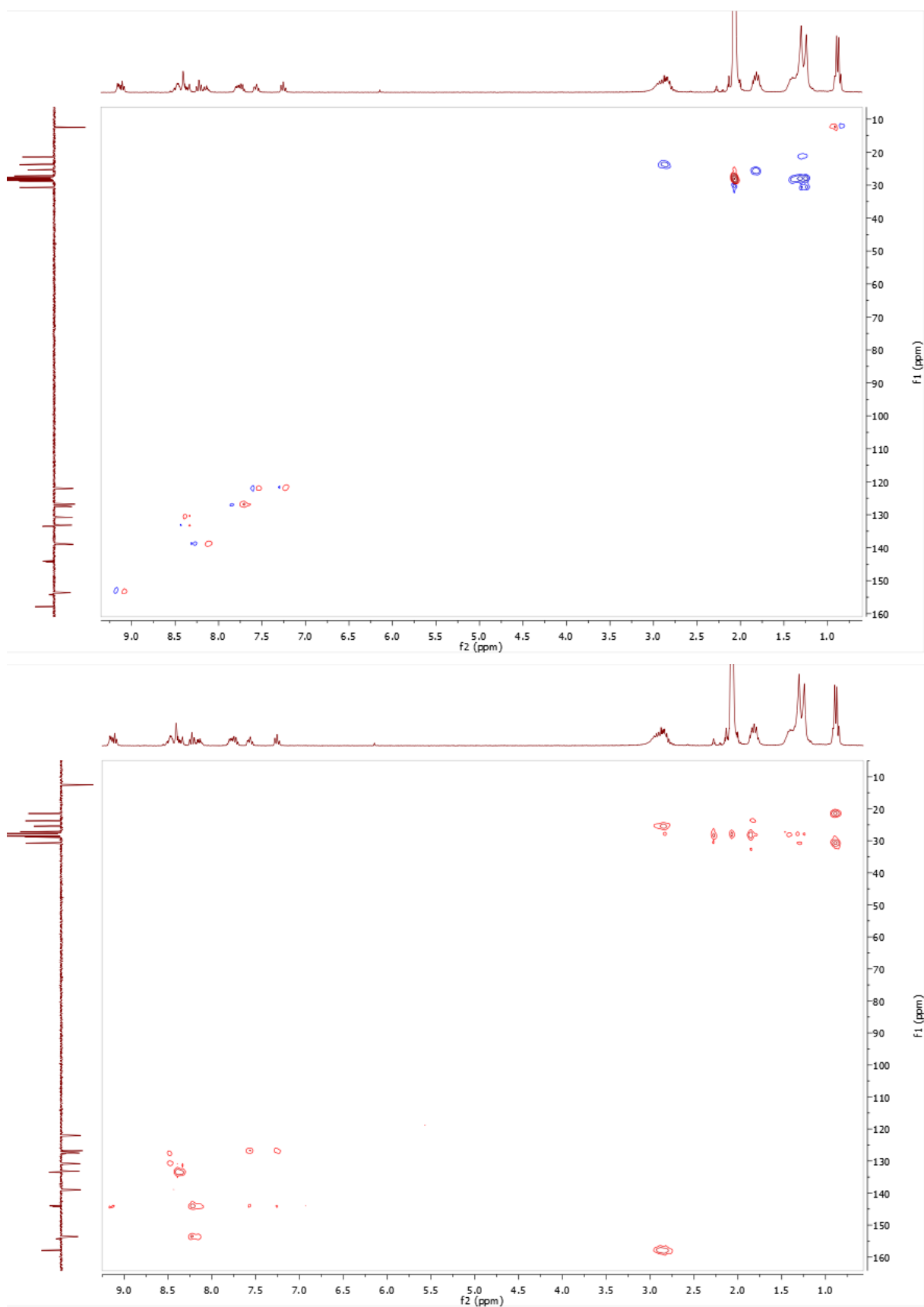


Figure S21. HSQC (top) and HMBC (bottom) NMR spectra of complex **Bi-Re-metaPhe** in acetone- d_6 at 25°C (300 MHz).

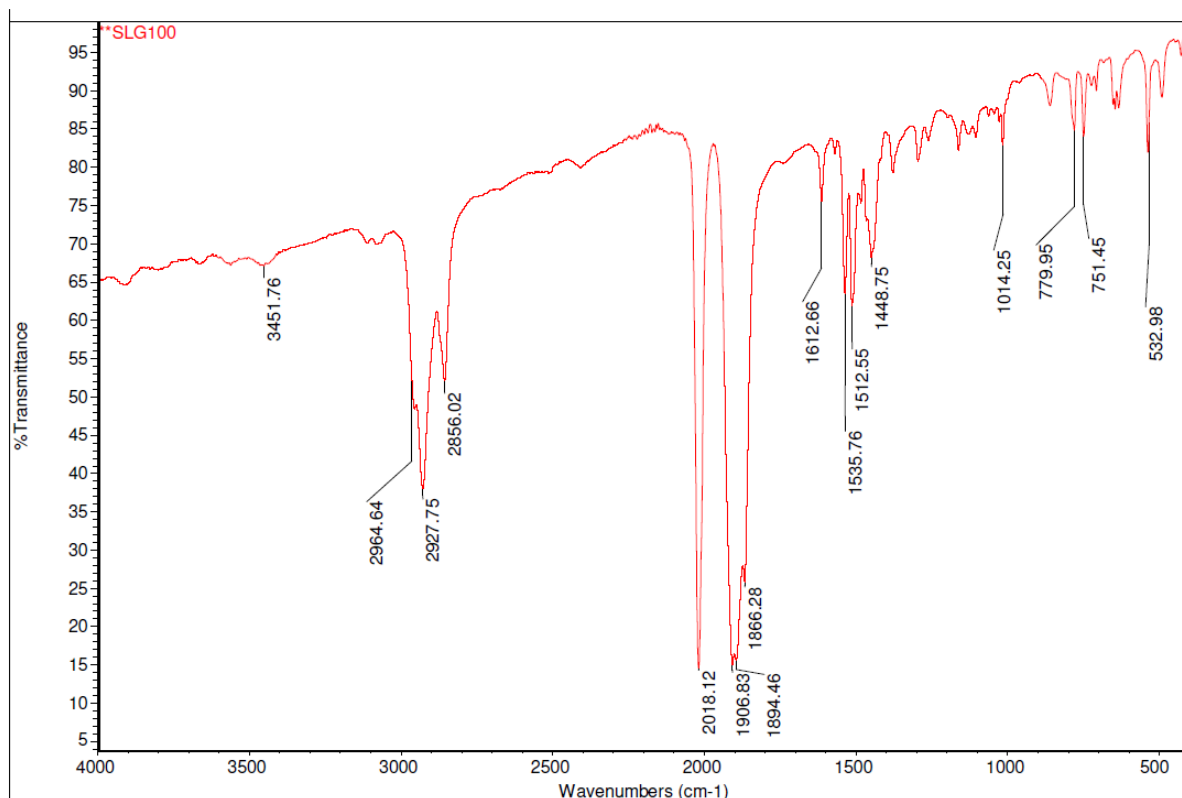
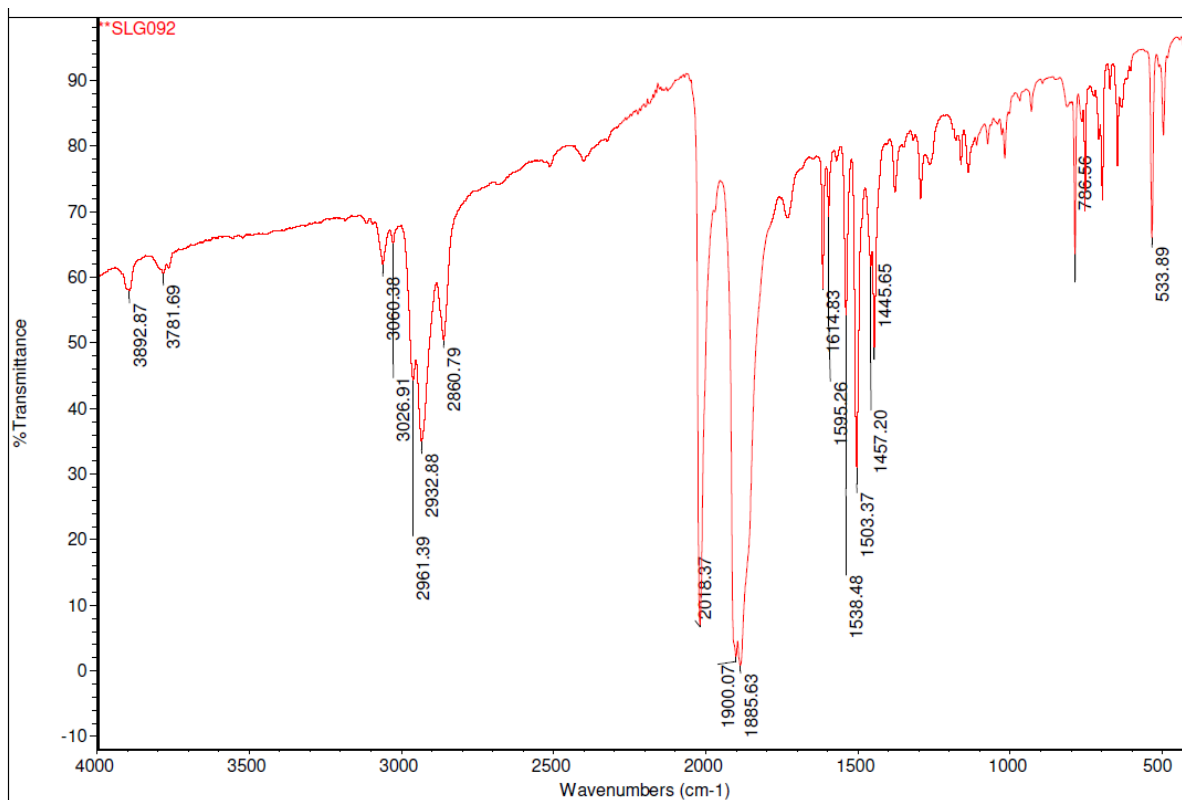


Figure S22. ATR FT-IR spectra of microcrystalline powders of complexes **Mono-Re-Phe** (top) and **Bi-Re-paraPhe** (bottom).

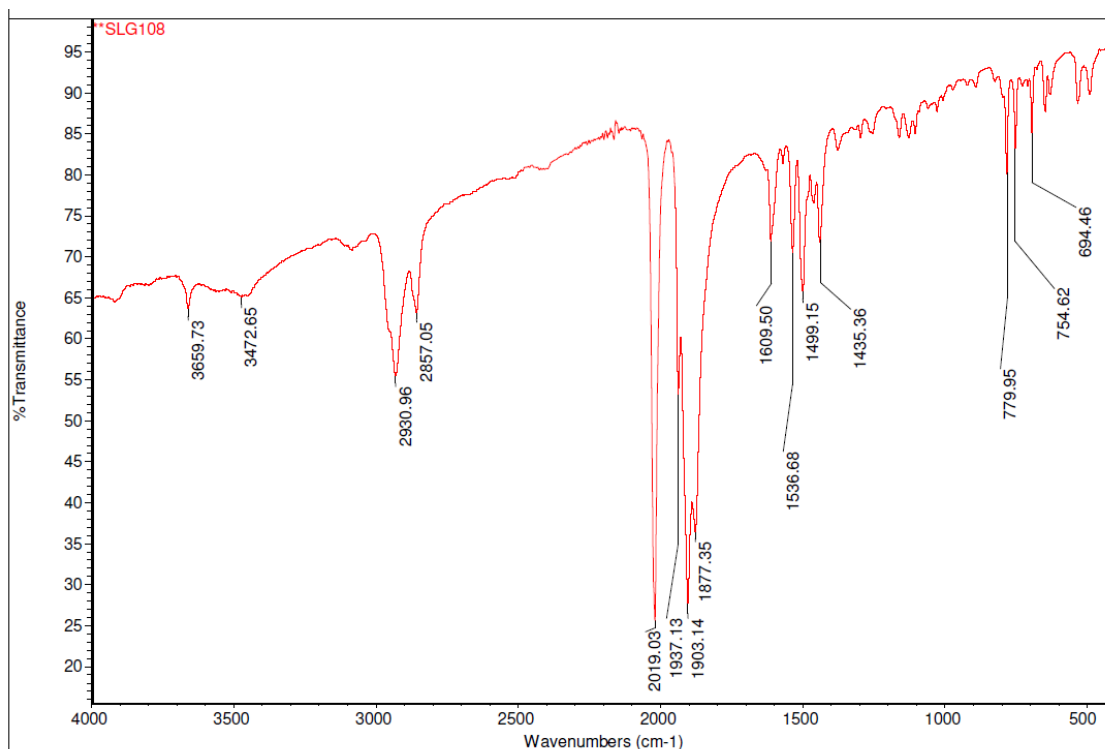


Figure S23. ATR FT-IR spectra of the microcrystalline powder of complex **Bi-Re-*meta*Phe**.

Crystallographic data

Table S1. Selected bond lengths (Å) for complexes **Mono-Re-Phe** and **Bi-Re-*meta*Phe**, and ligands **L-*para*Phe** and **L-*meta*Phe**. The atoms were numbered like on the molecular views. For the sake of comparison, each line corresponds to the same bond in each complex. For molecular views, the displacement ellipsoids are drawn at the 50% probability level.

Bond	Mono-Re-Phe	Bi-Re- <i>meta</i> Phe	Bond	L- <i>para</i> Phe	L- <i>meta</i> Phe
Re1-C1	1.904(2)	1.923(13)	C6-N2	1.3161(18)	1.312(3)
Re1-C2	1.913(4)	1.911(2)	N2-N3	1.3919(19)	1.394(3)
Re1-C3	1.912(2)	1.898(10)	C7- N3	1.3154(18)	1.310(3)
Re1-N1	2.1974 (17)	2.205(8)	C7-N4	1.3717(17)	1.374(2)
Re1-N2	2.1411 (16)	2.154(7)	C6-N4	1.3777(17)	1.373(2)
Re1-C11	2.4747(6)	2.472(3)	C36- N4	1.4396(15)	---
O1-C1	1.149(3)	1.089(15)	C35- N4	---	1.437(2)
O2-C2	1.148(3)	1.134(14)	C5-C6	1.472(2)	1.471(3)
O3-C3	1.154(3)	1.163(13)	C4-C5	1.391(2)	1.391(3)
			C5-N1	1.3363(19)	1.344(3)

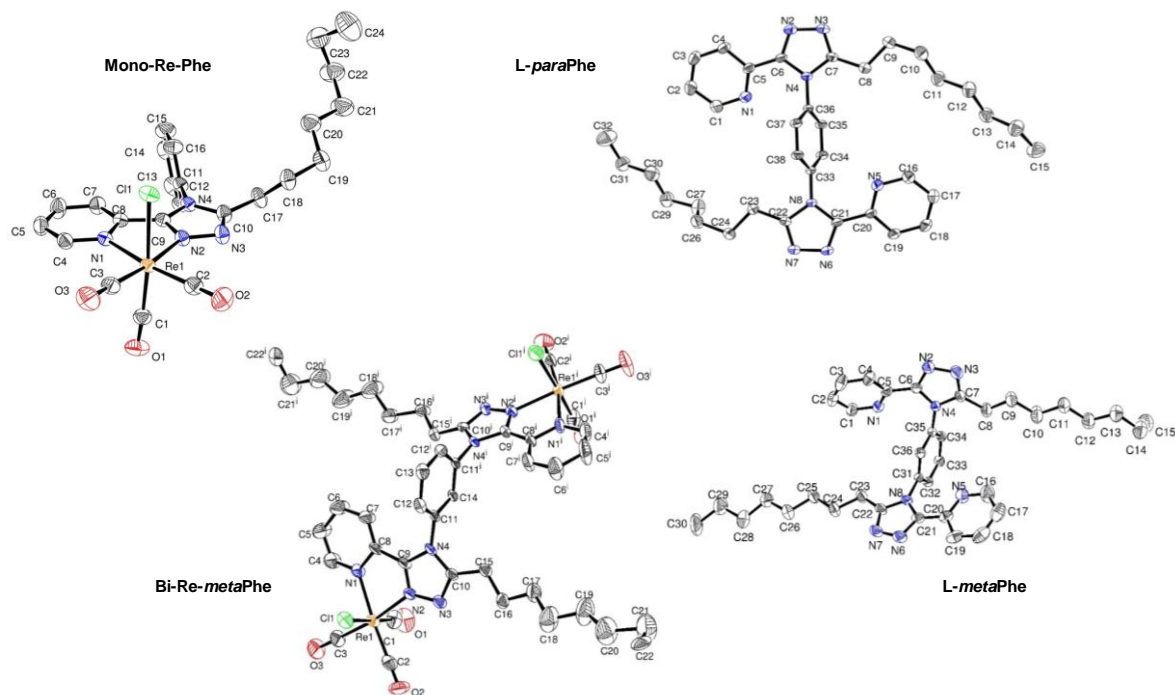


Table S2. Selected angles ($^{\circ}$) for complexes **Mono-Re-Phe** and **Bi-Re-metaPhe**, and ligands **L-paraPhe** and **L-metaPhe**. For the sake of comparison, each line corresponds to the same bond in each complex. The atoms were numbered like on the molecular views.

Angle	Mono-Re-Phe	Bi-Re-metaPhe	Angle	L-paraPhe	L-metaPhe
C1-Re1-C2	90.34(10)	90.4(5)	C4-C5-C6	120.23(14)	118.86(19)
C1-Re1-C3	87.66(10)	89.0(5)	N1-C5-C6	116.55(12)	117.55(18)
C2-Re1-C3	87.92(10)	90.0(5)	N2-C6-C5	124.60(12)	124.66(18)
C1-Re1-N1	91.22(8)	95.2(5)	N4-C6-C5	125.55(12)	125.73(18)
C2-Re1-N1	171.22(8)	170.5(4)	C6-N2-N3	107.63(11)	107.80(17)
C3-Re1-N1	100.78(8)	97.8(4)	C7-N3-N2	107.27(12)	107.32(17)
C1-Re1-N2	96.75(8)	94.4(4)	N3-C7-N4	110.28(13)	109.96(18)
C2-Re1-N2	97.23(8)	97.7(4)	C6-N4-C7	104.99(11)	105.34(16)
C3-Re1-N2	173.18(8)	171.6(4)	C7-N4-C36	125.31(11)	---
N1-Re1-N2	74.01(6)	74.2(3)	C6-N4-C36	129.70(11)	---
C1-Re1-C11	174.68(7)	177.8(4)	C35-C36-N4	118.87(11)	---
C2-Re1-C11	94.92(7)	91.0(3)	C37-C36-N4	119.41(11)	---
C3-Re1-C11	91.76(7)	92.7(4)	C7-N4-C35	---	124.68(16)
N1-Re1-C11	83.69(5)	83.2(2)	C6-N4-C35	---	129.37(16)
N2-Re1-C11	83.37(5)	83.8(2)	C36-C35-N4	---	118.89(17)
O1-C1-Re1	175.7(2)	176.4(13)	C34-C35-N4	---	119.98(16)
O2-C2-Re1	179.0(2)	177.2(10)			
O3-C3-Re1	177.7(2)	178.9(13)			

Comment S1. Crystal lattice of Re-Phe

In the crystal lattice of **Re-Phe**, two neighboring molecules, each with Re2 centre, interact with each other *via* two C26–H26(trz)···Cl2 interactions to form centrosymmetric $R_2^2(12)$ dimers (Fig. S24). These dimers are connected into loop chain *via* intermolecular C20–H20(py)_{Re2}···Cl1_{Re1} and C22–H22(py)_{Re2}···O3(CO)_{Re1} interactions along the *ab* plane (Fig. S25). They are also linked into stair chain by an aromatic intermolecular parallel displaced $\pi(\text{py})_{\text{Re2}}-\pi(\text{py})_{\text{Re2}}$ stacking interactions with a centroid–centroid distance of 3.871(5)Å, a dihedral angle of 29.0° and a slip angle of 1.877° along *a*-axis (Fig. S26). The neighboring molecules with Re1 and Re2 centres share intermolecular C22–H22(py)_{Re2}···O3(CO)_{Re1} and C10–H10(trz)_{Re1}···O4(CO)_{Re2} interactions forming a zig-zag chain along the *ac* plane (Fig. S26). The presence of intramolecular C23–H23(py)··· $\pi(\text{Ph})$ interactions was also detected in the crystal lattice of **Re-Phe**.

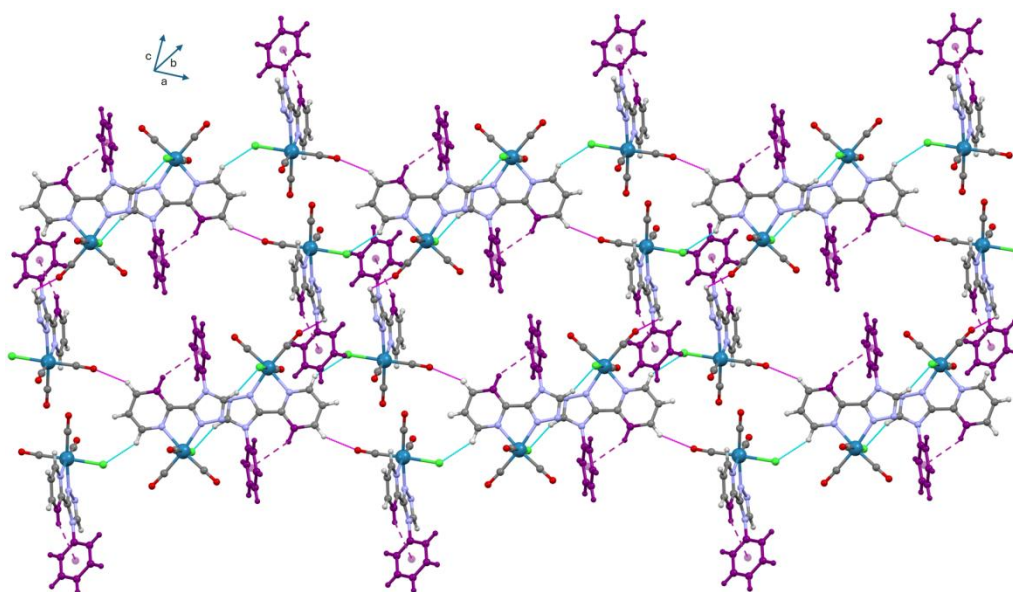


Figure S24. (a) Centrosymmetric $R_2^2(12)$ dimers of **Re-Phe** formed *via* intermolecular C26–H26(trz)···Cl2 (cyan color) interactions of two antiparallel Re2 molecules. (b) Dimers linked through C20–H20(py)_{Re2}···Cl1_{Re1} (cyan color) and C22–H22(py)_{Re2}···O3(CO)_{Re1} (magenta color) interactions viewed along the *ab* plane and C10–H10(trz)_{Re1}···O4(CO)_{Re2} (magenta color) interactions viewed along the *ac* plane and stabilized by intramolecular C23–H23(py)··· $\pi(\text{Ph})$ (tyrian purple color) interactions.

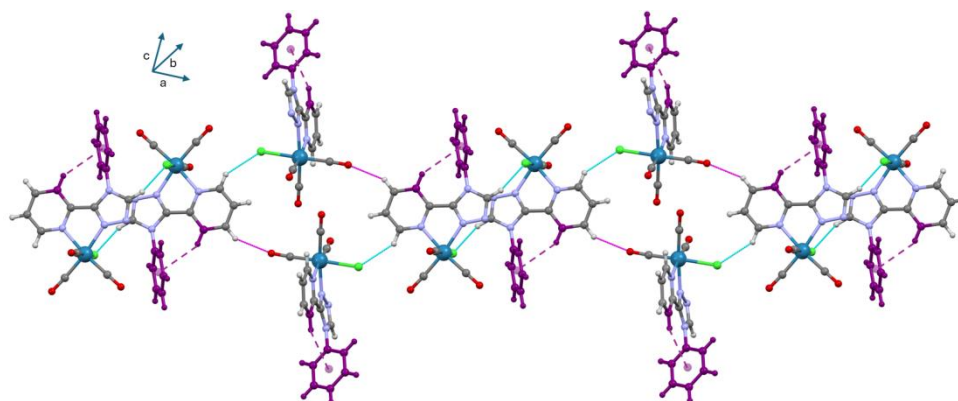


Figure S25. Dimers of **Re-Phe** connected *via* intermolecular C20–H20(py)_{Re2}···Cl1_{Re1} (cyan color) and C22–H22(py)_{Re2}···O3(CO)_{Re1} (magenta color) interactions into loop chain viewed along *ab* plane and stabilized by intramolecular C23–H23(py)··· $\pi(\text{Ph})$ (tyrian purple color) interactions.

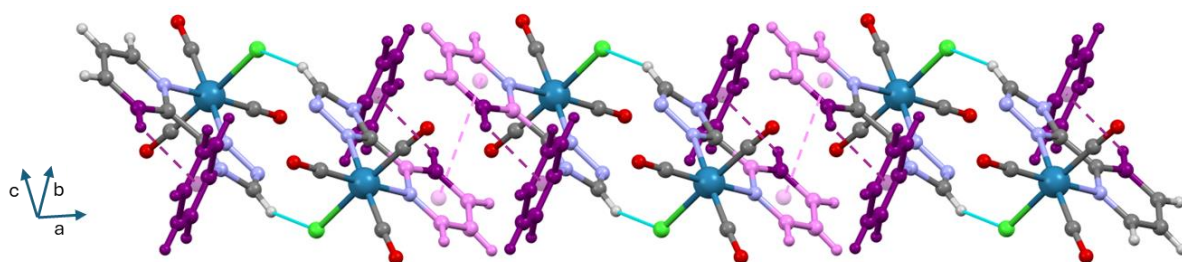


Figure S26. Dimers of **Re-Phe** linked by aromatic intermolecular parallel displaced $\pi(\text{py})_{\text{Re}2}-\pi(\text{py})_{\text{Re}2}$ stacking interactions (violet color) into stair chain viewed along a -axis and stabilized by intramolecular $\text{C}23-\text{H}23(\text{py})\cdots\pi(\text{Ph})$ (tyrian purple color) interactions.

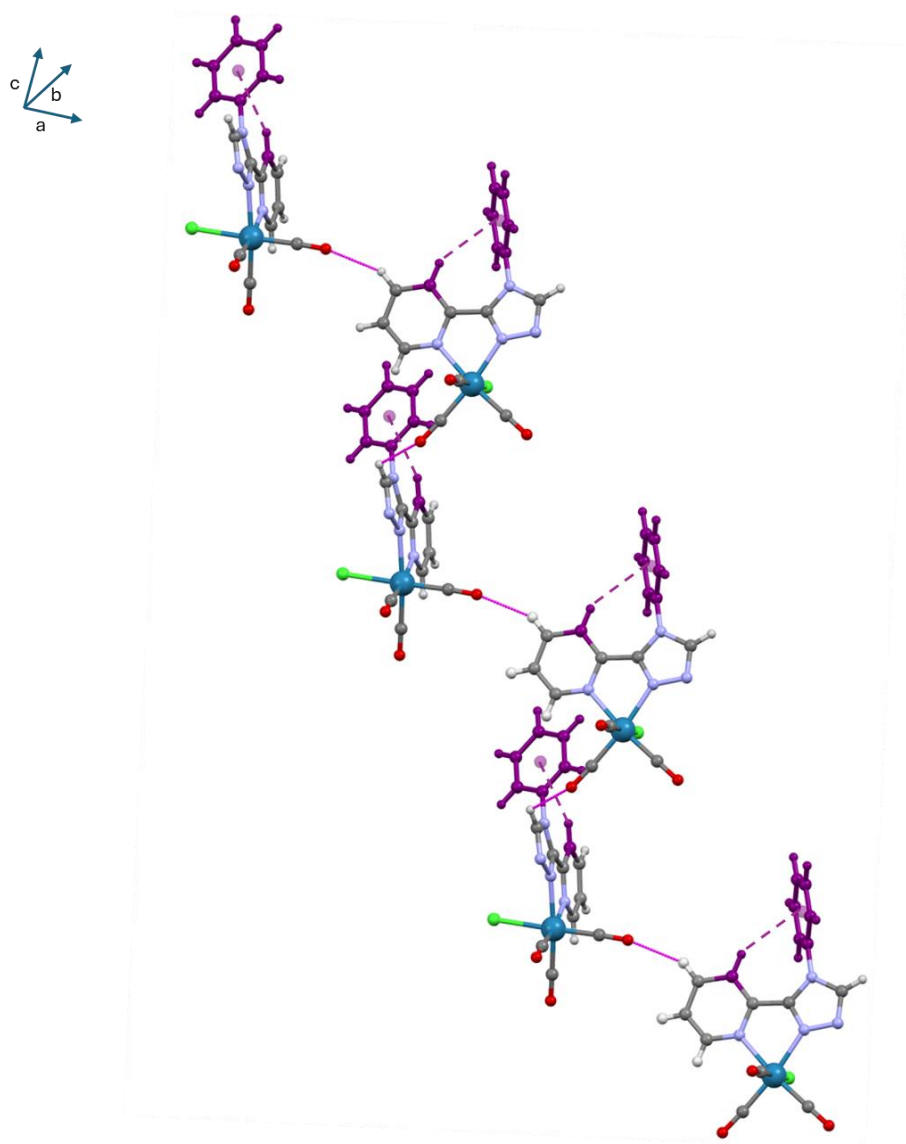


Figure S27. Neighboring molecules of **Re-Phe** with $\text{Re}1$ and $\text{Re}2$ centres connected *via* intermolecular $\text{C}22-\text{H}22(\text{py})_{\text{Re}2}\cdots\text{O}3(\text{CO})_{\text{Re}1}$ and $\text{C}10-\text{H}10(\text{trz})_{\text{Re}1}\cdots\text{O}4(\text{CO})_{\text{Re}2}$ (magenta color) interactions into a zig-zag chain viewed along the ac plane and stabilized by intramolecular $\text{C}23-\text{H}23(\text{py})\cdots\pi(\text{Ph})$ (tyrian purple color) interactions.

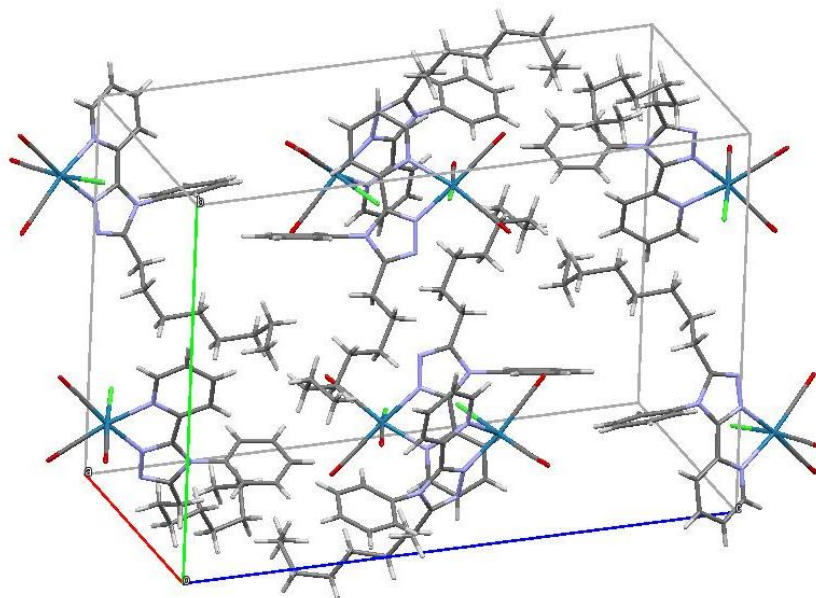


Figure S28. Crystal cell of complex **Mono-Re-Phe**.

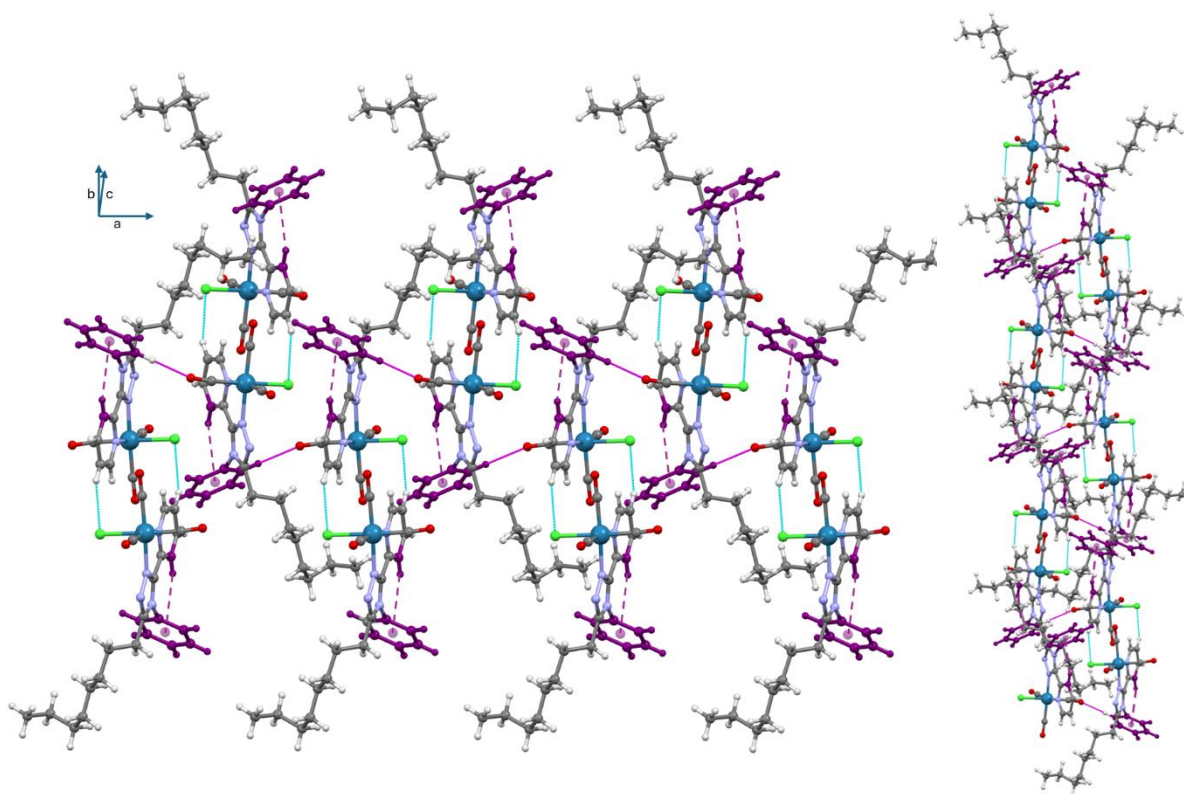


Figure S29. Centrosymmetric $R_2^2(12)$ dimers of complex **Mono-Re-Phe** formed *via* intermolecular C5–H5(trz)···C11 (cyan color) interactions of two antiparallel Re1 molecules. Dimers linked through C16–H16(Ph)···O1(CO) (magenta color) interactions are viewed along the *ab*-plane and stabilized by intramolecular C7–H7(py)··· π (Ph) (tyrian purple color) interactions.

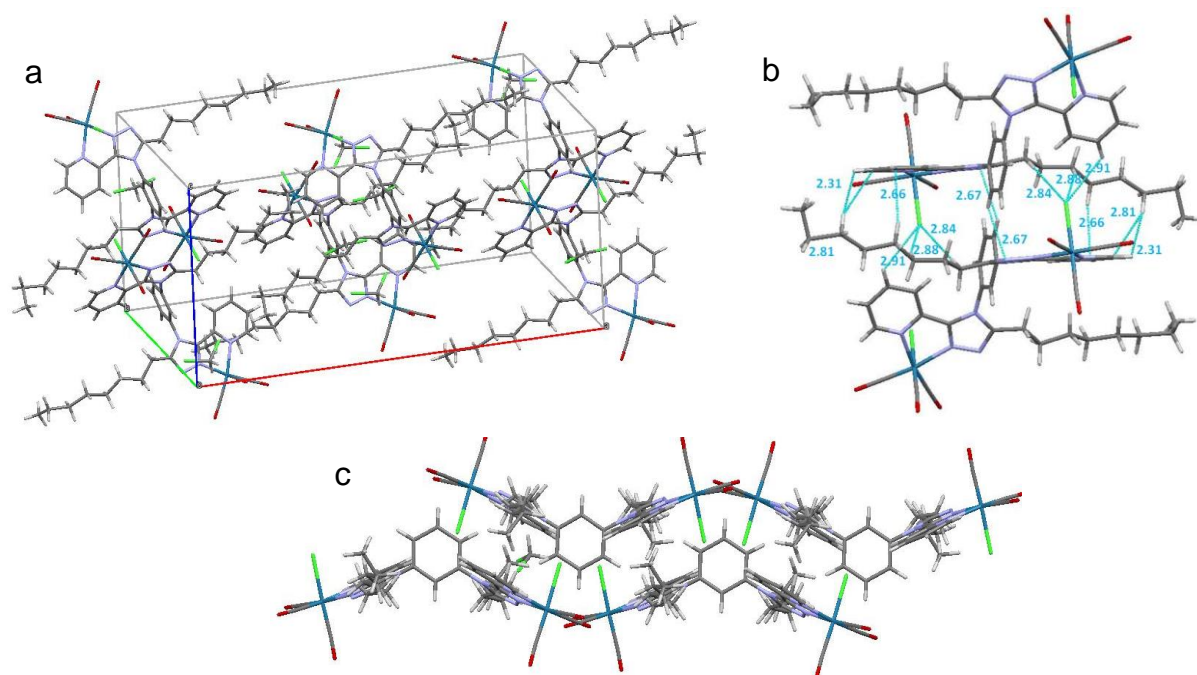


Figure S30. (a) Crystal cell of complex **Bi-Re-*meta*Phe**, (b) neighboring molecules forming dimers with short contact distances indicated in blue ink (in Å), and (c) molecular view perpendicular to the central phenyl ring.

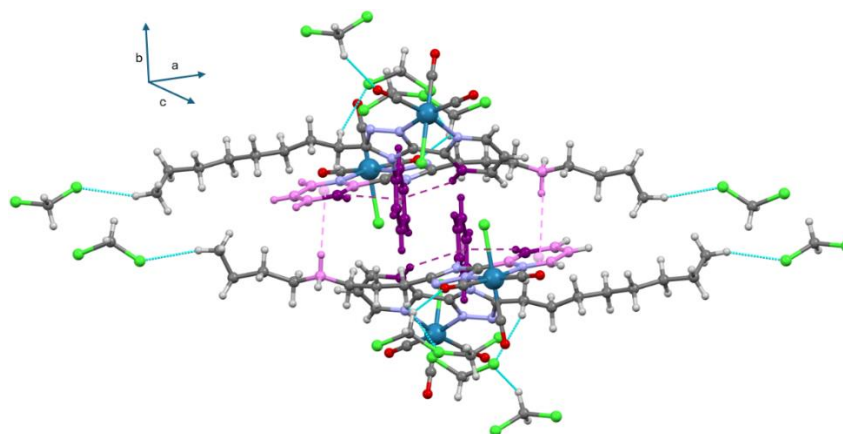


Figure S31. Intermolecular C7–H7(py)⋯ π (*m*-Xyl) (violet color) and intramolecular C18–H18A(CH₂)_{octyl}⋯ π (py) (tyrian purple color) interactions in **Bi-Re-*meta*Phe**.

Table S3. Octahedral distortion parameters of **Re-Phe**, **Mono-Re-Phe** and **Bi-Re-*meta*Phe**.

Metal complex	Octahedral distortion parameters			
	ζ , Å	Σ , °	Θ , °	Volume, Å ³
Re-Phe	1.15/1.13	63.3/66.7	169/164	11.85/11.83
Mono-Re-Phe	1.08	66.4	188	11.87
Bi-Re-<i>meta</i>Phe	1.10	59.3	157	11.97

Table S4. Experimental and DFT-optimized octahedral distortion parameters in the singlet (S_0 , ground; S_1 , excited) and triplet (T_1 , excited) states of **Re-Phe**, **Mono-Re-Phe** and **Bi-Re-meta-Phe**.

Metal Complex	Re-Phe				Mono-Re-Phe				Bi-Re-meta-Phe			
	Exp.	Calc.			Exp.	Calc.			Exp.	Calc.		
		S_0	S_1	T_1		S_0	S_1	T_1		S_0	S_1	T_1
ζ , Å	1.15/1.13	1.16	0.81	0.84	1.08	1.15	0.80	0.87	1.10	1.15	1.15/0.81	1.15/0.86
Σ , °	63.3/66.7	58.7	51.8	49.2	66.4	58.4	50.8	47.7	59.3	58.8	58.6/51.4	58.7/48.1
Θ , °	169/164	166	182	171	188	166	180	164	157	167	167/181	167/165
V , Å ³	11.9/11.8	12.1	11.9	11.9	11.87	12.06	11.88	11.91	11.97	12.06	12.06/11.89	12.06/11.91
μ , D	–	7.90	3.82	4.25	–	7.94	4.13	4.82	–	4.19	4.51	4.10

Metal Complex	Bi-Re-para-Phe		
	Calc.		
	S_0	S_1	T_1
ζ , Å	1.15	1.15 / 0.80	1.15 / 0.85
Σ , °	58.7	58.6 / 51.5	58.8 / 48.2
Θ , °	167	166 / 181	167 / 165
V , Å ³	12.1	12.1 / 11.9	12.1 / 11.9
μ , D	0.00	4.20	3.91

Octahedral distortion parameters are composed of three parameters: one bond-length distortion parameter ζ and two bond-angle distortion parameters Σ and Θ . ζ is the average of the sum of the deviation of six unique metal–ligand bond lengths around the central metal atom (d_i) from the average value (d_{mean}). Σ can be defined as the sum of the deviation of the twelve *cis* L–Re–L angles ϕ_i from 90°. Σ is a general measure of the deviation of a metal ion from an ideal octahedral geometry. Θ can be defined as the sum of the deviation of the 24 torsional angles between the ligand atoms on opposite triangular faces of the octahedron viewed along the pseudo-threefold axis (θ_i) from 60°. Θ represents the distortion of the MX_6 geometry from perfectly octahedral (O_h) to trigonal prismatic (D_{3h}). Distortion parameters ζ , Σ and Θ were calculated using the OctaDist software (R. Ketkaew, Y. Tantirungrotechai, P. Harding, G. Chastanet, P. Guionneau, M. Marchivie, D. J. Harding, *Dalton Trans.*, 2021, **50**, 1086–1096). All values lie in the expected range observed for distorted quasi-octahedral Re(I) complexes. In fact, a perfectly octahedral complex would give $\zeta = \Sigma = \Theta = 0$.

Table S5. Short contacts detected in structures of **Re-Phe**, **Mono-Re-Phe** and **Bi-Re-meta-Phe**.

D—H...A	D—H [Å]	H...A [Å]	D...A [Å]	D—H...A [°]	Symmetry codes
Re-Phe					
C10—H10...O4	0.95	2.42	2.994(11)	119	x, y, z
C10—H10...C11	0.95	2.75	3.552(10)	142' / 92' / 353	$2-x, 1-y, 1-z$
C20—H20...C11	0.95	2.72	3.492(9)	139	$2-x, 1-y, 1-z$
C22—H22...O3	0.95	2.47	3.337(12)	151	$1+x, y, -1+z$
C26—H26...C12	0.95	2.67	3.454(10)	140	$1-x, 2-y, -z$
Mono-Re-Phe					
C5—H5...C11	0.95	2.77	3.659(3)	157	$1-x, -y, 1-z$
C16—H16...O1	0.95	2.61	3.721	163	$-1/2+x, 1/2-y, 1-z$
Bi-Re-meta-Phe					
C15—H15B...C12	0.99	2.61	3.40(3)	137	$-1/2+x, 3/2-y, -1/2+z$
C22—H22A...O3	0.98	2.55	3.51(2)	164	x, y, z
C22—H22B...C13	0.98	2.72	3.64(2)	157	$1/2+x, 1/2+y, z$
C23—H23B...O2	0.99	2.44	3.25(2)	138	x, y, z

Table S6. Geometrical parameters (\AA , $^\circ$) for C–H $\cdots\pi$ interactions detected in structures of **Re-Phe**, **Mono-Re-Phe** and **Bi-Re-metaPhe**.

X—H(i) \cdots Cg(i)	H \cdots Cg [\AA]	X \cdots Cg [\AA]	X—H \cdots Cg [$^\circ$]	H-Perp	Gamma
Re-Phe					
C23—H23 \cdots Cg(8) ^{#1}	2.98	3.817(10)	148	2.57	30.42
Mono-Re-Phe					
C7—H7 \cdots Cg(4) ^{#1}	2.96	3.817(3)	150	-2.62	27.80
Bi-Re-meta-Phe					
C7—H7 \cdots Cg(4) ^{#1}	2.93	3.791(10)	151	-2.61	26.99
C7—H7 \cdots Cg(4) ^{#2}	2.93	3.791(10)	151	2.61	26.99
C18—H18A \cdots Cg(3) ^{#3}	2.91	3.86(5)	162	2.65	24.37

Cg(i) = center of gravity of ring i; X \cdots Cg = distance of X to Cg; X—H \cdots Cg = X—H—Cg angle; H—Perp = perpendicular distance of H to ring plane J; γ = angle between Cg—H vector and ring J normal.

For complex **Re-Phe**, Cg8 is the centroid of the ring (C27–C32).

For complex **Mono-Re-Phe**, Cg4 is the centroid of the ring (C11–C16).

For complex **Bi-Re-meta-Phe**, Cg3 and Cg4 are the centroids of the rings (N1/C4–C8) and (C11/C12/C13/C12_a/C11_a/C14), respectively.

Symmetry codes: #1: x, y, z; #2: 1-x, y, 1/2-z; #3: 1-x, 2-y, 1-z.

Table S7. Geometrical parameters (\AA , $^\circ$) for $\pi\cdots\pi$ interactions detected in structure of **Re-Phe**.

Cg(i) \cdots Cg(j)	Cg \cdots Cg [\AA]	α [$^\circ$]	β [$^\circ$]	γ [$^\circ$]	Cg(i)_Perp	Cg(j)_Perp	Slippage
Cg(7) \cdots Cg(7) ^{#1}	3.871(5)	0.0(4)	29.0	29.0	3.385(4)	3.385(4)	1.877

Cg(i) = plane number i; α = dihedral angle between planes i and j; β = angle Cg(i) \rightarrow Cg(j) or Cg(i) \rightarrow Me vector and normal to plane i; γ = angle Cg(i) \rightarrow Cg(j) vector and normal to plane j; Cg—Cg = distance between ring centroids; Cg(i)_Perp = perpendicular distance of Cg(i) on ring j; Cg(j)_Perp = perpendicular distance of Cg(j) on ring i; Slippage = distance between Cg(i) and perpendicular projection of Cg(j) on ring i.

Cg7 is the centroid of the ring (N5/C20–C24).

Symmetry code: #1: 2-x, 2-y, -z;

Comment S2. Hirshfeld surfaces (HS) analysis of **Re-Phe**, **Mono-Re-Phe** and **Bi-Re-metaPhe**

HS of **Re-Phe** showed a surface having an area of 360.35 \AA^2 , which is spread over volume of 414.76 \AA^3 . The surface is generated between -0.1882 a.u. (red spot) and 1.6948 a.u. (blue colour) (cf. Fig. 4a). The shape index plot is generated from -1.0000 to 1.0000 a.u. (cf. Fig. 4d). 2D Fingerprint plots (FP) of HS for **Re-Phe** with relative contributions of different interactions are shown in Fig. S32. The presence of the short contacts C—H_(trz) \cdots O_(CO), C—H_(py) \cdots O_(CO), C—H_(trz) \cdots Cl and C—H_(py) \cdots Cl and [O \cdots H/H \cdots O = 30.7%, Cl \cdots H/H \cdots Cl = 12.3%] between the neighboring molecules are detected in the 2D FP of **Re-Phe**. These interactions are viewed on the d_{norm} surface by light and bright red spots, respectively (cf. Fig. 4a). In addition, $\pi_{\text{(py)}}\cdots\pi_{\text{(py)}}$ stacking interactions [C \cdots C = 3.9%, C \cdots N/N \cdots C = 1.6%], C—H_(py) $\cdots\pi_{\text{(Ph)}}$ [C \cdots H/H \cdots C = 14.6%, N \cdots H/H \cdots N = 7.8%] and various other interactions [H \cdots H = 14.7%, C \cdots O/O \cdots C = 5.7%] stabilizing the structure of **Re-Phe** are also found in the 2D FP.

For **Mono-Re-Phe**, the HS analysis reveals that the surface covers an area of 544.58 \AA^2 and the volume is 501.67 \AA^3 . The colour scale on the HS ranges from -1.8444 a.u. (red spot) and 1.2872 a.u. (blue colour) (cf. Fig. 4b). 2D FP of Hirshfeld surface with relative contributions of different interactions are shown in Fig. S33. Weak intermolecular interactions C—H_(Ph) \cdots O_(CO) and C—H_(py) \cdots Cl [O \cdots H/H \cdots O = 17.2%, Cl \cdots H/H \cdots Cl = 4.4%], through which the adjacent molecules interact, are detected in 2D FP. **Mono-Re-Phe** is further stabilized by C—H_(py) $\cdots\pi_{\text{(Ph)}}$ [C \cdots H/H \cdots C = 13.2%, N \cdots H/H \cdots N = 1.8%] and various other interactions [H \cdots H = 51.8%, C \cdots O/O \cdots C = 1.8%].

In **Bi-Re-metaPhe**, the HS spreads over an area of 914.71 \AA^2 and volume of 944.84 \AA^3 . The colour scale on the HS ranges from -1.8116 a.u. (red spot) and 1.2967 a.u. (blue colour) (cf. Fig. 4c). 2D FP with relative contributions of different interactions are shown in Fig. S34. Weak intermolecular interactions C—H_(octyl) \cdots O_(CO), C—H_(DCM) \cdots O_(CO) and C—H_(octyl) \cdots Cl_(DCM) [O \cdots H/H \cdots O = 20.5%, Cl \cdots H/H \cdots Cl = 11.1%], which are linking the adjacent molecules, are found in 2D FP. **Bi-Re-metaPhe** is further stabilized by C—H_(py) $\cdots\pi_{\text{(m-Xyl)}}$, C—H_(octyl) $\cdots\pi_{\text{(py)}}$ [C \cdots H/H \cdots C = 12.7%, N \cdots H/H \cdots N = 6.9%] and various other interactions [H \cdots H = 40.7%, C \cdots C = 4.3%, C \cdots O/O \cdots C = 2.7%].

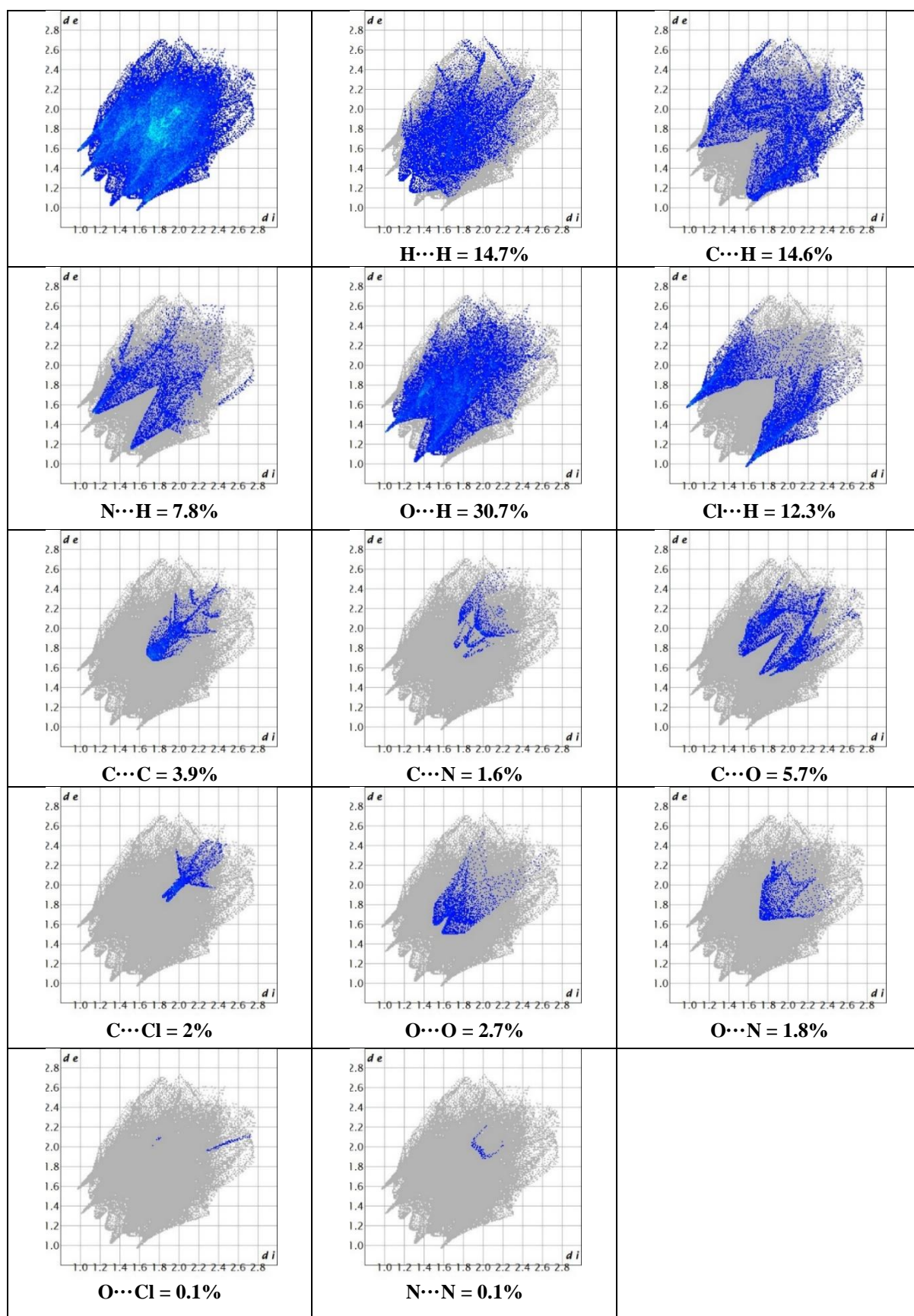


Figure S32. Two-dimensional fingerprint plots for overall interactions and individual interactions in crystal packing of **Re-Phe**.

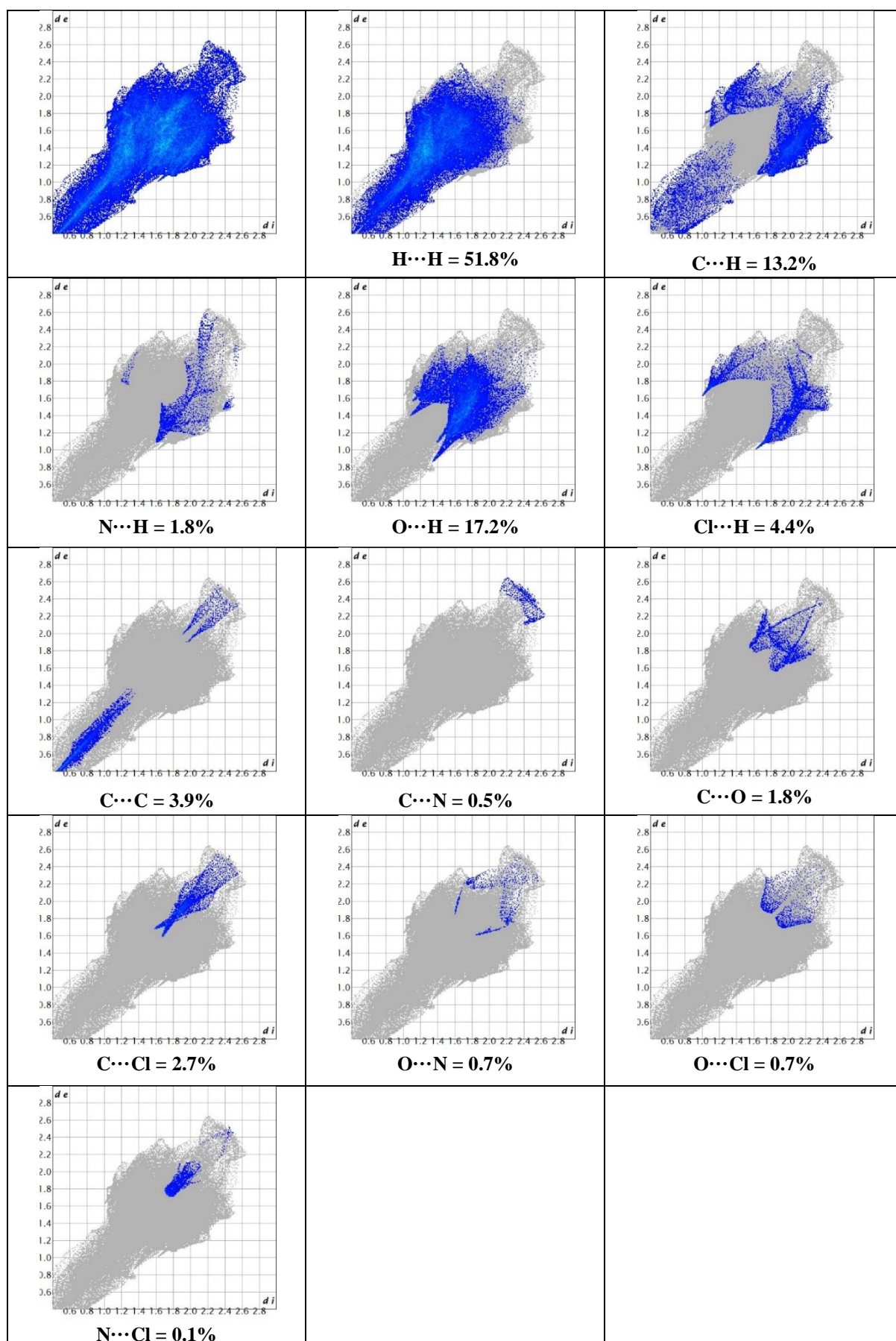


Figure S33. Two-dimensional fingerprint plots for overall interactions and individual interactions in crystal packing of **Mono-Re-Phe**.

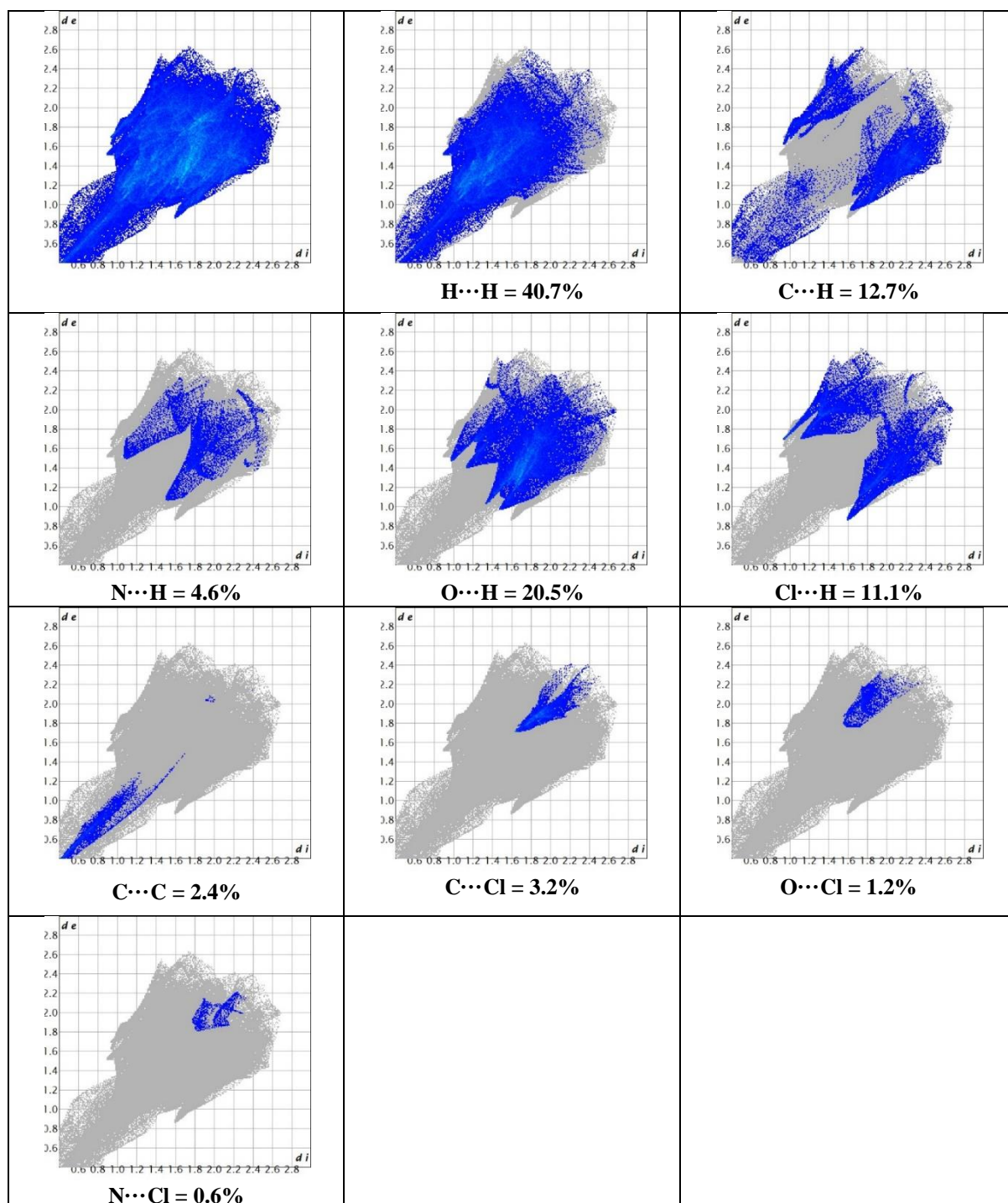


Figure S34. Two-dimensional fingerprint plots for overall interactions and individual interactions in crystal packing of *Bi-Re-metaPhe*.

Calculations

Table S8. Selected calculated bond lengths [\AA] and angles [$^\circ$] in the ground (S_0) first singlet excited (S_1) and first triplet excited (T_1) states for **Re-Phe**, together with the experimental data.

Bond lengths	Exp.	Optimized			Bond angles	Exp.	Optimized		
		S_0	S_1	T_1			S_0	S_1	T_1
Re1-C1	1.935(10)	1.915	1.956	1.984	C2-Re1-C1	90.1(4)	89.33	84.78	87.53
Re1-C2	1.902(11)	1.911	1.947	1.934	C2-Re1-C3	89.0(4)	89.84	93.01	92.64
Re1-C3	1.869(10)	1.896	1.954	1.953	C1-Re1-C3	89.5(4)	90.02	89.90	88.43
Re1-N1	2.200(7)	2.214	2.157	2.166	C2-Re1-N1	171.9(3)	171.15	174.35	172.25
Re1-N2	2.147(7)	2.152	2.105	2.054	C1-Re1-N1	97.7(3)	98.74	100.71	99.65
Re1-C11	2.474(2)	2.511	2.401	2.429	C3-Re1-N1	93.0(3)	93.77	88.38	90.51
					C2-Re1-N2	98.1(3)	97.98	98.65	96.71
C1-O1	1.140(11)	1.152	1.143	1.140	C1-Re1-N2	169.5(3)	171.65	176.55	175.53
C2-O2	1.171(11)	1.151	1.143	1.145	C3-Re1-N2	97.2(3)	94.03	90.25	92.64
C3-O3	1.182(10)	1.156	1.140	1.141	N1-Re1-N2	73.9(3)	73.72	75.85	76.20
					C2-Re1-C11	94.5(3)	92.75	92.13	91.99
					C1-Re1-C11	90.7(3)	91.71	91.01	88.03
					C3-Re1-C11	176.5(3)	176.90	174.84	174.04
					N1-Re1-C11	83.53(19)	83.43	86.46	85.37
					N2-Re1-C11	82.09(18)	83.94	88.54	93.23
					O1-C1-Re1	178.3(9)	179.48	178.45	178.61
					O2-C2-Re1	177.5(9)	178.92	179.60	179.16
					O3-C3-Re1	177.1(8)	179.51	179.29	179.31

Table S9. Selected calculated bond lengths [\AA] and angles [$^\circ$] in the ground (S_0) first singlet excited (S_1) and first triplet excited (T_1) states for complex **Mono-Re-Phe**, together with the experimental data.

Bond lengths	Exp.	Optimized			Bond angles	Exp.	Optimized		
		S_0	S_1	T_1			S_0	S_1	T_1
Re1-C1	1.904(2)	1.895	1.953	1.948	C2-Re1-C1	90.34(10)	89.84	93.03	91.99
Re1-C2	1.913(2)	1.911	1.946	1.931	C2-Re1-C3	87.92(10)	89.38	84.89	88.27
Re1-C3	1.912(2)	1.915	1.958	1.984	C1-Re1-C3	87.66(10)	90.01	89.85	88.65
Re1-N1	2.1974(17)	2.214	2.154	2.167	C2-Re1-N1	171.22(8)	171.09	174.29	172.05
Re1-N2	2.1411(16)	2.150	2.101	2.047	C1-Re1-N1	91.22(8)	93.79	88.50	91.46
Re1-Cl1	2.4747(6)	2.512	2.406	2.441	C3-Re1-N1	100.78(8)	98.75	100.63	98.97
					C2-Re1-N2	97.23(8)	97.95	98.54	96.49
C1-O1	1.149(3)	1.156	1.140	1.142	C1-Re1-N2	96.75(8)	93.95	90.10	90.01
C2-O2	1.148(3)	1.151	1.143	1.146	C3-Re1-N2	173.18(8)	171.68	176.58	175.10
C3-O3	1.154(3)	1.152	1.143	1.141	N1-Re1-N2	74.01(6)	73.70	75.95	76.35
					C2-Re1-Cl1	94.92(7)	92.68	91.99	91.74
					C1-Re1-Cl1	174.68(7)	176.98	174.97	174.67
					C3-Re1-Cl1	91.76(7)	91.69	90.95	87.67
					N1-Re1-Cl1	83.69(5)	83.49	86.47	85.32
					N2-Re1-Cl1	83.37(5)	84.05	88.81	93.35
					O1-C1-Re1	175.7(2)	179.52	179.31	179.44
					O2-C2-Re1	179.0(2)	178.89	179.64	179.09
					O3-C3-Re1	177.7(2)	179.49	178.34	178.72

Table S10. Selected calculated bond lengths [\AA] and angles [$^\circ$] in the ground (S_0) first singlet excited (S_1) and first triplet excited (T_1) states for complex **Bi-Re-metaPhe**, together with the experimental data.

Bond lengths	Exp.	Optimized			Bond angles	Exp.	Optimized		
		S_0	S_1	T_1			S_0	S_1	T_1
Re1-C1	1.923(13)	1.896	1.896	1.896	C2-Re1-C1	90.4(5)	89.83	89.84	89.83
Re1-C2	1.912(12)	1.911	1.911	1.911	C2-Re1-C3	90.0(5)	89.31	89.32	89.32
Re1-C3	1.898(10)	1.915	1.915	1.915	C1-Re1-C3	89.0(5)	89.96	89.96	89.96
Re1-N1	2.205(8)	2.214	2.214	2.214	C2-Re1-N1	170.5(4)	171.00	171.00	171.00
Re1-N2	2.154(7)	2.150	2.150	2.150	C1-Re1-N1	95.2(5)	93.89	93.89	93.89
Re1-Cl1	2.472(3)	2.511	2.511	2.511	C3-Re1-N1	97.8(4)	98.87	98.85	98.86
					C2-Re1-N2	97.7(4)	97.93	97.93	97.93
C1-O1	1.089(15)	1.156	1.156	1.156	C1-Re1-N2	94.4(4)	93.83	93.78	93.80
C2-O2	1.134(14)	1.151	1.151	1.151	C3-Re1-N2	171.6(4)	171.82	171.84	171.83
C3-O3	1.163(13)	1.152	1.152	1.152	N1-Re1-N2	74.2(3)	73.66	73.68	73.68
					C2-Re1-Cl1	91.0(3)	92.74	92.73	92.73
					C1-Re1-Cl1	177.8(4)	176.91	176.92	176.93
					C3-Re1-Cl1	92.7(4)	91.79	91.76	91.76
					N1-Re1-Cl1	83.2(2)	83.32	83.33	83.33
					N2-Re1-Cl1	83.8(2)	84.11	84.19	84.17
					O1-C1-Re1	176.4(13)	179.55	179.54	179.54
					O2-C2-Re1	177.2(10)	178.86	178.87	178.87
					O3-C3-Re1	178.9(13)	179.55	179.55	179.54

Table S11. Selected calculated bond lengths [\AA] and angles [$^\circ$] in the ground (S_0) first singlet excited (S_1) and first triplet excited (T_1) states for complex **Bi-Re-*para*Phe**.

Bond lengths	Optimized			Bond angles	Optimized		
	S_0	S_1	T_1		S_0	S_1	T_1
Re1-C37	1.896	1.896	1.896	C38-Re1-C37	89.83	89.83	89.82
Re1-C38	1.911	1.911	1.911	C38-Re1-C39	89.34	89.34	89.33
Re1-C39	1.915	1.915	1.915	C37-Re1-C39	90.03	90.02	90.01
Re1-N1	2.214	2.214	2.214	C38-Re1-N1	171.05	171.06	171.06
Re1-N2	2.150	2.150	2.150	C37-Re1-N1	93.75	93.75	93.73
Re1-Cl1	2.512	2.512	2.512	C39-Re1-N1	98.85	98.84	98.86
				C38-Re1-N2	97.92	97.92	97.91
C37-O37	1.156	1.156	1.156	C37-Re1-N2	94.06	94.05	93.99
C38-O38	1.151	1.151	1.151	C39-Re1-N2	171.67	171.67	171.73
C39-O39	1.152	1.152	1.152	N1-Re1-N2	73.66	73.67	73.68
				C38-Re1-Cl1	92.69	92.69	92.77
				C37-Re1-Cl1	176.96	176.97	176.89
				C39-Re1-Cl1	91.69	91.67	91.74
				N1-Re1-Cl1	83.51	83.51	83.46
				N2-Re1-Cl1	83.93	83.96	83.95
				O37-C37-Re1	179.54	179.53	179.55
				O38-C38-Re1	178.85	178.86	178.87
				O39-C39-Re1	179.52	179.53	179.54

Table S12. Torsion angle value between pyta and R calculated using the density functional theory (DFT) method at the PBE1PBE/LANL2DZ level for the ground state (S_0), first singlet excited (S_1) and first triplet excited state (T_1) of **Re-Phe**, **Mono-Re-Phe**, **Bi-Re-metaPhe** and **Bi-Re-paraPhe**, and obtained from crystallographic data.

Complex	Bond angle [°]	SXRD	S_0	S_1	T_1
Re-Phe	C(9)–N(4)–C(11)–C(12)	-70.19	-86.492	-67.652	-60.178
Mono-Re-Phe		-94.96	-92.478	-93.866	-93.472
Bi-Re-metaPhe		-99.09	-91.332	-89.813	-90.661
Bi-Re-paraPhe		–	-93.631	-95.975	-92.532

Table S13. The frontier molecular orbital compositions (%) and energy levels for **Re-Phe** (in dichloromethane).

Orbital		Energy (eV)	MO Contribution (%)					Main bond type
			Re	CO	Cl	pyta	R	
96	L+5	-0.63	38	56	-2	1	8	p(Re)+ π^* (CO)
95	L+4	-0.76	31	65	0	6	0	p(Re)+ π^* (CO)
94	L+3	-1.01	0	1	0	13	87	π^* (R)
93	L+2	-1.15	0	1	0	3	96	π^* (R)
92	L+1	-1.65	0	1	0	94	5	π^* (pyta)
91	L	-2.51	2	4	0	92	2	π^* (pyta)
HOMO–LUMO gap (E = 4.01 eV)								
90	H	-6.52	50	25	21	4	0	d(Re)+ π (CO)/ π (Cl)
89	H-1	-6.63	49	23	23	5	0	d(Re)+ π (CO)/ π (Cl)
88	H-2	-7.11	67	31	1	1	0	d(Re)+ π (CO)
87	H-3	-7.79	2	1	32	66	0	π (pyta)/ π (Cl)
86	H-4	-8.07	1	0	5	6	88	π (R)
85	H-5	-8.09	2	1	8	11	78	π (R)
84	H-6	-8.10	13	4	58	11	14	π (Cl)/d(Re)
83	H-7	-8.26	12	4	39	34	11	π (Cl)/ π (pyta)/d(Re)
82	H-8	-8.78	7	15	72	6	0	π (Cl)/ π (CO)
81	H-9	-9.33	0	4	0	89	7	π (pyta)
80	H-10	-9.46	4	2	4	88	2	π (pyta)

R = -C₆H₅

Table S14. The frontier molecular orbital compositions (%) and energy levels for **Mono-Re-Phe** (in dichloromethane).

Orbital		Energy (eV)	MO Contribution (%)					Main bond type	
			Re	CO	Cl	pyta	R _a		
128	L+5	-0.58	41	57	-2	0	4	1	p(Re)+ π^* (CO)
127	L+4	-0.73	33	64	0	7	-1	0	p(Re)+ π^* (CO)
126	L+3	-0.95	0	0	0	6	94	0	π^* (R _a)
125	L+2	-1.14	0	1	0	6	96	-2	π^* (R _a)
124	L+1	-1.59	0	1	0	95	4	0	π^* (pyta)
123	L	-2.45	2	5	0	90	2	0	π^* (pyta)
HOMO–LUMO gap (E = 4.03 eV)									
122	H	-6.48	49	25	19	6	0	0	d(Re)+ π (CO)/ π (Cl)
121	H-1	-6.60	49	23	23	5	0	0	d(Re)+ π (CO)/ π (Cl)
120	H-2	-7.07	68	31	1	0	0	0	d(Re)+ π (CO)
119	H-3	-7.60	0	0	24	71	0	4	π (pyta)/ π (Cl)
118	H-4	-8.03	2	1	7	9	81	0	π (R _a)
117	H-5	-8.06	1	0	4	7	88	0	π (R _a)
116	H-6	-8.07	13	4	62	12	9	0	π (Cl)/d(Re)
115	H-7	-8.20	12	4	44	28	12	0	π (Cl)/ π (pyta)/d(Re)
114	H-8	-8.62	0	0	0	3	0	97	σ (R _b)
113	H-9	-8.75	7	15	69	6	0	4	π (Cl)/ π (CO)/d(Re)
112	H-10	-8.78	0	1	3	1	0	96	σ (R _b)

R_a = -C₆H₅; R_b = octyl chain

Table S15. The frontier molecular orbital compositions (%) and energy levels for **Bi-Re-*meta*Phe** (in dichloromethane).

Orbital		Energy (eV)	MO Contribution (%)						Main bond type
			Re	CO	Cl	pyta	R _a	R _b	
233	L+9	-0.64	39	58	-1	3	3	0	p(Re)+π*(CO)
232	L+8	-0.64	41	57	-2	1	4	0	p(Re)+π*(CO)
231	L+7	-0.79	34	64	0	6	0	-1	p(Re)+π*(CO)
230	L+6	-0.80	33	63	0	8	-3	1	p(Re)+π*(CO)
229	L+5	-1.52	0	1	0	50	48	0	π*(pyta)/π*(R _a)
228	L+4	-1.62	0	1	0	71	28	0	π*(pyta)/π*(R _a)
227	L+3	-1.79	0	0	0	52	50	-1	π*(pyta)/π*(R _a)
226	L+2	-1.84	0	0	0	34	66	0	π*(pyta)/π*(R _a)
225	L+1	-2.56	2	5	0	90	3	0	π*(pyta)
224	L	-2.58	2	4	0	91	1	1	π*(pyta)
HOMO–LUMO gap (E = 3.96 eV)									
223	H	-6.54	49	25	20	7	0	0	d(Re)+π(CO)/π(Cl)
222	H-1	-6.55	50	25	20	6	0	0	d(Re)+π(CO)/π(Cl)
221	H-2	-6.66	49	23	23	7	-2	0	d(Re)+π(CO)/π(Cl)
220	H-3	-6.66	49	23	23	5	0	0	d(Re)+π(CO)/π(Cl)
219	H-4	-7.14	68	31	1	1	0	0	d(Re)+π(CO)
218	H-5	-7.14	67	31	1	1	0	0	d(Re)+π(CO)
217	H-6	-7.72	0	0	27	69	0	4	π(pyta)/π(Cl)
216	H-7	-7.73	1	0	27	69	0	3	π(pyta)/π(Cl)
215	H-8	-8.13	14	5	68	13	0	0	π(Cl)/d(Re)
214	H-9	-8.13	14	5	68	13	0	0	π(Cl)/d(Re)
213	H-10	-8.26	14	5	44	34	2	1	π(Cl)/π(pyta)/d(Re)
212	H-11	-8.26	14	5	46	35	0	1	π(Cl)/π(pyta)/d(Re)
211	H-12	-8.57	1	1	3	28	63	5	π(R _a)/π(pyta)
210	H-13	-8.61	0	0	0	14	84	1	π(R _a)/π(pyta)
209	H-14	-8.75	0	0	0	1	2	97	σ(R _b)
208	H-15	-8.75	0	0	0	1	2	96	σ(R _b)

R_a = -C₆H₄- (*m*-); R_b = octyl chain

Table S16. The frontier molecular orbital compositions (%) and energy levels for **Bi-Re-*para*Phe** (in dichloromethane).

Orbital		Energy (eV)	MO Contribution (%)						Main bond type
			Re	CO	Cl	pyta	R _a	R _b	
233	L+9	-0.64	39	58	-2	4	1	0	p(Re)+π*(CO)
232	L+8	-0.64	40	57	-1	2	3	0	p(Re)+π*(CO)
231	L+7	-0.79	33	64	0	4	0	0	p(Re)+π*(CO)
230	L+6	-0.80	33	63	0	9	-5	1	p(Re)+π*(CO)
229	L+5	-1.44	0	1	0	36	63	0	π*(R _a)/π*(pyta)
228	L+4	-1.66	0	1	0	98	0	0	π*(pyta)
227	L+3	-1.78	0	0	0	62	37	0	π*(pyta)/π*(R _a)
226	L+2	-1.88	0	0	0	12	87	1	π*(R _a)
225	L+1	-2.56	2	4	0	92	1	0	π*(pyta)
224	L	-2.57	2	4	0	89	3	1	π*(pyta)
HOMO–LUMO gap (E = 3.98 eV)									
223	H	-6.55	50	25	20	6	0	0	d(Re)+π(CO)/π(Cl)
222	H-1	-6.55	50	25	20	6	0	0	d(Re)+π(CO)/π(Cl)
221	H-2	-6.66	49	23	23	7	-1	0	d(Re)+π(CO)/π(Cl)
220	H-3	-6.66	49	23	23	6	0	0	d(Re)+π(CO)/π(Cl)
219	H-4	-7.14	67	31	1	1	0	0	d(Re)+π(CO)
218	H-5	-7.14	68	31	1	1	0	0	d(Re)+π(CO)

217	H-6	-7.72	0	0	27	69	0	4	$\pi(\text{pyta})/\pi(\text{Cl})$
216	H-7	-7.72	0	0	27	69	0	3	$\pi(\text{pyta})/\pi(\text{Cl})$
215	H-8	-8.13	14	5	68	13	0	0	$\pi(\text{Cl})/\text{d}(\text{Re})$
214	H-9	-8.13	14	5	68	13	0	0	$\pi(\text{Cl})/\text{d}(\text{Re})$
213	H-10	-8.25	13	5	43	35	4	0	$\pi(\text{Cl})/\pi(\text{pyta})/\text{d}(\text{Re})$
212	H-11	-8.26	14	5	46	35	0	0	$\pi(\text{Cl})/\pi(\text{pyta})/\text{d}(\text{Re})$
211	H-12	-8.56	1	1	3	33	59	3	$\pi(\text{R}_a)/\pi(\text{pyta})$
210	H-13	-8.65	0	0	1	3	95	1	$\pi(\text{R}_a)$
209	H-14	-8.74	0	0	0	1	0	99	$\sigma(\text{R}_b)$
208	H-15	-8.75	0	0	0	2	2	96	$\sigma(\text{R}_b)$

$\text{R}_a = -\text{C}_6\text{H}_4-$ (*p*-); $\text{R}_b =$ octyl chain

Table S17. The main electronic transitions for **Re-Phe**, calculated with TDDFT method at the PBE1PBE/LANL2DZ level (in dichloromethane).

Electronic transition	Contribution	Assignment		E_{calc} /eV	λ_{calc} /nm	f	λ_{exp} /nm
$\text{S}_0 \rightarrow \text{S}_1$	H→L	$\text{d}(\text{Re})+\pi(\text{CO})/\pi(\text{Cl}) \rightarrow \pi^*(\text{pyta})$	MLCT/LLCT	3.01	412.0	0.0009	
$\text{S}_0 \rightarrow \text{S}_2$	H-1→L	$\text{d}(\text{Re})+\pi(\text{CO})/\pi(\text{Cl}) \rightarrow \pi^*(\text{pyta})$	MLCT/LLCT	3.21	386.5	0.1099	
$\text{S}_0 \rightarrow \text{S}_3$	H-2→L	$\text{d}(\text{Re})+\pi(\text{CO}) \rightarrow \pi^*(\text{pyta})$	MLCT/LLCT	3.55	348.9	0.0006	
$\text{S}_0 \rightarrow \text{S}_8$	H-3→L	$\pi(\text{pyta})/\pi(\text{Cl}) \rightarrow \pi^*(\text{pyta})$	ILCT/LLCT	4.41	281.5	0.1451	
$\text{S}_0 \rightarrow \text{S}_{12}$	H-5→L	$\pi(\text{R}) \rightarrow \pi^*(\text{pyta})$	ILCT	4.72	262.6	0.0577	
$\text{S}_0 \rightarrow \text{S}_{16}$	H-7→L	$\pi(\text{Cl})/\pi(\text{pyta})/\text{d}(\text{Re}) \rightarrow \pi^*(\text{pyta})$	LLCT/ILCT	4.86	255.2	0.0915	
$\text{S}_0 \rightarrow \text{S}_{21}$	H-2→L+4	$\text{d}(\text{Re})+\pi(\text{CO}) \rightarrow \text{p}(\text{Re})+\pi^*(\text{CO})$	MLCT/LLCT	5.10	243.2	0.0637	
	H-1→L+3	$\text{d}(\text{Re})+\pi(\text{CO})/\pi(\text{Cl}) \rightarrow \pi^*(\text{R})$	MLCT/LLCT				
$\text{S}_0 \rightarrow \text{S}_{22}$	H-3→L+1	$\pi(\text{pyta})/\pi(\text{Cl}) \rightarrow \pi^*(\text{pyta})$	LLCT	5.30	234.1	0.1168	
$\text{S}_0 \rightarrow \text{S}_{30}$	H-6→L+1	$\pi(\text{Cl})/\text{d}(\text{Re}) \rightarrow \pi^*(\text{pyta})$	LLCT	5.57	222.5	0.0776	
$\text{S}_0 \rightarrow \text{S}_{36}$	H-5→L+1	$\pi(\text{R}) \rightarrow \pi^*(\text{pyta})$	ILCT	5.74	216.0	0.0453	
$\text{S}_0 \rightarrow \text{S}_{50}$	H-10→L	$\pi(\text{pyta}) \rightarrow \pi^*(\text{pyta})$	ILCT	6.15	201.5	0.0855	
	H-11→L	$\pi(\text{pyta}) \rightarrow \pi^*(\text{pyta})$	ILCT				

MLCT: metal-to-ligand charge transfer; LMCT: ligand-to-metal charge transfer; LLCT: ligand-to-ligand charge transfer; ILCT: intraligand charge transfer.

Table S18. The main electronic transitions for **Mono-Re-Phe**, calculated with TDDFT method at the PBE1PBE/LANL2DZ level and experimental (in dichloromethane).

Electronic transition	Contribution	Assignment		E_{calc} /eV	λ_{calc} /nm	f	λ_{exp} /nm
$\text{S}_0 \rightarrow \text{S}_1$	H→L	$\text{d}(\text{Re})+\pi(\text{CO})/\pi(\text{Cl}) \rightarrow \pi^*(\text{pyta})$	MLCT/LLCT	3.04	408.3	0.0017	
$\text{S}_0 \rightarrow \text{S}_2$	H-1→L	$\text{d}(\text{Re})+\pi(\text{CO})/\pi(\text{Cl}) \rightarrow \pi^*(\text{pyta})$	MLCT/LLCT	3.24	382.8	0.1088	379
$\text{S}_0 \rightarrow \text{S}_3$	H-2→L	$\text{d}(\text{Re})+\pi(\text{CO}) \rightarrow \pi^*(\text{pyta})$	MLCT/LLCT	3.58	346.1	0.0009	
$\text{S}_0 \rightarrow \text{S}_6$	H-3→L	$\pi(\text{pyta})/\pi(\text{Cl}) \rightarrow \pi^*(\text{pyta})$	ILCT/LLCT	4.32	287.3	0.1891	287
$\text{S}_0 \rightarrow \text{S}_{11}$	H-6→L	$\pi(\text{Cl})/\text{d}(\text{Re}) \rightarrow \pi^*(\text{pyta})$	LLCT	4.64	267.0	0.0398	
$\text{S}_0 \rightarrow \text{S}_{12}$	H-4→L	$\pi(\text{R}_a) \rightarrow \pi^*(\text{pyta})$	ILCT	4.73	261.9	0.0650	
$\text{S}_0 \rightarrow \text{S}_{15}$	H-7→L	$\pi(\text{Cl})/\pi(\text{pyta})/\text{d}(\text{Re}) \rightarrow \pi^*(\text{pyta})$	LLCT/ILCT	4.82	257.2	0.0730	
	H-5→L	$\pi(\text{R}_a) \rightarrow \pi^*(\text{pyta})$	ILCT				
$\text{S}_0 \rightarrow \text{S}_{22}$	H-3→L+1	$\pi(\text{pyta})/\pi(\text{Cl}) \rightarrow \pi^*(\text{pyta})$	ILCT/LLCT	5.20	238.7	0.1576	232
$\text{S}_0 \rightarrow \text{S}_{30}$	H-6→L+1	$\pi(\text{Cl})/\text{d}(\text{Re}) \rightarrow \pi^*(\text{pyta})$	LLCT	5.57	222.6	0.0520	
$\text{S}_0 \rightarrow \text{S}_{41}$	H-2→L+8	$\text{d}(\text{Re})+\pi(\text{CO}) \rightarrow \pi^*(\text{CO})/\pi^*(\text{pyta})$	MLCT/LLCT	5.88	211.0	0.0743	
$\text{S}_0 \rightarrow \text{S}_{52}$	H-19→L	$\pi(\text{pyta})/\pi(\text{R}_b) \rightarrow \pi^*(\text{pyta})$	ILCT	6.10	203.1	0.0405	
	H-20→L	$\pi(\text{pyta})/\pi(\text{R}_b) \rightarrow \pi^*(\text{pyta})$	ILCT				

MLCT: metal-to-ligand charge transfer; LMCT: ligand-to-metal charge transfer; LLCT: ligand-to-ligand charge transfer; ILCT: intraligand charge transfer

Table S19. The main electronic transitions for **Bi-Re-*meta*Phe** calculated with TDDFT method at the PBE1PBE/LANL2DZ level and experimental (in dichloromethane).

Electronic transition	Contribution	Assignment		E_{calc} /eV	λ_{calc} /nm	f	λ_{exp} /nm
$S_0 \rightarrow S_1$	H→L	$d(\text{Re})+\pi(\text{CO})/\pi(\text{Cl}) \rightarrow \pi^*(\text{pyta})$	MLCT/LLCT	2.98	416.0	0.0028	
	H-1→L+1	$d(\text{Re})+\pi(\text{CO})/\pi(\text{Cl}) \rightarrow \pi^*(\text{pyta})$	MLCT/LLCT				
$S_0 \rightarrow S_2$	H-1→L	$d(\text{Re})+\pi(\text{CO})/\pi(\text{Cl}) \rightarrow \pi^*(\text{pyta})$	MLCT/LLCT	2.98	415.9	0.0003	
	H→L+1	$d(\text{Re})+\pi(\text{CO})/\pi(\text{Cl}) \rightarrow \pi^*(\text{pyta})$	MLCT/LLCT				
$S_0 \rightarrow S_3$	H-3→L+1	$d(\text{Re})+\pi(\text{CO})/\pi(\text{Cl}) \rightarrow \pi^*(\text{pyta})$	MLCT/LLCT	3.18	389.6	0.1809	394
	H-2→L	$d(\text{Re})+\pi(\text{CO})/\pi(\text{Cl}) \rightarrow \pi^*(\text{pyta})$	MLCT/LLCT				
$S_0 \rightarrow S_4$	H-3→L	$d(\text{Re})+\pi(\text{CO})/\pi(\text{Cl}) \rightarrow \pi^*(\text{pyta})$	MLCT/LLCT	3.19	389.0	0.0455	
	H-2→L+1	$d(\text{Re})+\pi(\text{CO})/\pi(\text{Cl}) \rightarrow \pi^*(\text{pyta})$	MLCT/LLCT				
$S_0 \rightarrow S_{20}$	H-7→L	$\pi(\text{pyta})/\pi(\text{Cl}) \rightarrow \pi^*(\text{pyta})$	ILCT/LLCT	4.31	287.8	0.2731	289
	H-6→L+1	$\pi(\text{pyta})/\pi(\text{Cl}) \rightarrow \pi^*(\text{pyta})$	ILCT/LLCT				
$S_0 \rightarrow S_{22}$	H-2→L+2	$d(\text{Re})+\pi(\text{CO})/\pi(\text{Cl}) \rightarrow \pi^*(\text{pyta})/\pi^*(\text{R}_a)$	MLCT/LLCT	4.33	286.5	0.0566	
	H-2→L+2	$d(\text{Re})+\pi(\text{CO})/\pi(\text{Cl}) \rightarrow \pi^*(\text{pyta})/\pi^*(\text{R}_a)$	MLCT/LLCT				
$S_0 \rightarrow S_{37}$	H-8→L	$\pi(\text{Cl})/d(\text{Re}) \rightarrow \pi^*(\text{pyta})$	LLCT	4.59	269.9	0.0791	
	H-9→L+1	$\pi(\text{Cl})/d(\text{Re}) \rightarrow \pi^*(\text{pyta})$	LLCT				
$S_0 \rightarrow S_{43}$	H-11→L	$\pi(\text{Cl})/\pi(\text{pyta})/d(\text{Re}) \rightarrow \pi^*(\text{pyta})$	LLCT/ILCT	4.78	259.7	0.3733	
	H-10→L+1	$\pi(\text{Cl})/\pi(\text{pyta})/d(\text{Re}) \rightarrow \pi^*(\text{pyta})$	LLCT/ILCT				
$S_0 \rightarrow S_{54}$	H-4→L+6	$d(\text{Re})+\pi(\text{CO}) \rightarrow p(\text{Re})+\pi^*(\text{CO})$	MLCT/ILCT	5.08	244.0	0.0633	
	H-5→L+7	$d(\text{Re})+\pi(\text{CO}) \rightarrow p(\text{Re})+\pi^*(\text{CO})$	MLCT/ILCT				
$S_0 \rightarrow S_{58}$	H-7→L+2	$\pi(\text{pyta})/\pi(\text{Cl}) \rightarrow \pi^*(\text{pyta})/\pi^*(\text{R}_a)$	ILCT/LLCT	5.14	241.1	0.1848	236
$S_0 \rightarrow S_{61}$	H-6→L+3	$\pi(\text{pyta})/\pi(\text{Cl}) \rightarrow \pi^*(\text{pyta})/\pi^*(\text{R}_a)$	ILCT/LLCT	5.21	238.2	0.0500	
$S_0 \rightarrow S_{69}$	H-16→L	$\pi(\text{Cl})/\pi(\text{pyta}) \rightarrow \pi^*(\text{pyta})$	LLCT/ILCT	5.36	231.4	0.0467	
$S_0 \rightarrow S_{81}$	H-9→L+3	$\pi(\text{Cl})/d(\text{Re}) \rightarrow \pi^*(\text{pyta})/\pi^*(\text{R}_a)$	LLCT	5.53	224.2	0.1371	
	H-8→L+2	$\pi(\text{Cl})/d(\text{Re}) \rightarrow \pi^*(\text{pyta})/\pi^*(\text{R}_a)$	LLCT				
$S_0 \rightarrow S_{96}$	H→L+10	$d(\text{Re})+\pi(\text{CO})/\pi(\text{Cl}) \rightarrow \pi^*(\text{pyta})/\pi^*(\text{R}_b)$	MLCT/LLCT	5.72	216.8	0.0421	
$S_0 \rightarrow S_{100}$	H-2→L+26	$d(\text{Re})+\pi(\text{CO})/\pi(\text{Cl}) \rightarrow p(\text{Re})/\pi^*(\text{pyta})/\pi^*(\text{R}_b)$	MLCT/LLCT	5.74	216.0	0.0674	
	H-2→L+31	$d(\text{Re})+\pi(\text{CO})/\pi(\text{Cl}) \rightarrow p(\text{Re})/\pi^*(\text{pyta})/\pi^*(\text{R}_b)$	MLCT/LLCT				
$S_0 \rightarrow S_{147}$	H-1→L+12	$d(\text{Re})+\pi(\text{CO})/\pi(\text{Cl}) \rightarrow \pi^*(\text{pyta})/\pi^*(\text{R}_b)$	MLCT/LLCT	6.11	202.9	0.0591	
	H→L+11	$d(\text{Re})+\pi(\text{CO})/\pi(\text{Cl}) \rightarrow \pi^*(\text{pyta})/\pi^*(\text{R}_b)$	MLCT/LLCT				
$S_0 \rightarrow S_{150}$	H-20→L+1	$\pi(\text{R}_b) \rightarrow \pi^*(\text{pyta})$	ILCT	6.13	202.2	0.0783	

MLCT: metal-to-ligand charge transfer; LMCT: ligand-to-metal charge transfer; LLCT: ligand-to-ligand charge transfer; ILCT: intraligand charge transfer.

Table S20. The main electronic transitions for **Bi-Re-*para*Phe** calculated with TDDFT method at the PBE1PBE/LANL2DZ level (in dichloromethane).

Electronic transition	Contribution	Assignment		E_{calc} /eV	λ_{calc} /nm	f	λ_{exp} /nm
$S_0 \rightarrow S_1$	H-1→L	$d(\text{Re})+\pi(\text{CO})/\pi(\text{Cl}) \rightarrow \pi^*(\text{pyta})$	MLCT/LLCT	2.99	414.9	0.0027	
	H→L+1	$d(\text{Re})+\pi(\text{CO})/\pi(\text{Cl}) \rightarrow \pi^*(\text{pyta})$	MLCT/LLCT				
$S_0 \rightarrow S_3$	H-3→L	$d(\text{Re})+\pi(\text{CO})/\pi(\text{Cl}) \rightarrow \pi^*(\text{pyta})$	MLCT/LLCT	3.19	388.7	0.2357	391
	H-2→L+1	$d(\text{Re})+\pi(\text{CO})/\pi(\text{Cl}) \rightarrow \pi^*(\text{pyta})$	MLCT/LLCT				
$S_0 \rightarrow S_{22}$	H-7→L+1	$\pi(\text{pyta})/\pi(\text{Cl}) \rightarrow \pi^*(\text{pyta})$	LLCT/ILCT	4.31	287.5	0.3775	289
	H-6→L	$\pi(\text{pyta})/\pi(\text{Cl}) \rightarrow \pi^*(\text{pyta})$	LLCT/ILCT				
$S_0 \rightarrow S_{35}$	H-9→L	$\pi(\text{Cl})/d(\text{Re}) \rightarrow \pi^*(\text{pyta})$	LLCT	4.60	269.6	0.0971	
	H-8→L+1	$\pi(\text{Cl})/d(\text{Re}) \rightarrow \pi^*(\text{pyta})$	LLCT				
$S_0 \rightarrow S_{45}$	H-11→L+1	$\pi(\text{Cl})/\pi(\text{pyta})/d(\text{Re}) \rightarrow \pi^*(\text{pyta})$	LLCT/ILCT	4.78	259.5	0.3732	
	H-10→L	$\pi(\text{Cl})/\pi(\text{pyta})/d(\text{Re}) \rightarrow \pi^*(\text{pyta})$	LLCT/ILCT				
$S_0 \rightarrow S_{47}$	H-3→L+8	$d(\text{Re})+\pi(\text{CO})/\pi(\text{Cl}) \rightarrow p(\text{Re})+\pi^*(\text{CO})$	MLCT/ILCT/LLCT	4.80	258.4	0.0732	
	H-2→L+9	$d(\text{Re})+\pi(\text{CO})/\pi(\text{Cl}) \rightarrow p(\text{Re})+\pi^*(\text{CO})$	MLCT/ILCT/LLCT				
$S_0 \rightarrow S_{55}$	H-5→L+6	$d(\text{Re})+\pi(\text{CO}) \rightarrow p(\text{Re})+\pi^*(\text{CO})$	MLCT/ILCT	5.08	244.0	0.0655	
	H-4→L+7	$d(\text{Re})+\pi(\text{CO}) \rightarrow p(\text{Re})+\pi^*(\text{CO})$	MLCT/ILCT				

$S_0 \rightarrow S_{60}$	H-7→L+4	$\pi(\text{pyta})/\pi(\text{Cl}) \rightarrow \pi^*(\text{pyta})$	ILCT/LLCT	5.18	239.4	0.2658	236
	H-3→L+3	$d(\text{Re})+\pi(\text{CO})/\pi(\text{Cl}) \rightarrow \pi^*(\text{pyta})/\pi^*(\text{R}_a)$	MLCT/LLCT				
$S_0 \rightarrow S_{68}$	H-17→L	$\pi(\text{Cl}) \rightarrow \pi^*(\text{pyta})$	LLCT	5.38	230.4	0.0522	
	H-16→L+1	$\pi(\text{Cl}) \rightarrow \pi^*(\text{pyta})$	LLCT				
$S_0 \rightarrow S_{75}$	H-6→L+5	$\pi(\text{pyta})/\pi(\text{Cl}) \rightarrow \pi^*(\text{R}_a)/\pi^*(\text{pyta})$	ILCT/LLCT	5.44	228.0	0.0504	
	H-7→L+4	$\pi(\text{pyta})/\pi(\text{Cl}) \rightarrow \pi^*(\text{pyta})$	ILCT/LLCT				
$S_0 \rightarrow S_{81}$	H-9→L+3	$\pi(\text{Cl})/d(\text{Re}) \rightarrow \pi^*(\text{pyta})/\pi^*(\text{R}_a)$	LLCT	5.54	224.0	0.0964	
	H-8→L+4	$\pi(\text{Cl})/d(\text{Re}) \rightarrow \pi^*(\text{pyta})$	LLCT				
$S_0 \rightarrow S_{122}$	H-12→L+2	$\pi^*(\text{R})/\pi(\text{pyta}) \rightarrow \pi^*(\text{R}_a)$	ILCT	5.94	208.6	0.1155	
$S_0 \rightarrow S_{128}$	H-8→L+4	$\pi(\text{Cl})/d(\text{Re}) \rightarrow \pi^*(\text{pyta})$	LLCT	6.00	206.7	0.1292	
$S_0 \rightarrow S_{145}$	H-21→L	$\pi^*(\text{R}_b) \rightarrow \pi^*(\text{pyta})$	ILCT	6.13	202.3	0.1293	

MLCT: metal-to-ligand charge transfer; LMCT: ligand-to-metal charge transfer; LLCT: ligand-to-ligand charge transfer; ILCT: intraligand charge transfer.

Table S21. Excitation energies and oscillator strengths calculated on the optimized geometry of the first singlet excited state (S_1) of complexes **Re-Phe**, **Mono-Re-Phe**, **Bi-Re-metaPhe** and **Bi-Re-paraPhe** (in dichloromethane) with TDDFT method at the PBE1PBE/LANL2DZ level.

State	Contribution	Assignment	E_{calc} /eV	λ_{calc} /nm	f
Re-Phe					
1	HOMO→LUMO	$d(\text{Re})+\pi(\text{CO})/\pi(\text{Cl}) \rightarrow \pi^*(\text{pyta})$	2.22	559.0	0.0016
2	H-1→LUMO	$d(\text{Re})+\pi(\text{CO})/\pi(\text{Cl}) \rightarrow \pi^*(\text{pyta})$	2.62	472.9	0.1674
3	H-2→LUMO	$d(\text{Re})+\pi(\text{CO}) \rightarrow \pi^*(\text{pyta})$	2.95	419.7	0.0006
4	HOMO→L+1	$d(\text{Re})+\pi(\text{CO})/\pi(\text{Cl}) \rightarrow \pi^*(\text{pyta})$	3.60	344.1	0.0377
Mono-Re-Phe					
1	HOMO→LUMO	$d(\text{Re})+\pi(\text{CO})/\pi(\text{Cl}) \rightarrow \pi^*(\text{pyta})$	2.26	548.3	0.0027
2	H-1→LUMO	$d(\text{Re})+\pi(\text{CO})/\pi(\text{Cl}) \rightarrow \pi^*(\text{pyta})$	2.67	464.4	0.1655
3	H-2→LUMO	$d(\text{Re})+\pi(\text{CO}) \rightarrow \pi^*(\text{pyta})$	3.00	413.5	0.0024
4	HOMO→L+1	$d(\text{Re})+\pi(\text{CO})/\pi(\text{Cl}) \rightarrow \pi^*(\text{pyta})$	3.63	341.2	0.0389
Bi-Re-metaPhe					
1	HOMO→LUMO	$d(\text{Re})+\pi(\text{CO})/\pi(\text{Cl}) \rightarrow \pi^*(\text{pyta})$	2.21	560.8	0.0019
2	H-1→LUMO	$d(\text{Re})+\pi(\text{CO})/\pi(\text{Cl}) \rightarrow \pi^*(\text{pyta})$	2.62	473.1	0.1680
3	H-4→LUMO	$d(\text{Re})+\pi(\text{CO}) \rightarrow \pi^*(\text{pyta})$	2.95	420.9	0.0014
4	H-2→L+1	$d(\text{Re})+\pi(\text{CO})/\pi(\text{Cl}) \rightarrow \pi^*(\text{pyta})$	2.98	416.0	0.0026
Bi-Re-paraPhe					
1	HOMO→LUMO	$d(\text{Re})+\pi(\text{CO})/\pi(\text{Cl}) \rightarrow \pi^*(\text{pyta})$	2.21	560.6	0.0021
2	H-1→LUMO	$d(\text{Re})+\pi(\text{CO})/\pi(\text{Cl}) \rightarrow \pi^*(\text{pyta})$	2.62	472.8	0.1712
3	H-4→LUMO	$d(\text{Re})+\pi(\text{CO}) \rightarrow \pi^*(\text{pyta})$	2.95	420.6	0.0012
4	H-2→L+1	$d(\text{Re})+\pi(\text{CO})/\pi(\text{Cl}) \rightarrow \pi^*(\text{pyta})$	2.99	415.0	0.0021

Table S22. Phosphorescence emission energies of **Re-Phe**, **Mono-Re-Phe**, **Bi-Re-metaPhe** and **Bi-Re-paraPhe** calculated with DFT and TDDFT methods at the PBE1PBE/LANL2DZ level, in comparison with the experimental values.

Complex	DFT		Character	TDDFT				$\lambda_{\text{em}}(\text{Exp})$ nm
	$\Delta E_{T_1-S_0}$			eV	nm	Major contribution	Character	
	eV	nm						
Re-Phe	1.96	632.6	$^3\text{MLCT}/^3\text{LLCT}$	1.93	641.9	H→L	$^3\text{MLCT}/^3\text{LLCT}$	626 ^a
Mono-Re-Phe	1.99	623.0	$^3\text{MLCT}/^3\text{LLCT}$	1.94	639.7	H→L	$^3\text{MLCT}/^3\text{LLCT}$	616
Bi-Re-metaPhe	1.94	639.1	$^3\text{MLCT}/^3\text{LLCT}$	1.90	653.1	H→L	$^3\text{MLCT}/^3\text{LLCT}$	636
Bi-Re-paraPhe	1.92	645.8	$^3\text{MLCT}/^3\text{LLCT}$	1.88	660.2	H→L	$^3\text{MLCT}/^3\text{LLCT}$	636

$\Delta E_{T_1-S_0}$ is the energy difference between the ground singlet and triplet states.

^a From Poirot *et al. Dalton Trans.*, 2021, **50**, 13686–13698.

Table S23. Natural populations of the $5d_{xy}$, $5d_{xz}$, $5d_{yz}$, $5d_{x^2-y^2}$ and $5d_z^2$ orbitals of the central atom in **Re-Phe**, **Mono-Re-Phe**, **Bi-Re-metaPhe** and **Bi-Re-paraPhe**.

Orbital	Complex					
	Re-Phe	Mono-Re-Phe	Bi-Re-metaPhe		Bi-Re-paraPhe	
$5d_{xy}$	1.219	1.421	1.114	1.114	0.976	0.976
$5d_{xz}$	1.229	1.465	1.341	1.341	1.513	1.513
$5d_{yz}$	1.297	1.529	1.434	1.434	1.561	1.561
$5d_{x^2-y^2}$	1.554	1.141	1.556	1.556	1.564	1.564
$5d_z^2$	1.384	1.125	1.237	1.237	1.068	1.068

The population of $5d$ orbitals ($5d_{xy}$, $5d_{xz}$, $5d_{yz}$, $5d_{x^2-y^2}$ and $5d_z^2$) of the central atoms shows that in free Re (+1) state, the population of $5d_{xy}$, $5d_{xz}$ and $5d_{yz}$ orbitals are 2.0, 2.0 and 2.0 (e) and the other two ($5d_{x^2-y^2}$ and $5d_z^2$) orbitals remain vacant. On complex formation, some decrease in populations for the $5d_{xy}$, $5d_{xz}$ and $5d_{yz}$ orbital and some increase in the populations of $5d_{x^2-y^2}$ and $5d_z^2$ orbital can be observed in comparison to free Re (+1) state.

Table S24. Atomic charges from the Natural Population Analysis (NPA) for **Re-Phe**, **Mono-Re-Phe**, **Bi-Re-metaPhe** and **Bi-Re-paraPhe**.

Atom	Complex					
	Re-Phe	Mono-Re-Phe	Bi-Re-metaPhe		Bi-Re-paraPhe	
Re(1)	-0.99	-0.99	-0.99	-0.99	-0.99	-0.99
C(1)	+0.76	+0.74	+0.74	+0.74	+0.74	+0.74
C(2)	+0.77	+0.77	+0.77	+0.77	+0.77	+0.77
C(3)	+0.74	+0.76	+0.76	+0.76	+0.76	+0.76
N(1)	-0.39	-0.39	-0.39	-0.39	-0.39	-0.39
N(2)	-0.23	-0.26	-0.23	-0.23	-0.26	-0.25
Cl(1)	-0.46	-0.46	-0.46	-0.46	-0.46	-0.46
O(1)	-0.48	-0.49	-0.49	-0.49	-0.49	-0.49
O(2)	-0.47	-0.47	-0.47	-0.47	-0.47	-0.47
O(3)	-0.49	-0.48	-0.48	-0.48	-0.48	-0.48

Natural population analysis (NPA) calculates the charge that is transferred between the donor and acceptor moieties and this charge transfer indicates electrovalent bonding between the Re and ligand. The calculated charge on the rhenium atoms is -0.99 (e) in **Re-Phe**, **Mono-Re-Phe**, **Bi-Re-metaPhe** and **Bi-Re-paraPhe** which is slightly lower than the formal charge of +1, as a result of charge donation from the N atoms of the ligand. The charge on the nitrogen atoms is smaller and less negative, indicating that there is higher electron density delocalization from the N atoms to Re atoms. The positively charged carbon atoms of the carbonyl ligands are found to accept as much as ~0.74/0.77/0.76 (e) from Re atoms, while the Re atoms donates charge 0.99 (e). The negatively charged nitrogen atoms **N(1)**, **N(2)** and chlorine atom **Cl(1)** are found to donate as much as ~0.39 (e), -0.23 (e) and ~0.46 (e) to Re atoms, respectively.

Table S25. Absolute electronegativity, absolute hardness, dipole moment (μ), electrophilicity index (ω) and global softness (σ) of complexes **Re-Phe**, **Mono-Re-Phe**, **Bi-Re-metaPhe** and **Bi-Re-paraPhe**.

Parameter	Complex			
	Re-Phe	Mono-Re-Phe	Bi-Re-metaPhe	Bi-Re-paraPhe
Total Energy (Hartree)	-1153.6934814	-1467.8985047	-2703.7740894	-2703.7743660
E_{HOMO} (eV)	-6.52	-6.48	-6.54	-6.55
E_{LUMO} (eV)	-2.51	-2.45	-2.58	-2.57
Energy gap ΔE (eV)	4.01	4.03	3.96	3.98
Ionization Potential I	6.52	6.48	6.54	6.55
Electron Affinity A	2.51	2.45	2.58	2.57
Electronegativity χ (eV)	4.52	4.47	4.56	4.56
Chemical potential μ	-4.52	-4.47	-4.56	-4.56
Hardness η (eV)	2.01	2.02	1.98	1.99
Softness σ (eV)	0.50	0.50	0.51	0.50
Electrophilicity ω (D/eV)	5.08	4.95	5.25	5.22
Dipole moment μ (D)	7.90	7.94	4.19	0

The determination of HOMO and LUMO energies is very important in view of chemical reaction. The HOMO (Highest Occupied Molecular Orbitals) is the orbital that primarily acts as an electron donor and the LUMO (Lowest Unoccupied Molecular Orbital) is the orbital that largely acts as the electron acceptor. The gap between HOMO and LUMO reflects the chemical reactivity and stability of the molecule.

The frontier molecular orbital descriptors such as ionization potential ($IP = -E_{\text{HOMO}}$), electron affinity ($EA = -E_{\text{LUMO}}$), electronegativity ($\chi = (I + A)/2$), chemical potential ($\mu = -\chi$), hardness ($\eta = (I - A)/2$), softness ($\sigma = 1/\eta$) and electrophilicity index ($\omega = \mu^2/2\eta$) were calculated according to Koopmans theorem [T. Koopmans, *Physica*, 1933, 1, 104.]. Dipole moment was calculated using the equation: $\mu = 2.54 \times (x^2 + y^2 + z^2)^{1/2}$.

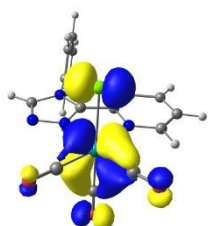
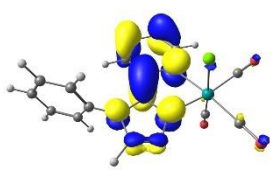
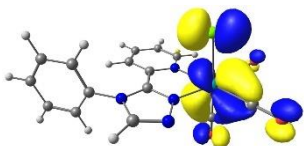
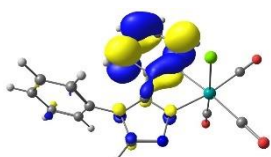

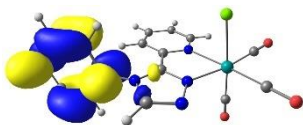
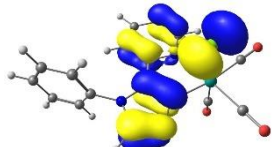
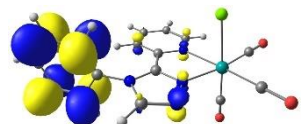
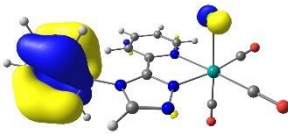
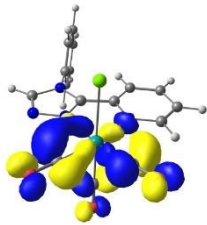
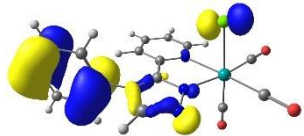
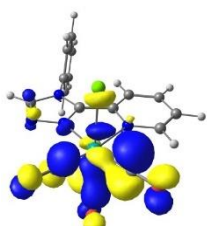
Occupied orbitals		Unoccupied orbitals	
HOMO / 90 (-6.52 eV)		LUMO / 91 (-2.51 eV)	
HOMO-1 / 89 (-6.63 eV)		LUMO+1 / 92 (-1.65 eV)	
HOMO-2 / 88 (-7.11 eV)		LUMO+2 / 93 (-1.15 eV)	
HOMO-3 / 87 (-7.79 eV)		LUMO+3 / 94 (-1.01 eV)	
HOMO-4 / 86 (-8.07 eV)		LUMO+4 / 95 (-0.76 eV)	
HOMO-5 / 85 (-8.09 eV)		LUMO+5 / 96 (-0.63 eV)	

Figure S35. The isodensity plots of the frontier molecular orbitals of **Re-Phe** (in dichloromethane).

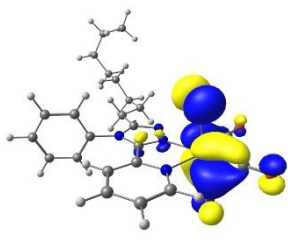
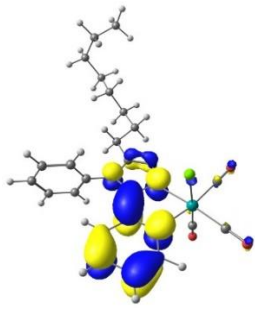
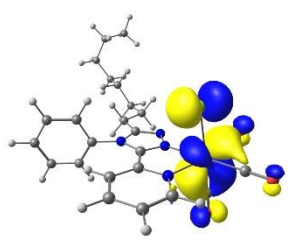
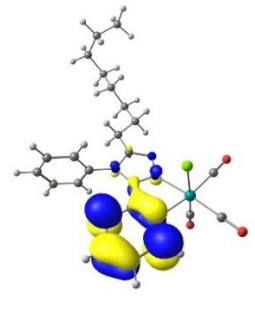
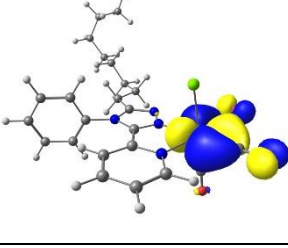
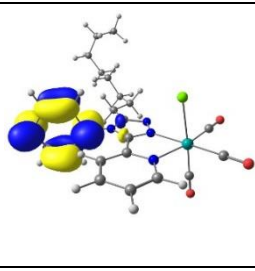
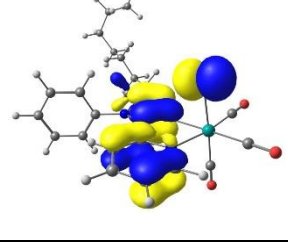
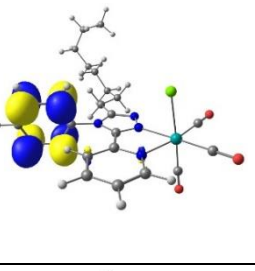
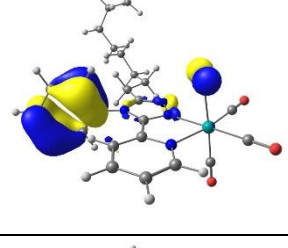
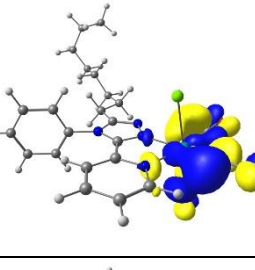
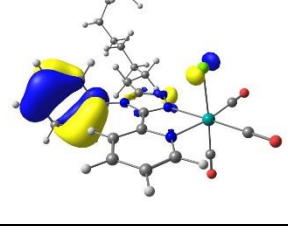
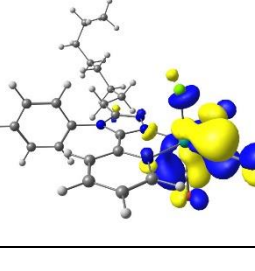
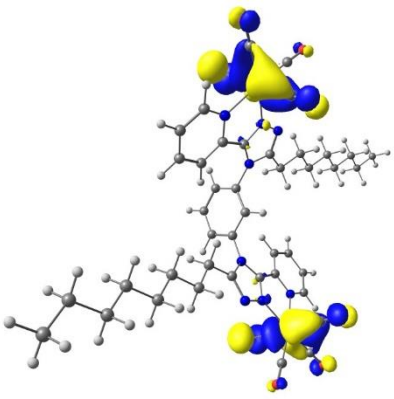
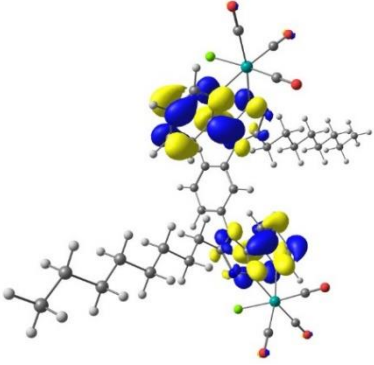
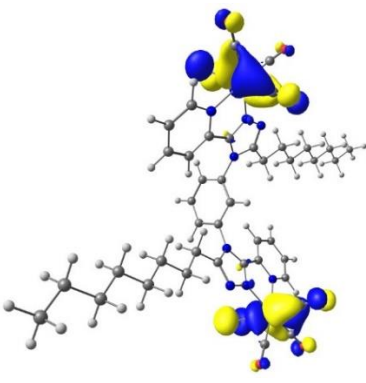
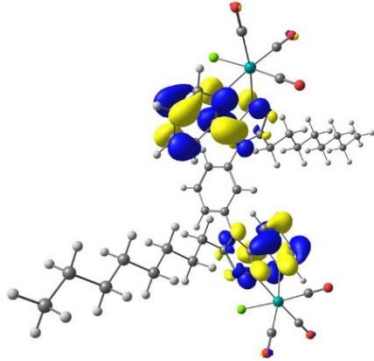
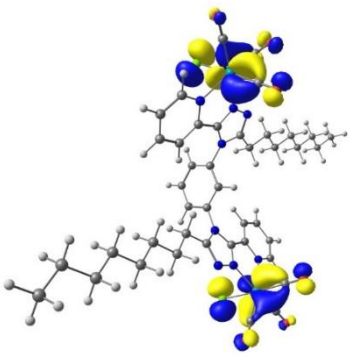
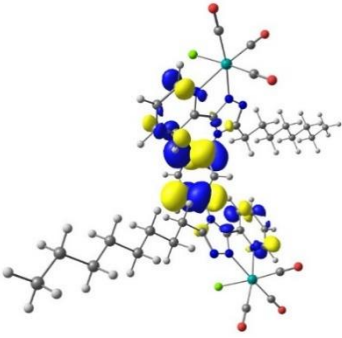
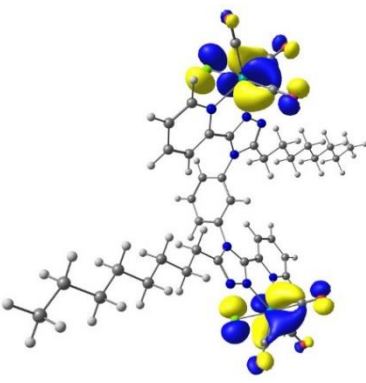
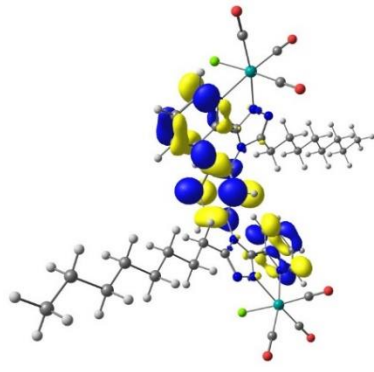
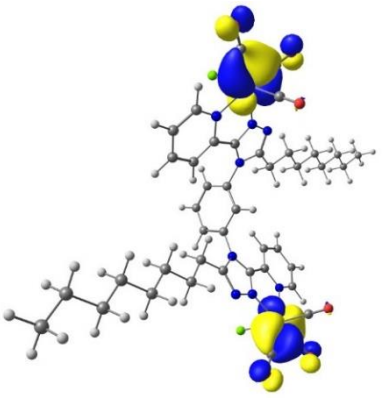
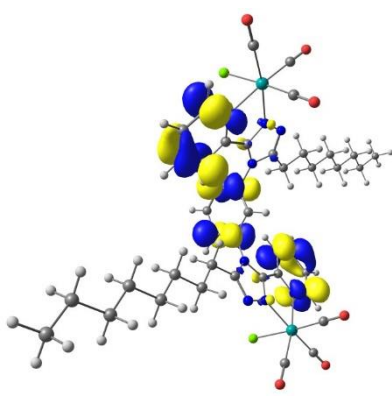
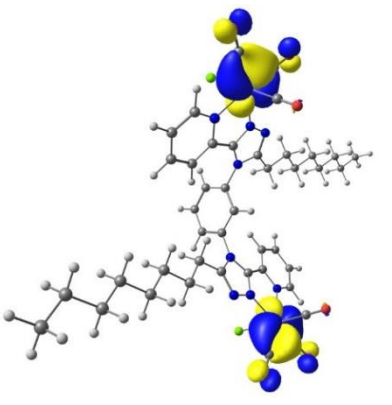
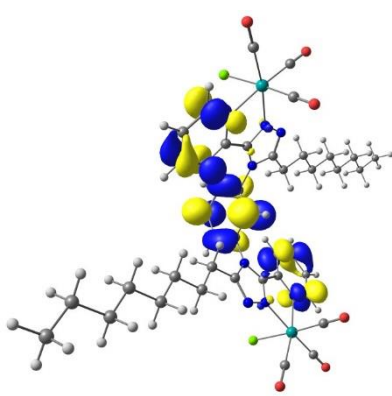
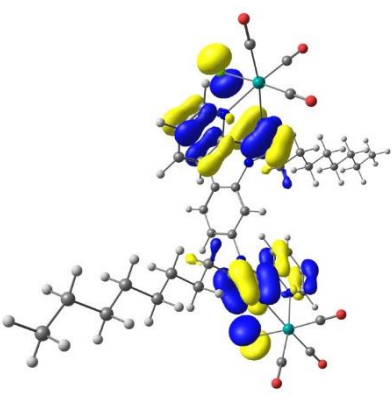
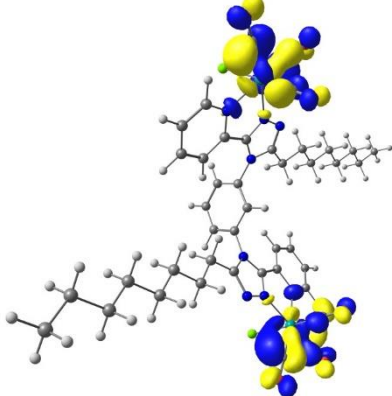
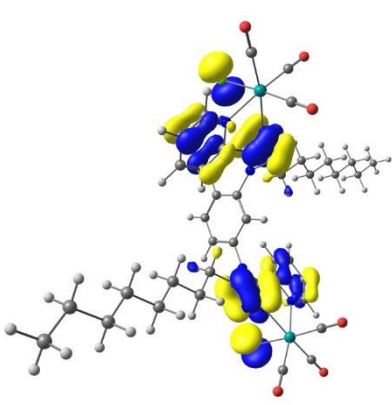
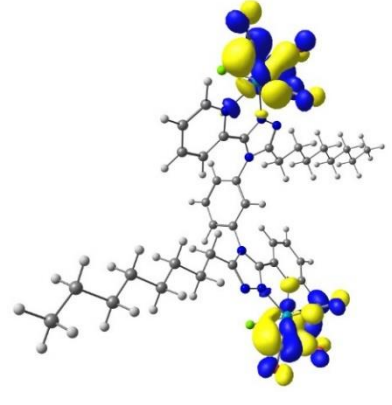
Occupied orbitals		Unoccupied orbitals	
HOMO / 122 (-6.48 eV)		LUMO / 123 (-2.45 eV)	
HOMO-1 / 121 (-6.60 eV)		LUMO+1 / 124 (-1.59 eV)	
HOMO-2 / 120 (-7.07 eV)		LUMO+2 / 125 (-1.14 eV)	
HOMO-3 / 119 (-7.60 eV)		LUMO+3 / 126 (-0.95 eV)	
HOMO-4 / 118 (-8.03 eV)		LUMO+4 / 127 (-0.73 eV)	
HOMO-5 / 117 (-8.06 eV)		LUMO+5 / 128 (-0.58 eV)	

Figure S36. The isodensity plots of the frontier molecular orbitals of **Mono-Re-Phe** (in dichloromethane).

Occupied orbitals		Unoccupied orbitals	
HOMO / 223 (-6.54 eV)		LUMO / 224 (-2.58 eV)	
HOMO-1 / 222 (-6.55 eV)		LUMO+1 / 225 (-2.56 eV)	
HOMO-2 / 221 (-6.66 eV)		LUMO+2 / 226 (-1.84 eV)	
HOMO-3 / 220 (-6.66 eV)		LUMO+3 / 227 (-1.79 eV)	

<p>HOMO-4 / 219 (-7.14 eV)</p>		<p>LUMO+4 / 228 (-1.62 eV)</p>	
<p>HOMO-5 / 218 (-7.14 eV)</p>		<p>LUMO+5 / 229 (-1.52 eV)</p>	
<p>HOMO-6 / 217 (-7.72 eV)</p>		<p>LUMO+6 / 230 (-0.80 eV)</p>	
<p>HOMO-7 / 216 (-7.73 eV)</p>		<p>LUMO+7 / 231 (-0.79 eV)</p>	

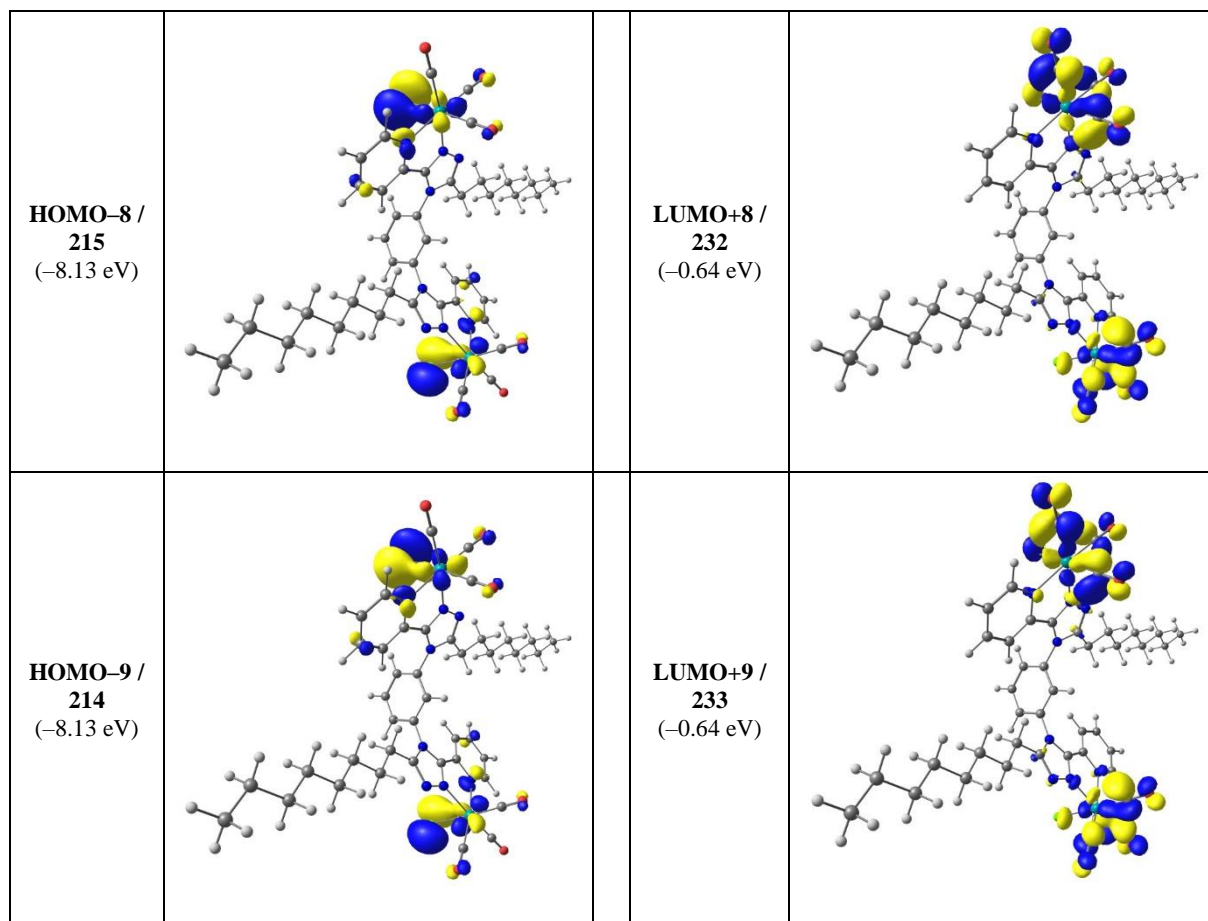
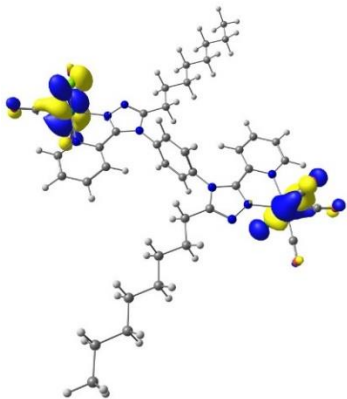
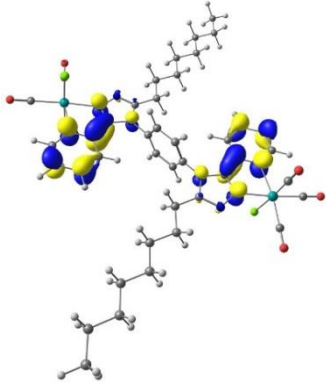
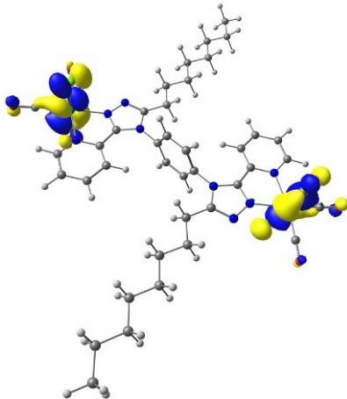
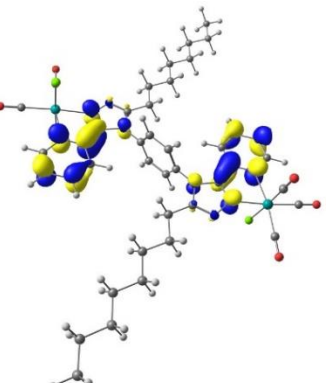
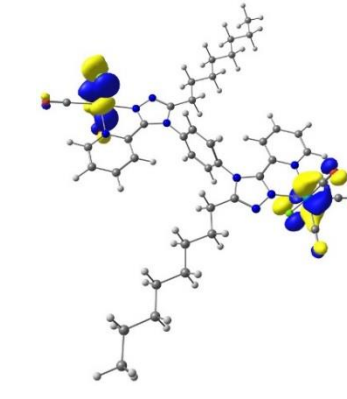
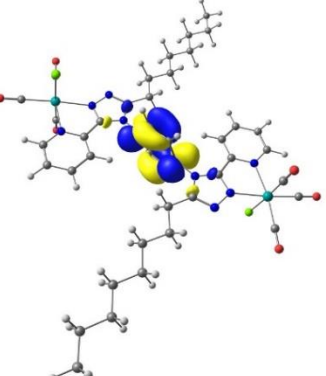
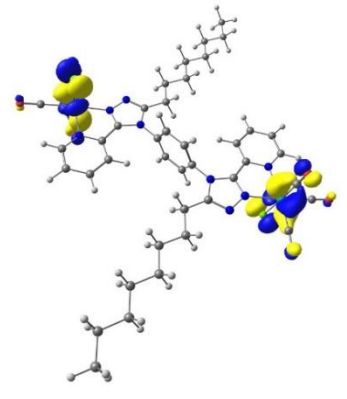
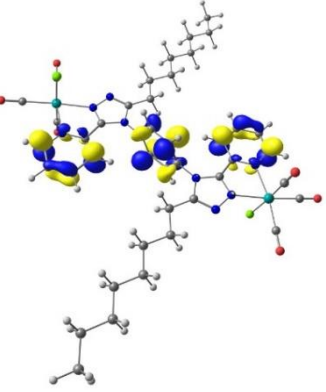
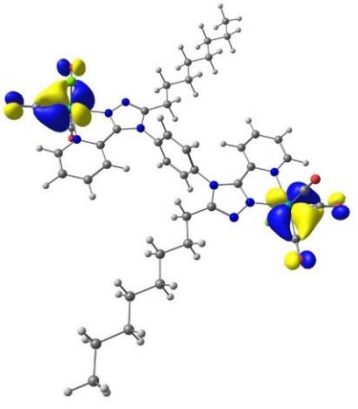
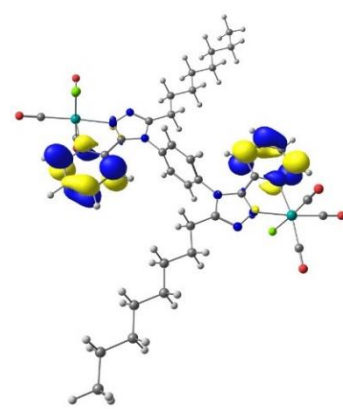
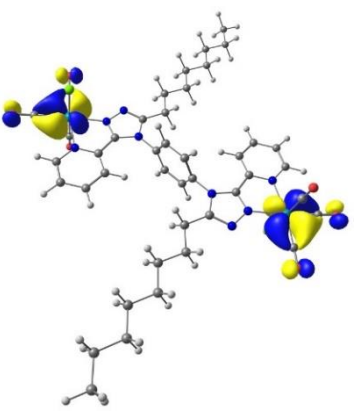
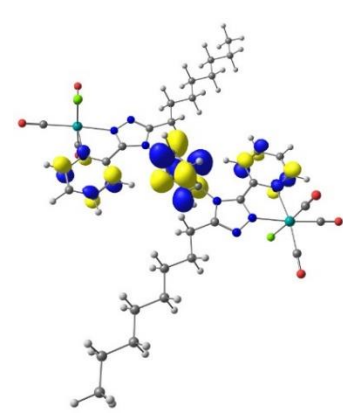
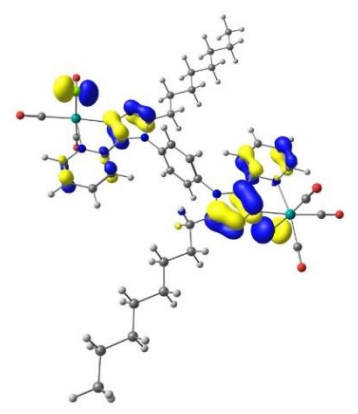
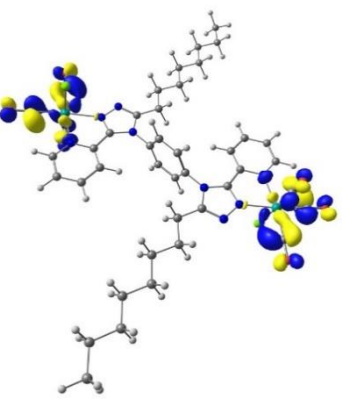
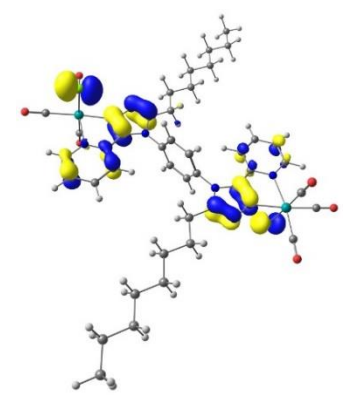
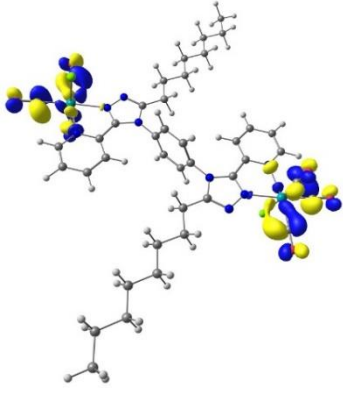


Figure S37. The isodensity plots of the frontier molecular orbitals of **Bi-Re-*meta*Phe** (in dichloromethane).

Occupied orbitals		Unoccupied orbitals	
HOMO / 223 (-6.55 eV)		LUMO / 224 (-2.57 eV)	
HOMO-1 / 222 (-6.55 eV)		LUMO+1 / 225 (-2.56 eV)	
HOMO-2 / 221 (-6.66 eV)		LUMO+2 / 226 (-1.88 eV)	
HOMO-3 / 220 (-6.66 eV)		LUMO+3 / 227 (-1.78 eV)	

<p>HOMO-4 / 219 (-7.14 eV)</p>		<p>LUMO+4 / 228 (-1.66 eV)</p>	
<p>HOMO-5 / 218 (-7.14 eV)</p>		<p>LUMO+5 / 229 (-1.44 eV)</p>	
<p>HOMO-6 / 217 (-7.72 eV)</p>		<p>LUMO+6 / 230 (-0.80 eV)</p>	
<p>HOMO-7 / 216 (-7.72 eV)</p>		<p>LUMO+7 / 231 (-0.79 eV)</p>	

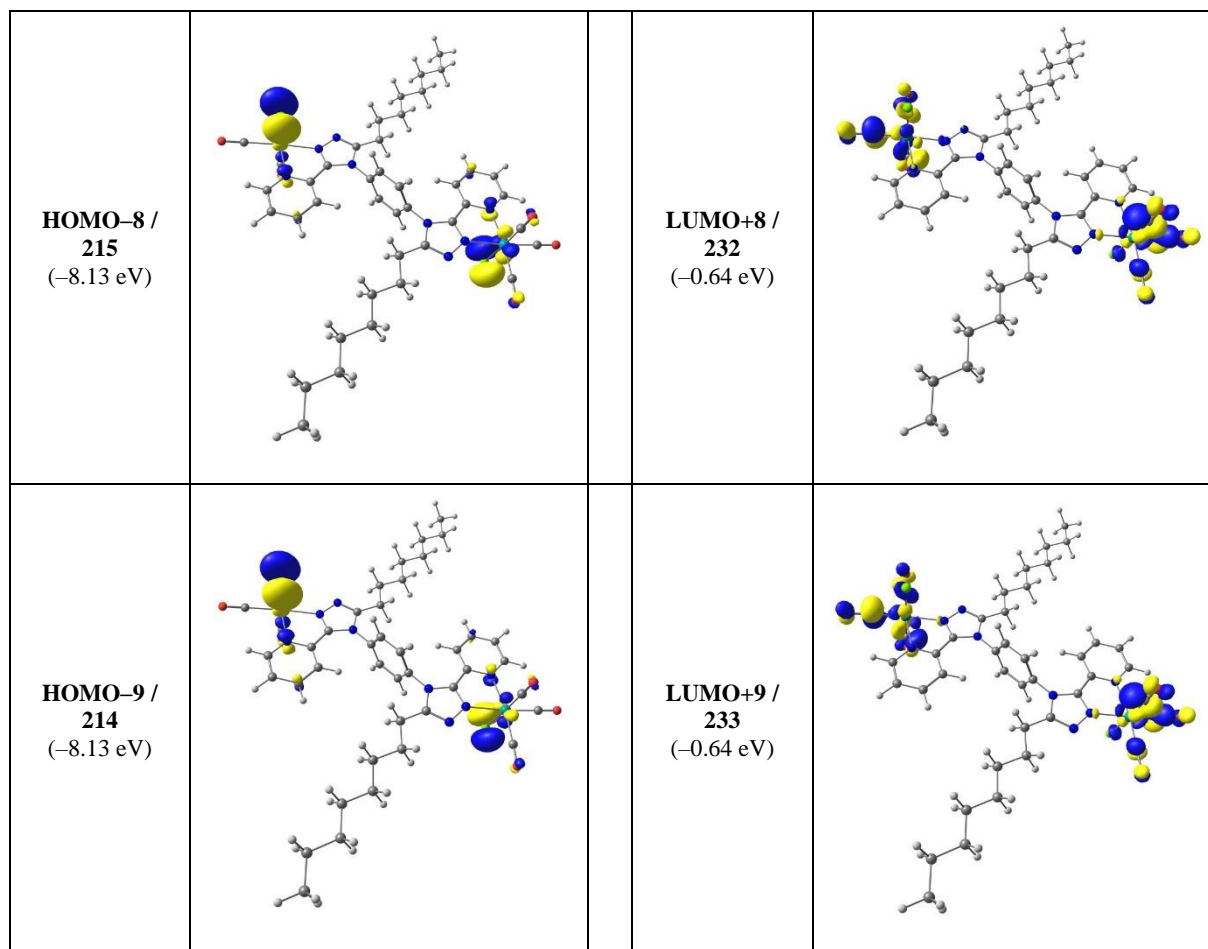


Figure S38. The isodensity plots of the frontier molecular orbitals of **Bi-Re-*para*Phe** (in dichloromethane).

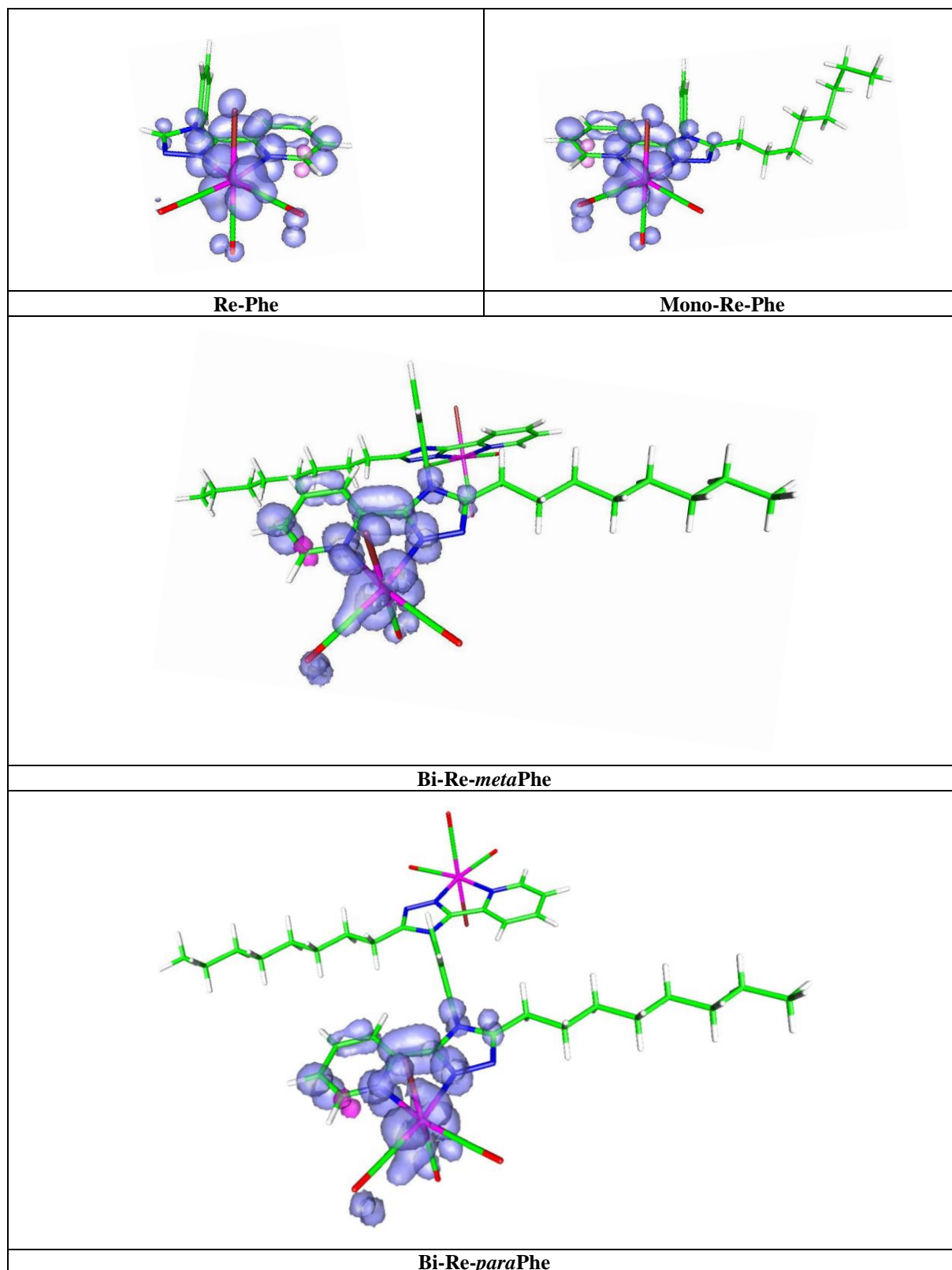


Figure S39. Spin density distribution for the lowest triplet state (T_1) of **Re-Phe**, **Mono-Re-Phe**, **Bi-Re-*meta*Phe** and **Bi-Re-*para*Phe** (in dichloromethane) calculated based on the optimized triplet state with DFT method at the PBE1PBE/LanL2DZ level (isovalue surface of 0.0045 au).

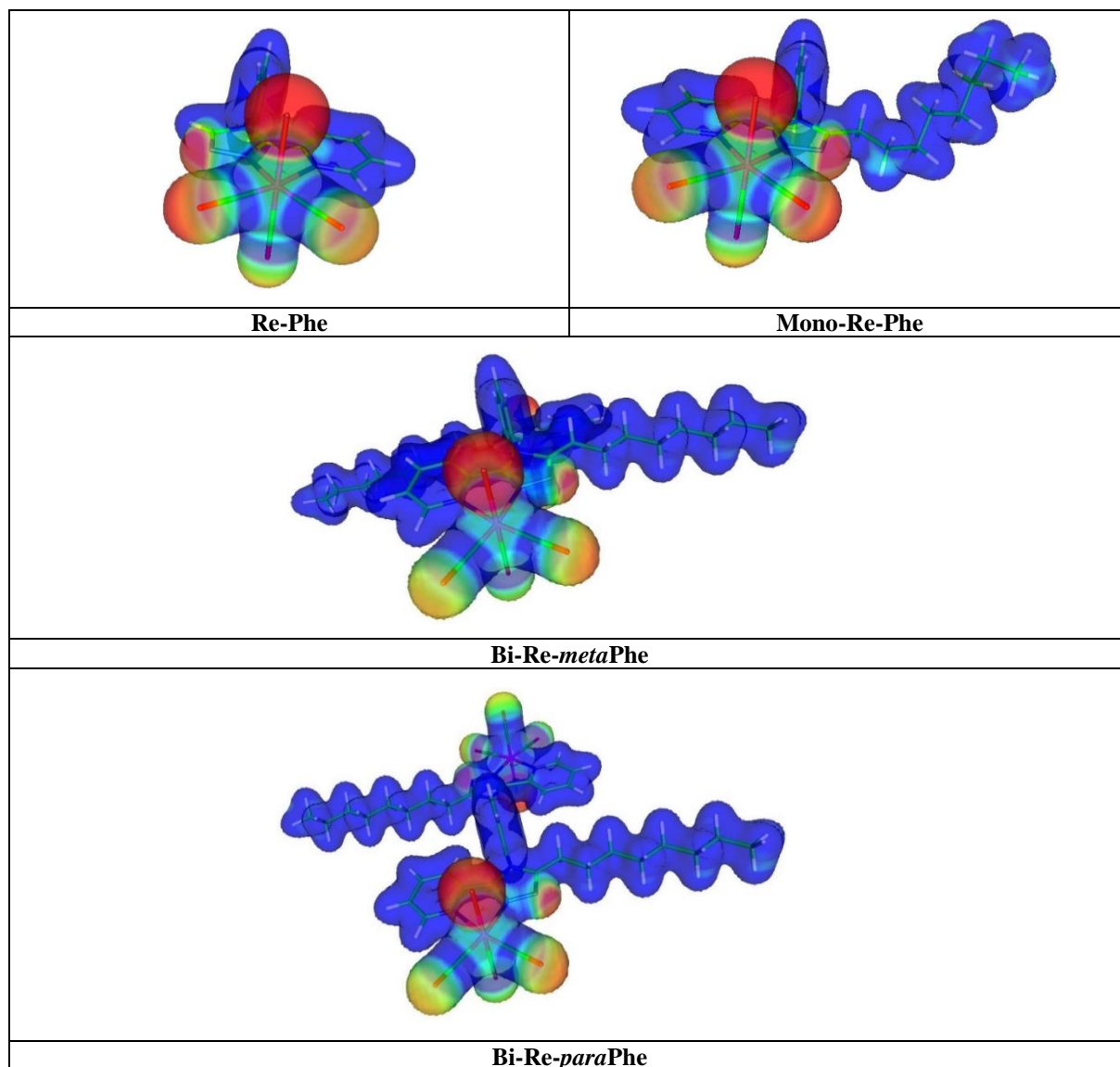


Figure S40. Molecular Electrostatic Potential (MEP) of **Re-Phe**, **Mono-Re-Phe**, **Bi-Re-*meta*Phe** and **Bi-Re-*para*Phe** (in dichloromethane) on the $\rho(r) = 0.02$ au isodensity surface, calculated based on the optimized ground state geometry with DFT method at the PBE1PBE/LanL2DZ level. Mapping colours range from red -0.05 au to blue $+0.05$ au.

MEP surface plot helps to understand visually the relative polarity of the molecule, as shown in Figure 9. It is also useful to explain quantitatively hydrogen bonding, reactivity and structure–activity relationship of molecules including the biomolecules and drugs. MEP helps to find the sites for electrophilic and nucleophilic attacks as well as hydrogen bonding interactions. The MEP surfaces of **Re-Phe**, **Mono-Re-Phe**, **Bi-Re-*meta*Phe** and **Bi-Re-*para*Phe** studied by PBE1PBE/LanL2DZ were generated by mapping electrostatic potential onto the molecular electron density surface. In the MEP surface map, regions are represented by different colors which corresponds to different values of the electrostatic potential. The maximum negative region which preferred site for electrophilic attack is indicated as red color, whereas the maximum positive region which preferred site for nucleophilic attack is indicated as blue color. Potential increases in the order red < orange < yellow < green < cyan < blue, where red shows the strongest repulsion and blue shows the strongest attraction. Regions having the negative potential are over the electronegative atoms while the regions having the positive potential are over the electropositive atoms.

Negative electrostatic potential regions (red colour) of complexes **Re-Phe**, **Mono-Re-Phe**, **Bi-Re-*meta*Phe** and **Bi-Re-*para*Phe** are mainly localized around the chlorine Cl, the nitrogens N of the ligand as well as carbonyl oxygens. The positive electrostatic potential regions (blue colour) are around the hydrogen atoms.

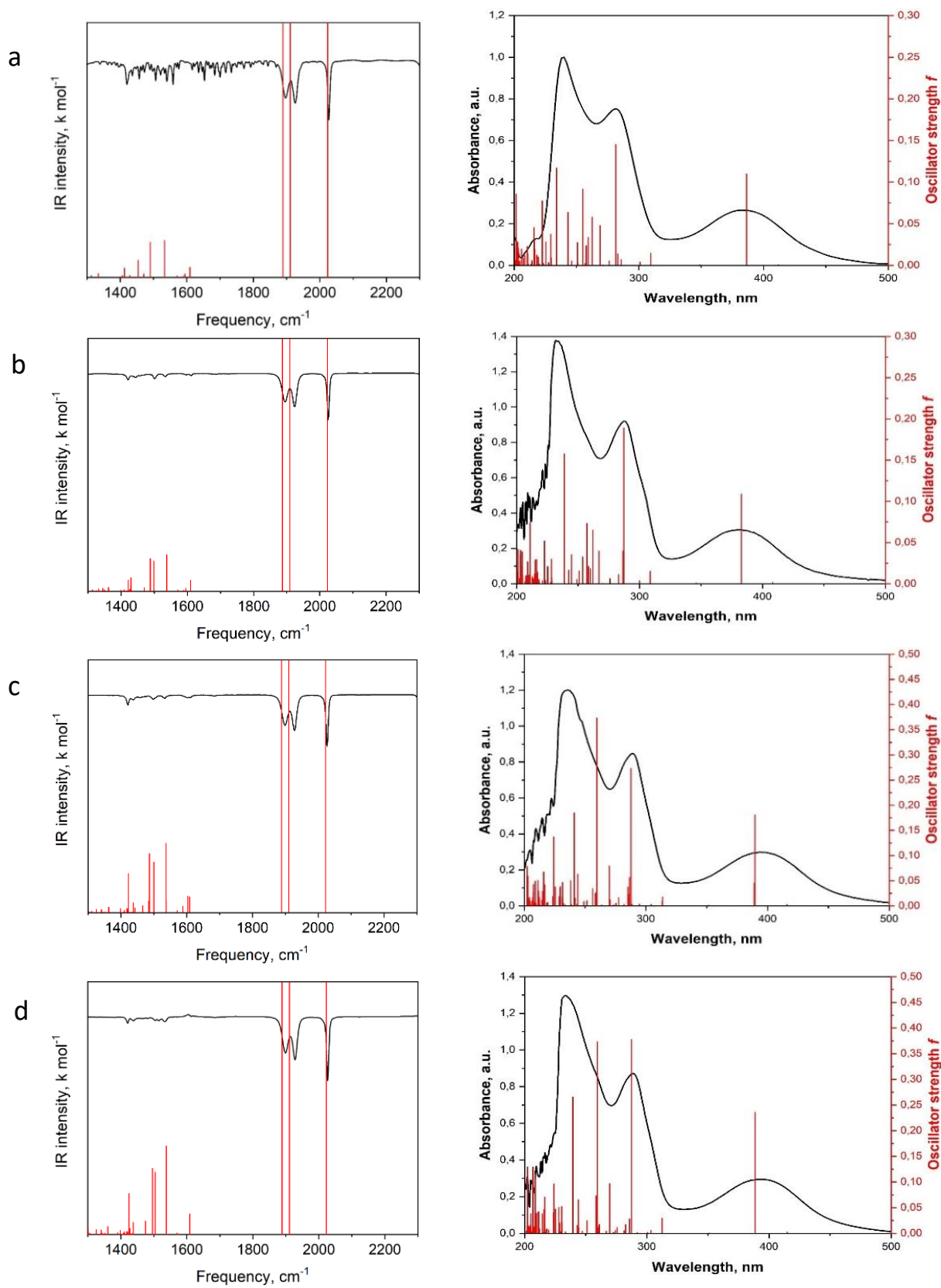


Figure S41. The experimental (black) and simulated (red) FT-IR spectra (left) and UV-Vis absorption spectra (right) of **Re-Phe** (a), **Mono-Re-Phe** (b), **Bi-Re-metaPhe** (c) and **Bi-Re-paraPhe** (d) in dichloromethane.

Electrochemistry

Table S26. Experimental electrochemical data used, and calculated values of the energy gaps (E_g) for complexes, **Mono-Re-Phe**, **Bi-Re-paraPhe**, and **Bi-Re-metaPhe**.

Compound	$E_{\text{onset ox}}$ (V)	$E_{\text{onset red}}$ (V)	E_{HOMO} (eV)	E_{LUMO} (eV)	E_g^{el} (eV)	$E_{\text{calc}}^{\text{a}}$ (eV)
Mono-Re-Phe	1.07	-1.48	-5.81	-3.26	2.55	2.67
Bi-Re-paraPhe	1.33	-1.13	-6.07	-3.61	2.46	2.62
Bi-Re-metaPhe	1.33	-1.13	-6.07	-3.61	2.46	2.62

^a The values were obtained using the TD-DFT method and considering the optimized geometry of the S_1 state (see the theoretical section).

Comment S3. Evaluation of the electrochemical energy gap values (E_g^{el}) for the Re complexes.

The onset oxidation and reduction potentials ($E_{\text{onset ox}}$, $E_{\text{onset red}}$) were measured by cyclic voltammetry in volt *versus* SCE. The CVs were carried out at a potential scan rate of 200 mV s⁻¹ at room temperature.

The HOMO and LUMO energy levels (E_{HOMO} and E_{LUMO}) in electron volt (eV) were calculated according to the empirical equations (1) and (2):^[1]

$$E_{\text{HOMO}} \text{ (eV)} = -e (E_{\text{onset ox}} \text{ (V vs. SCE)} + 4.74 \text{ V}) \quad \text{Eq(1)}$$

$$E_{\text{LUMO}} \text{ (eV)} = -e (E_{\text{onset red}} \text{ (V vs. SCE)} + 4.74 \text{ V}) \quad \text{Eq(2)}$$

and the energy gap value was obtained as follows: $E_g^{\text{el}} = (E_{\text{LUMO}} - E_{\text{HOMO}})$.

The differences observed for the estimation of the energy gaps using experimental methods or theoretical calculations are well known. See for example: R. Stowasser, R. Hoffmann, *J. Am. Chem. Soc.* 1999, *121*, 3414-3420.

[1] a) Y. Zhou, J. W. Kim, R. Nandhakumar, M. J. Kim, E. Cho, Y. S. Kim, Y. H. Jang, C. Lee, S. Han, K. M. Kim, J.-J. Kim and J. Yoon, *Chem. Commun.* 2010, **46**, 6512-6514 and references therein; b) G. V. Loukova, *Chem. Phys. Lett.* 2002, **353**, 244-252.

Electrochemical selected curves

OSWV study was performed on a Pt working electrode in $\text{CH}_2\text{Cl}_2 + 0.1 \text{ M } n[\text{Bu}_4\text{N}][\text{BF}_4]$ at room temperature in the presence of ferrocene used as internal reference. Frequency 20 Hz, amplitude 20 mV, step potential 5 mV. Cyclic voltammograms of the indicated compounds were performed on a Pt working electrode in $\text{CH}_2\text{Cl}_2 + 0.1 \text{ M } n[\text{Bu}_4\text{N}][\text{BF}_4]$ at room temperature at a scan rate of 0.2 V s^{-1} or at other mentioned scan rates.

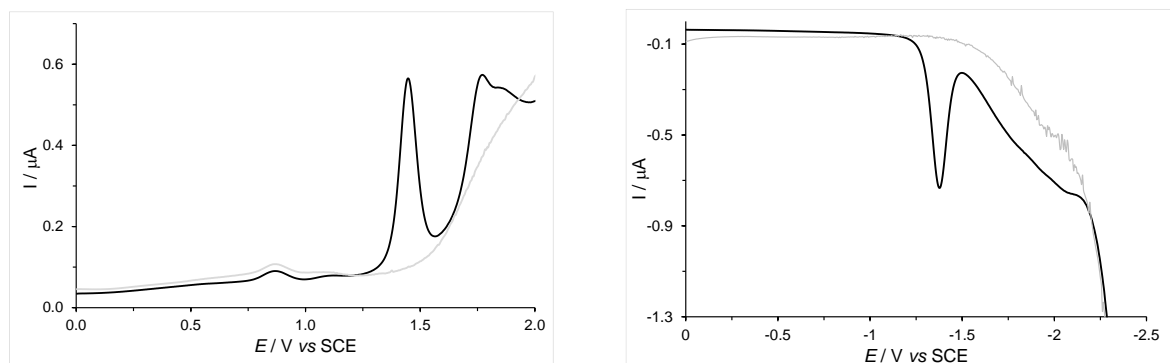


Figure S42. OSWVs: anodic (left) and cathodic (right) scans of complex **Mono-Re-Phe**.

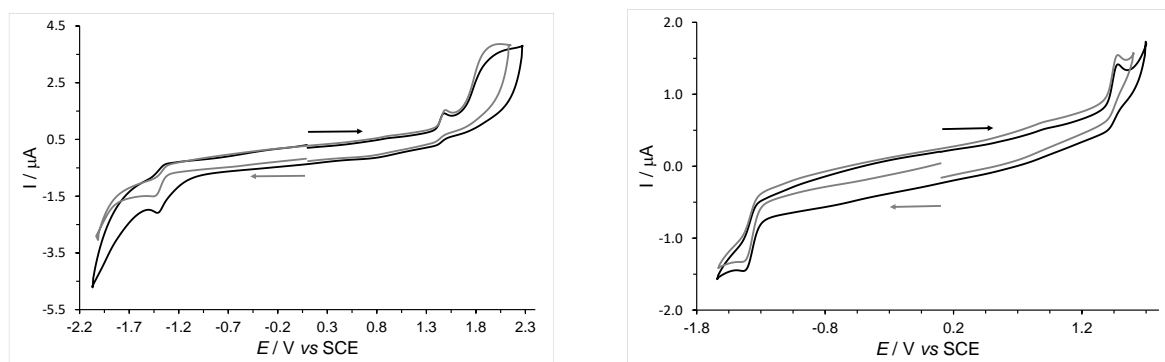


Figure S43. Cyclic voltammograms of complex **Mono-Re-Phe** (left), and of its first oxidation and reduction processes (right) at 0.2 V/s .

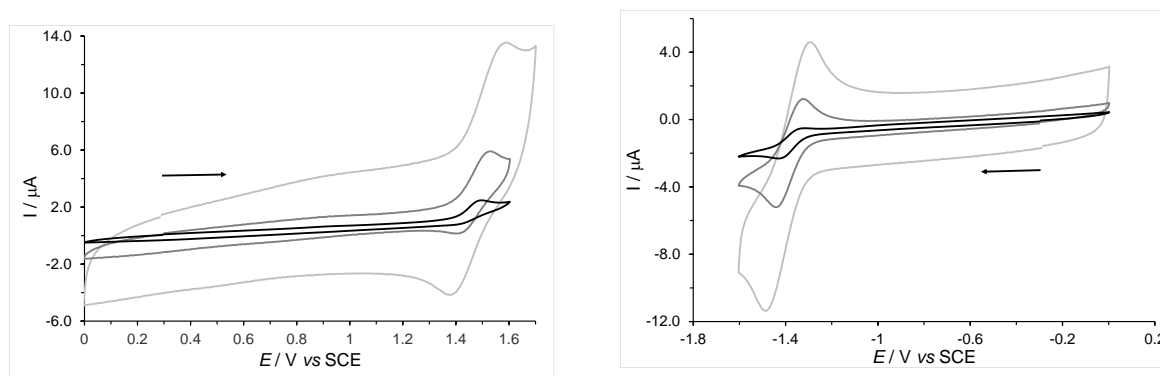


Figure S44. Cyclic voltammograms of the first oxidation process of complex **Mono-Re-Phe** at 1, 10, and 50 V/s from bottom-black line to top-light gray line (left), and of its first reduction process at 1, 10, and 50 V/s from bottom-black line to top-gray line (right).

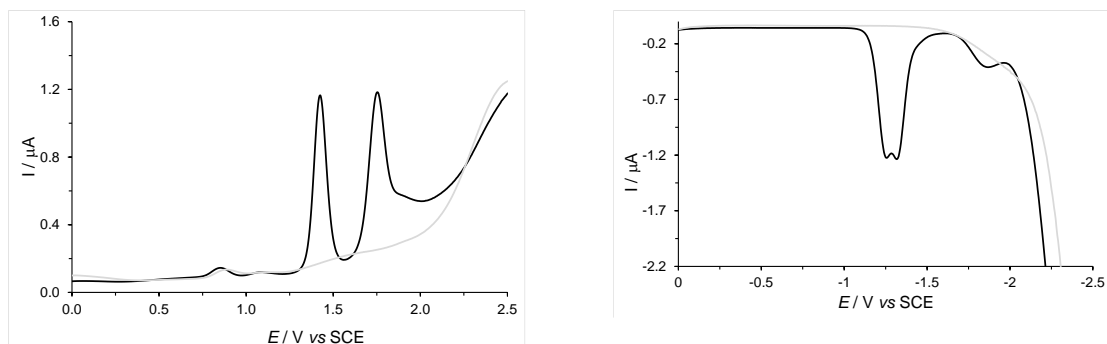


Figure S45. OSWVs: anodic (left) and cathodic (right) scans of complex **Bi-Re-paraPhe**.

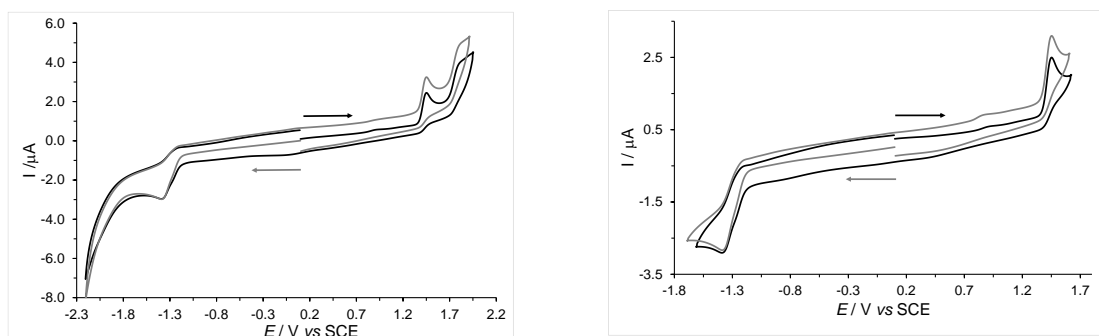


Figure S46. Cyclic voltammograms of complex **Bi-Re-paraPhe** (left), and of its first oxidation and reduction processes (right) at 0.2 V/s.

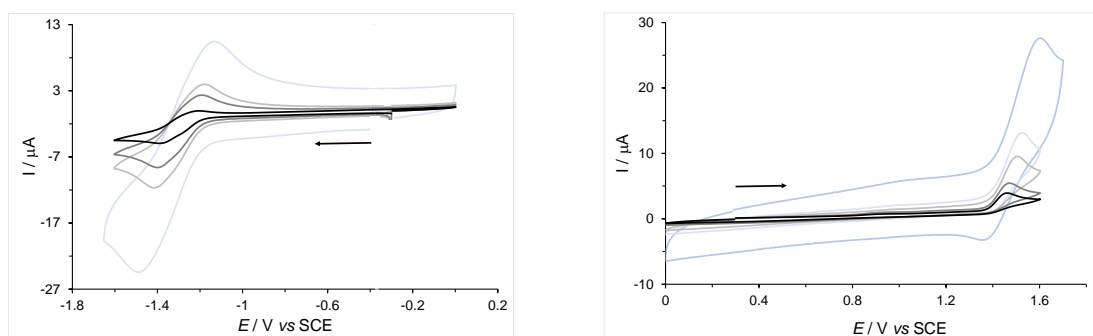


Figure S47. Cyclic voltammograms of the first reduction process of complex **Bi-Re-paraPhe** at 1, 5, 10, and 50 V/s from bottom-black line to top-light blue line (left), and of its first oxidation process at 1, 2, 5, 10, and 50 V/s from bottom-black line to top-gray line (right).

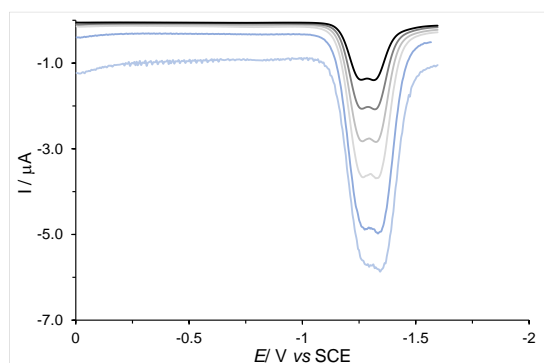


Figure S48. OSWVs: anodic scans of complex **Bi-Re-paraPhe** at different frequencies (20/50/100/200/500/1000) from black line to blue line with amplitude 20 mV and step potential 5 mV.

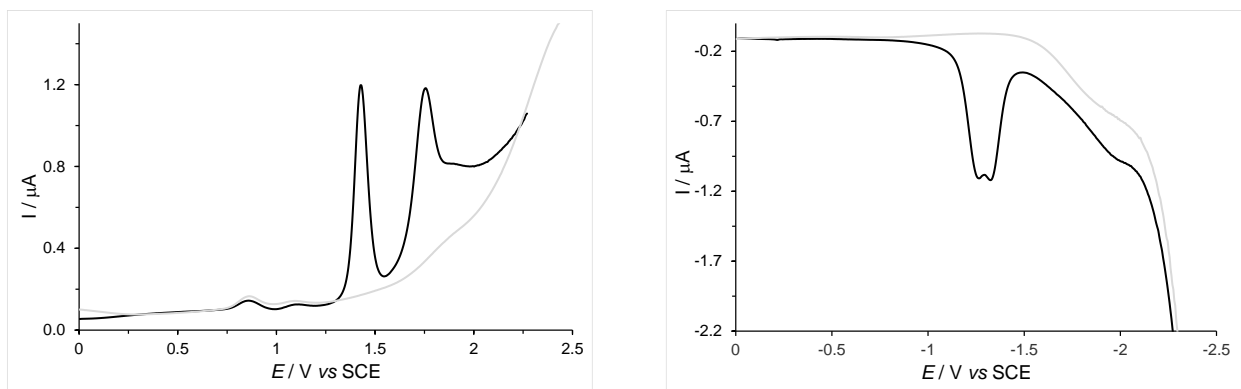


Figure S49. OSWVs: anodic (left) and cathodic (right) scans of complex **Bi-Re-metaPhe**.

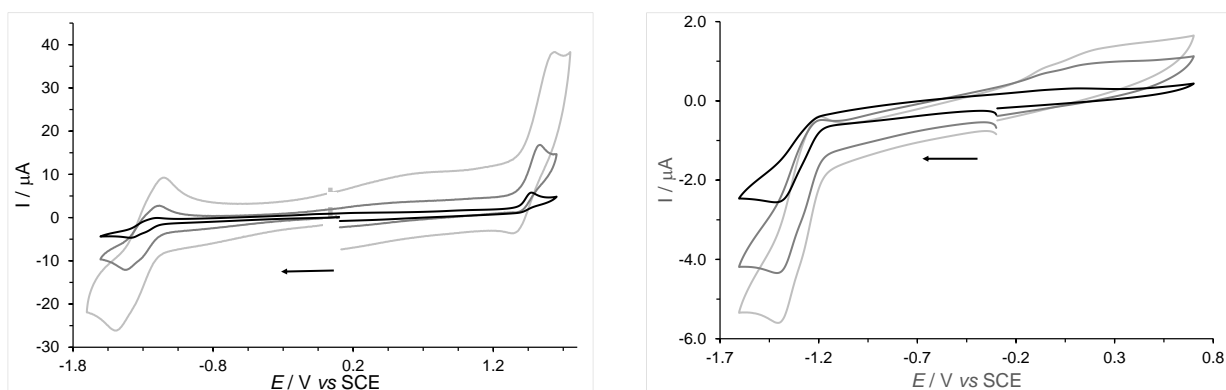


Figure S50. Cyclic voltammograms of complex **Bi-Re-metaPhe**, its first oxidation and reduction processes at 5, 10, 50 V/s from black to gray line (left) and its first reduction potential 0.1, 0.5, 1 V/s from black to gray line (right).

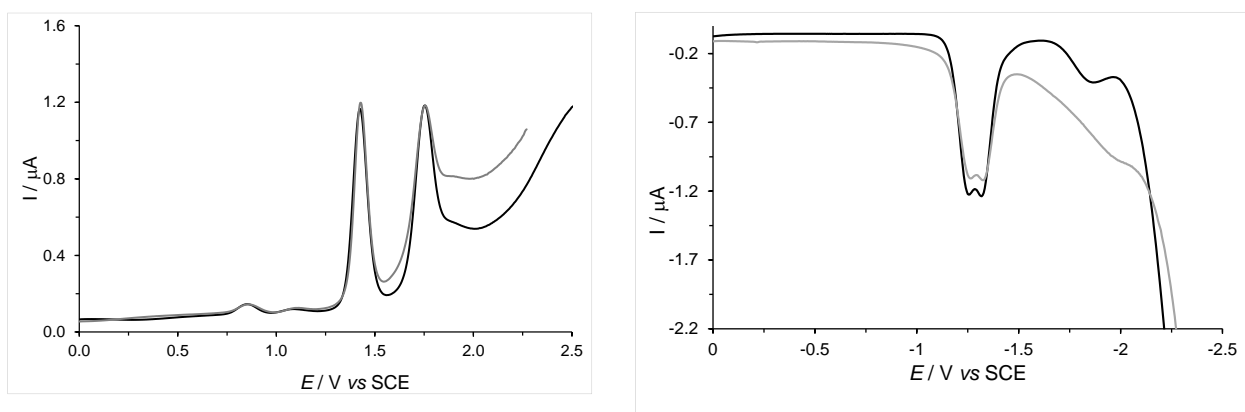


Figure S51. OSWVs: anodic (left) and cathodic (right) scans of complex **Bi-Re-paraPhe** (black) versus **Bi-Re-metaPhe** (gray).

Selected curves of the corresponding ligands

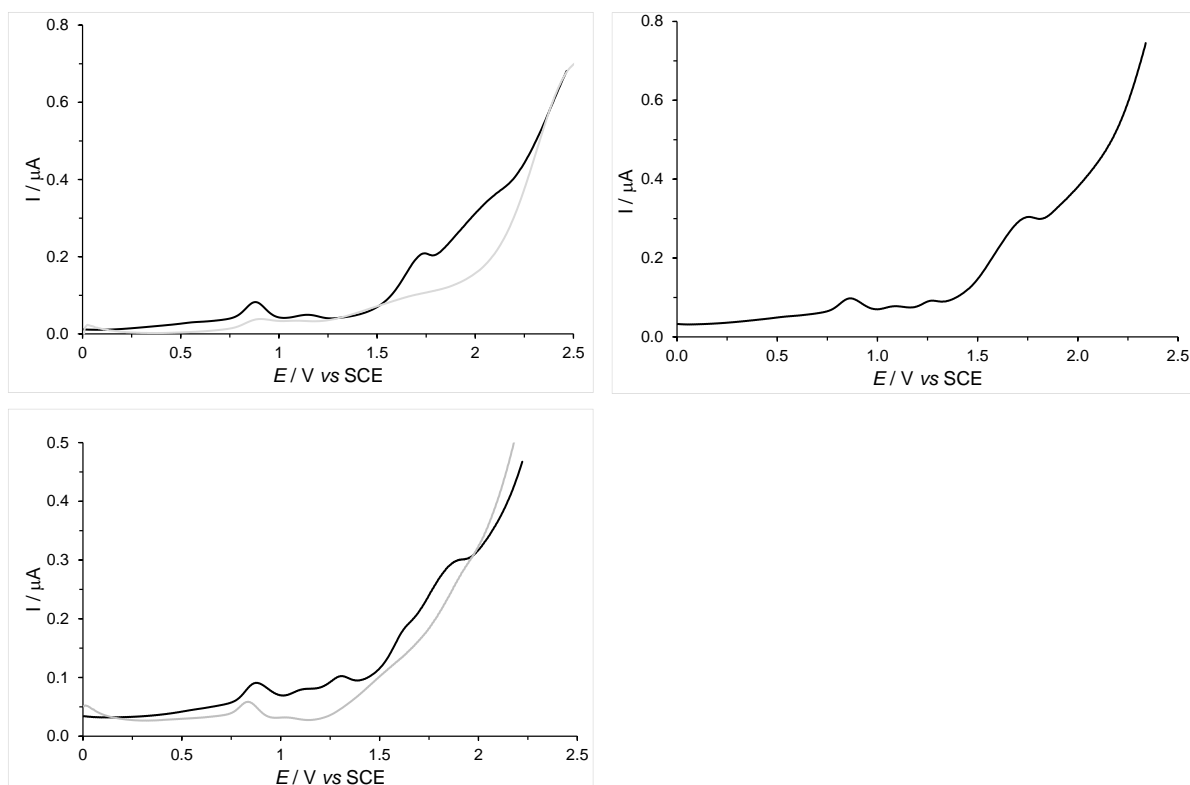


Figure S52. OSWVs: anodic scans of ligands **L-Phe** (top left), **L-paraPhe** (top right), and **L-metaPhe** (bottom), and of the corresponding electrochemical medium without the ligand (gray).

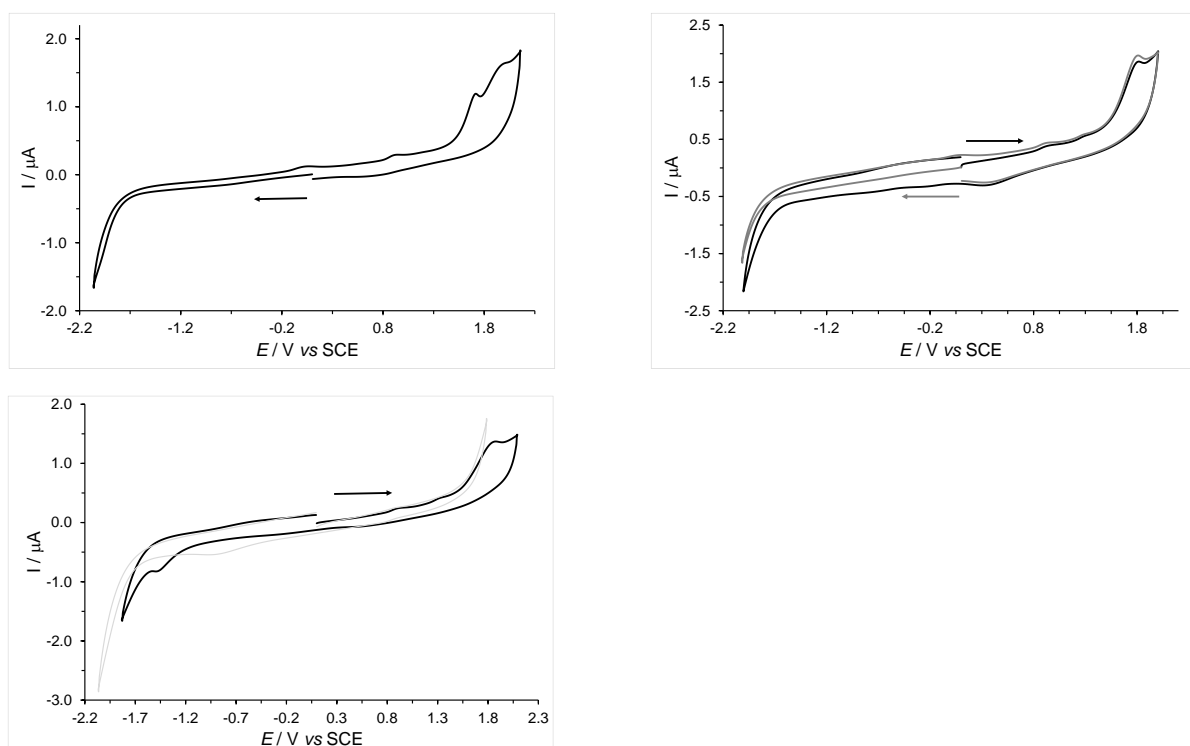


Figure S53. Cyclic voltammograms of ligands **L-Phe** (top left), **L-paraPhe** (top right), and **L-metaPhe** (bottom), and of the electrochemical medium without ligand in the last case in gray.

Spectroscopy

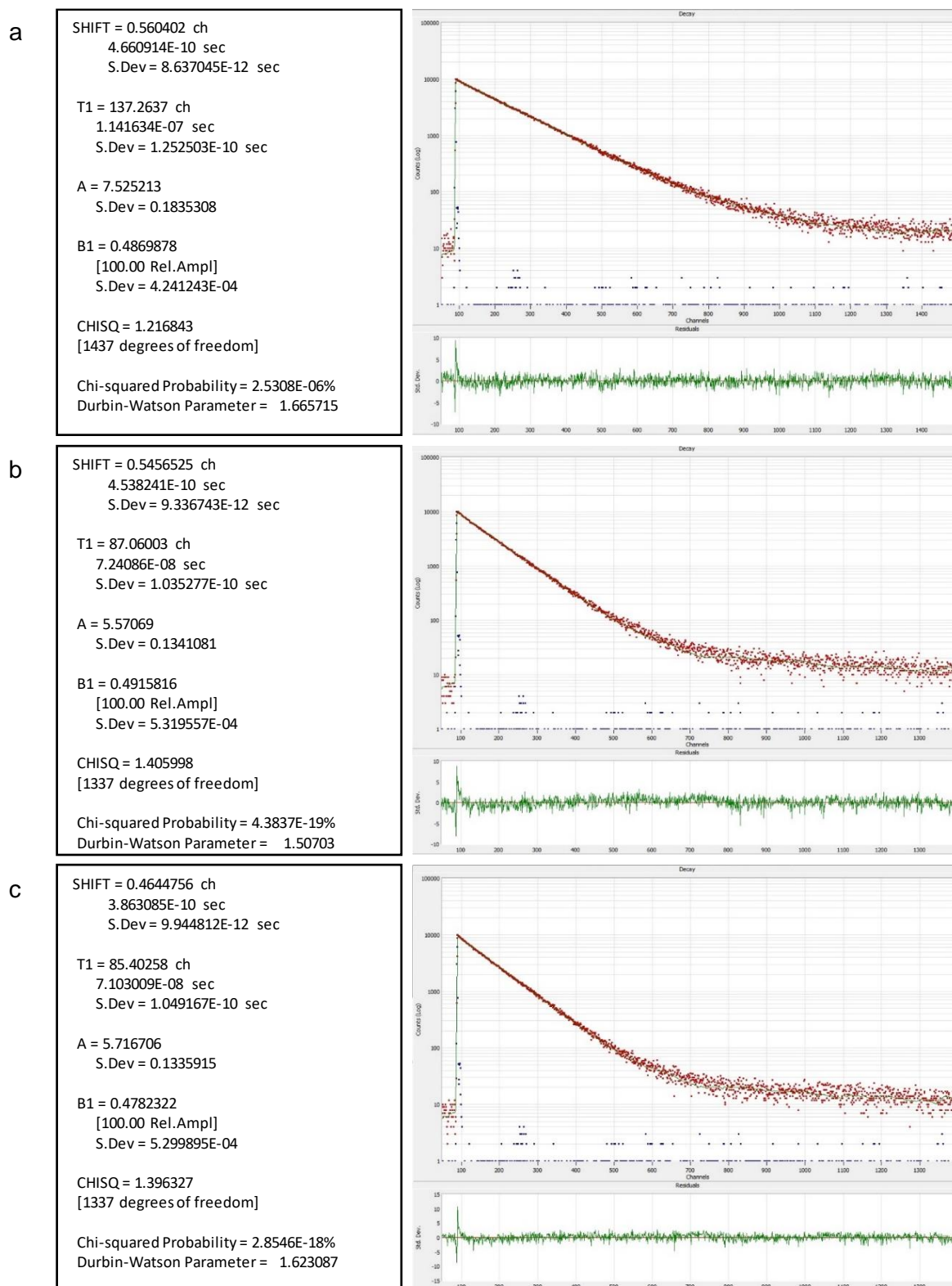


Figure S54. Emission decays of **Mono-Re-Phe** ($\sim 1.2 \times 10^{-5}$ M) (a), and bimetallic complexes ($\sim 6.6 \times 10^{-5}$ M) **Bi-Re-paraPhe** (b) and **Bi-Re-metaPhe** (c) in dichloromethane. $\lambda_{\text{ex}} = 370$ nm.

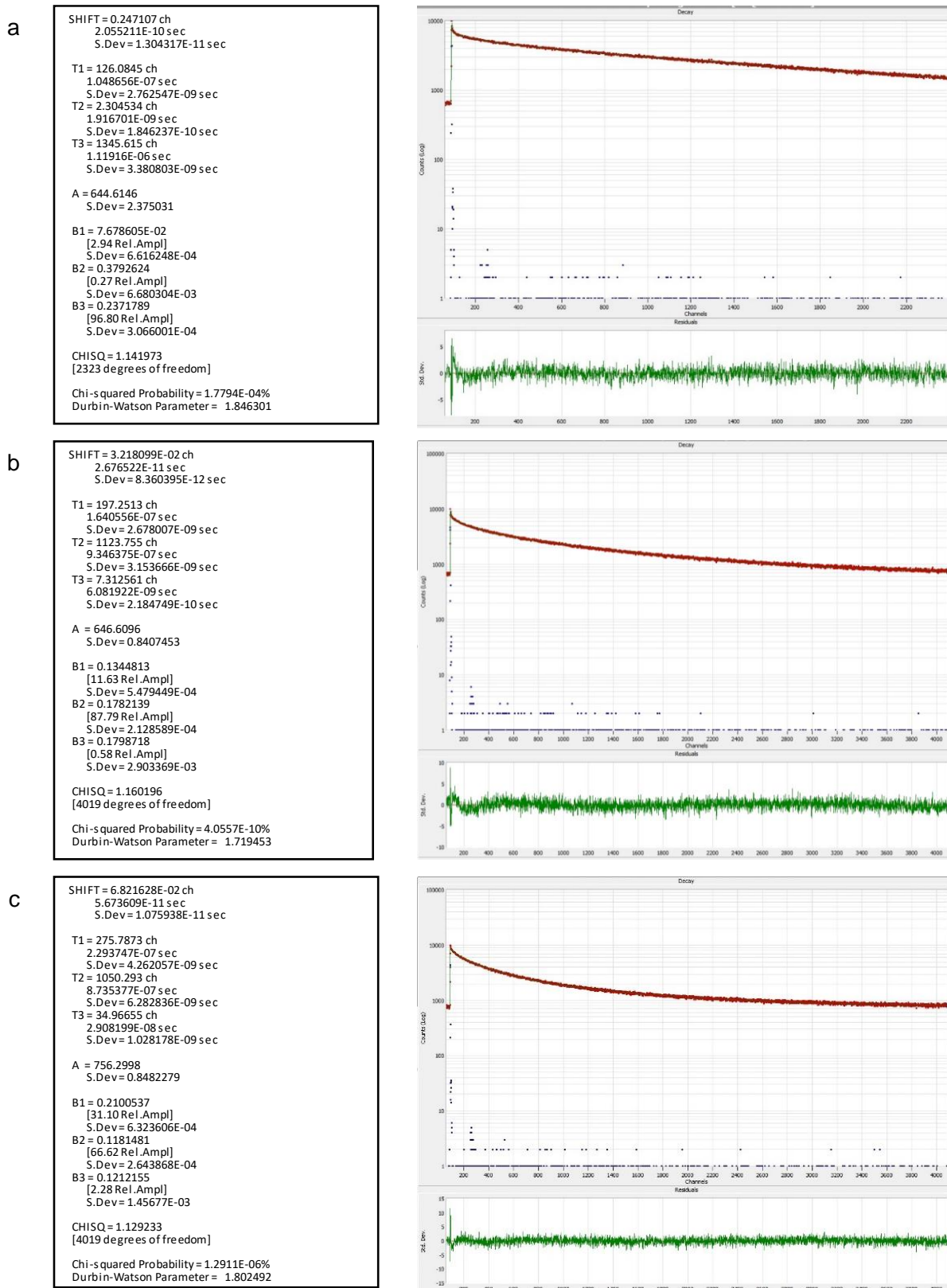


Figure S55. Emission decays of **Mono-Re-Phe** as pristine powder (a), and **Bi-Re-paraPhe** as pristine (b) and ground (c) powders. $\lambda_{ex} = 370$ nm.

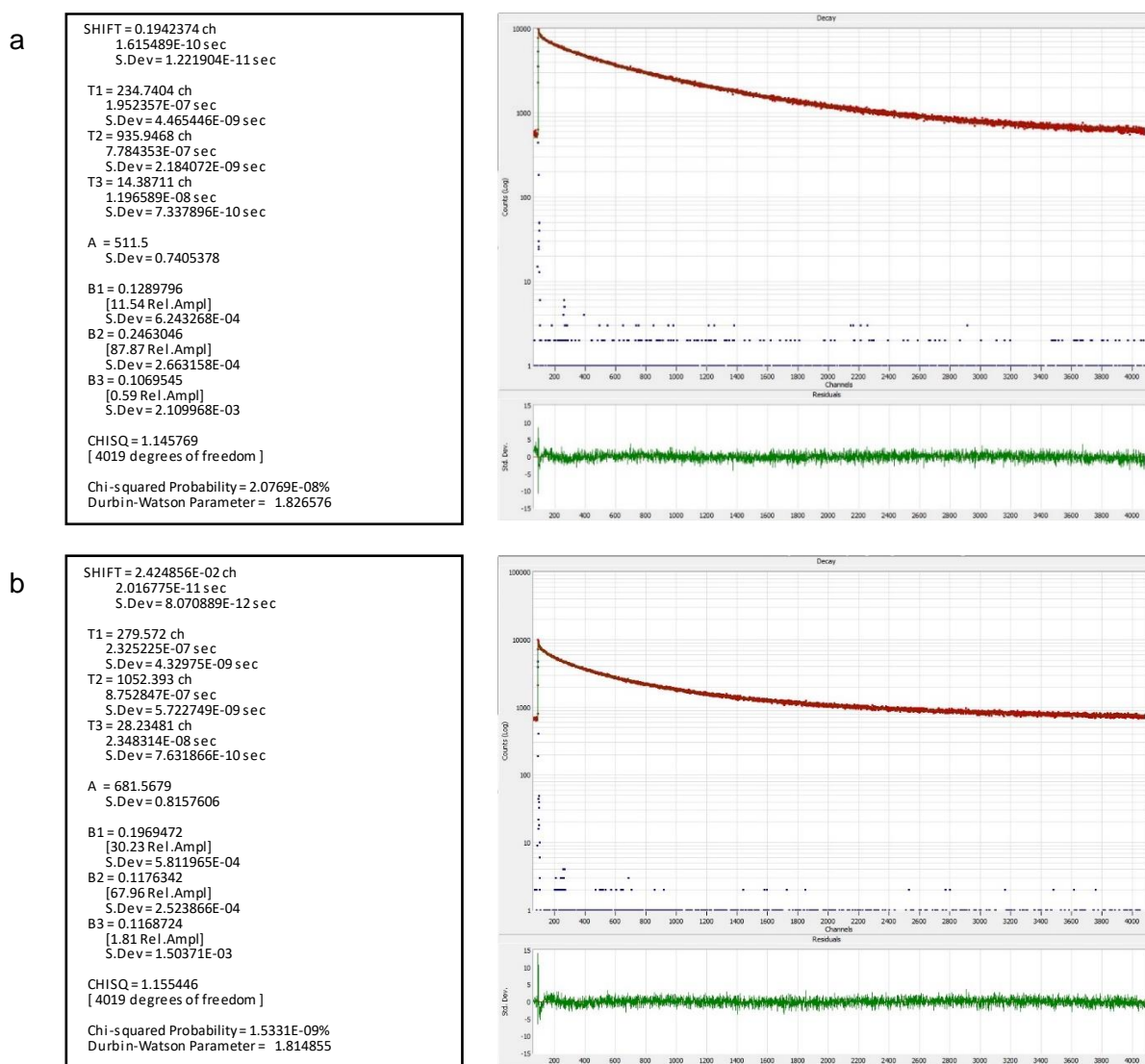


Figure S56. Emission decays of **Bi-Re-metaPhe** as pristine (a) and ground (b) powders. $\lambda_{\text{ex}} = 370 \text{ nm}$.

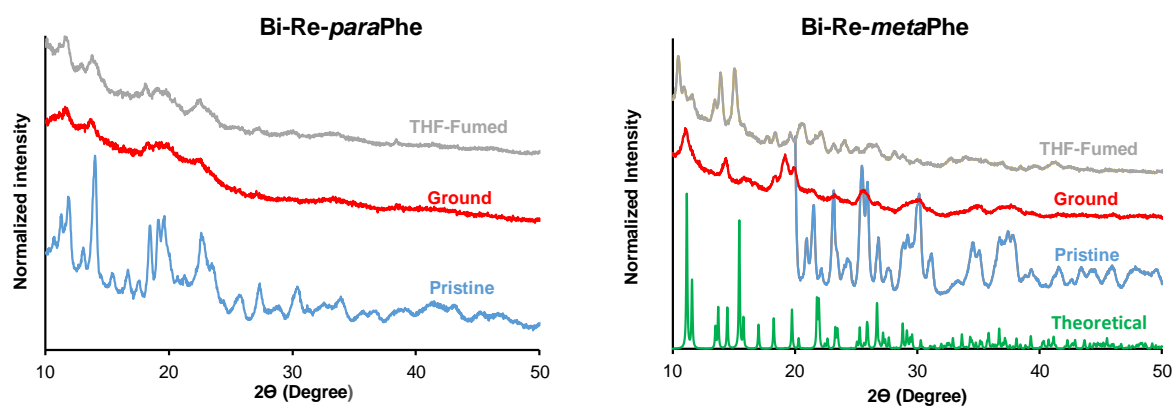


Figure S57. Powder XRD patterns of the pristine, ground and THF-fumed powders of **Bi-Re-paraPhe** (left) and **Bi-Re-meta-Phe** (right), and theoretical spectrum of **Bi-Re-meta-Phe** calculated from single crystal XRD analysis.

Calculations - Annex

Table S27. Cartesian coordinates of complex **Re-Phe** in S_0 (in dichloromethane).

75	11.148231000	5.511105000	9.662202000
17	12.737539000	3.596970000	9.323474000
8	9.825361000	4.105298000	12.045186000
8	13.059174000	6.946895000	11.575919000
8	9.165347000	7.816154000	9.927135000
7	10.017780000	4.528709000	8.031142000
7	11.991053000	6.238698000	7.821001000
7	12.987636000	7.104266000	7.544732000
7	12.215840000	6.254098000	5.664741000
6	10.324618000	4.638141000	11.153914000
6	12.333801000	6.402718000	10.867200000
6	9.917447000	6.944603000	9.820863000
6	9.003694000	3.681015000	8.222518000
1	8.709935000	3.507568000	9.249960000
6	8.348452000	3.047379000	7.177426000
1	7.531837000	2.369701000	7.392789000
6	8.759622000	3.300514000	5.878294000
1	8.270321000	2.822768000	5.037455000
6	9.812177000	4.179228000	5.663839000
1	10.155246000	4.398374000	4.661738000
6	10.419347000	4.774736000	6.760600000
6	11.518754000	5.723257000	6.702346000
6	13.111543000	7.102033000	6.244762000
1	13.820826000	7.683149000	5.675912000
6	12.092757000	6.002803000	4.257373000
6	12.792998000	4.941677000	3.696548000
1	13.413789000	4.310235000	4.322621000
6	12.678354000	4.710631000	2.330944000
1	13.218763000	3.885720000	1.880240000
6	11.877885000	5.536056000	1.547244000
1	11.792750000	5.351894000	0.481765000
6	11.189198000	6.598639000	2.123640000
1	10.568732000	7.243883000	1.511798000
6	11.293633000	6.839532000	3.488576000
1	10.762528000	7.661623000	3.955431000

Table S28. Cartesian coordinates of complex **Re-Phe** in S_1 (in dichloromethane).

75	11.208587000	5.457224000	9.620140000
17	12.790177000	3.655204000	9.488396000
8	9.945396000	4.251990000	12.179908000
8	12.977534000	7.028262000	11.607490000
8	9.013698000	7.638022000	9.590377000
7	10.105764000	4.424181000	8.080760000
7	12.002181000	6.213802000	7.822773000
7	12.959875000	7.131799000	7.533521000
7	12.151307000	6.299531000	5.648252000
6	10.405539000	4.680740000	11.225733000
6	12.326862000	6.443659000	10.872181000
6	9.828433000	6.840816000	9.603167000
6	9.123441000	3.523873000	8.276158000
1	8.898197000	3.288961000	9.310378000
6	8.429347000	2.917571000	7.259809000
1	7.655982000	2.197627000	7.493585000
6	8.745755000	3.264319000	5.919519000
1	8.205017000	2.818430000	5.092738000
6	9.740505000	4.173004000	5.681625000
1	9.995316000	4.456506000	4.668385000
6	10.440016000	4.756841000	6.762030000
6	11.482997000	5.699130000	6.686614000
6	13.035777000	7.170393000	6.239930000
1	13.709978000	7.789156000	5.667898000
6	12.054338000	6.050566000	4.247856000
6	12.504883000	4.838792000	3.732711000
1	12.913991000	4.088088000	4.400346000
6	12.423141000	4.611024000	2.364960000
1	12.771421000	3.668427000	1.956988000
6	11.908056000	5.591660000	1.521534000
1	11.850283000	5.411305000	0.453497000
6	11.470249000	6.802963000	2.046103000
1	11.068956000	7.568514000	1.391032000
6	11.536910000	7.036415000	3.415345000
1	11.187062000	7.971275000	3.839588000

Table S29. Cartesian coordinates of complex **Re-Phe** in T_1 (in dichloromethane).

75	11.218812000	5.467410000	9.599836000
17	12.718974000	3.557267000	9.575345000
8	9.902876000	4.283565000	12.174040000
8	13.096495000	7.049897000	11.457455000
8	9.056638000	7.680033000	9.645034000
7	10.111145000	4.394557000	8.079488000
7	11.956717000	6.216486000	7.835728000
7	12.883251000	7.170670000	7.542643000
7	12.085160000	6.326192000	5.647893000
6	10.379565000	4.700624000	11.226005000
6	12.391972000	6.459118000	10.774769000
6	9.859453000	6.870067000	9.625186000
6	9.167015000	3.464377000	8.287048000
1	8.968574000	3.214007000	9.323218000
6	8.469835000	2.842698000	7.275337000
1	7.725276000	2.095606000	7.518373000
6	8.743916000	3.212535000	5.934895000
1	8.194856000	2.760298000	5.116587000
6	9.706705000	4.148910000	5.681824000
1	9.930219000	4.451195000	4.666769000
6	10.416857000	4.739629000	6.758170000
6	11.433691000	5.695378000	6.678325000
6	12.946967000	7.219351000	6.252212000
1	13.601927000	7.860937000	5.682185000
6	12.024149000	6.073162000	4.248322000
6	12.398964000	4.826381000	3.754667000
1	12.721725000	4.048877000	4.438797000
6	12.358013000	4.598921000	2.385312000
1	12.647728000	3.629296000	1.995226000
6	11.962020000	5.613074000	1.517485000
1	11.936837000	5.432096000	0.448333000
6	11.601887000	6.858595000	2.020548000
1	11.292442000	7.650753000	1.347518000
6	11.625430000	7.093009000	3.390815000
1	11.330875000	8.055100000	3.795941000

Table S30. Cartesian coordinates of complex **Mono-Re-Phe** in S_0 (in dichloromethane).

6	-3.056002000	-1.054840000	-1.861291000
6	-2.104915000	-2.945839000	-0.204831000
6	-4.384954000	-1.654102000	0.404815000
6	-3.998934000	1.675362000	0.531492000
1	-4.870725000	1.035491000	0.583421000
6	-4.103460000	3.041125000	0.746396000
1	-5.070842000	3.473798000	0.968757000
6	-2.958556000	3.819030000	0.671023000
1	-3.002508000	4.889584000	0.834516000
6	-1.746613000	3.208529000	0.381684000
1	-0.836425000	3.788935000	0.315621000
6	-1.720229000	1.835487000	0.177632000
6	-0.539210000	1.052483000	-0.143469000
6	1.407254000	0.213114000	-0.622219000
6	2.864602000	0.119632000	-0.890878000
1	3.396753000	0.521216000	-0.020904000
1	3.108182000	0.789148000	-1.725598000
6	3.328410000	-1.298563000	-1.204702000
1	3.112582000	-1.948537000	-0.349304000
1	2.739019000	-1.686720000	-2.041285000
6	4.812751000	-1.376843000	-1.550732000
1	5.021058000	-0.731697000	-2.415180000
1	5.033226000	-2.400364000	-1.877663000
6	5.756437000	-1.014795000	-0.408348000
1	5.610773000	0.032269000	-0.111290000
1	5.498353000	-1.620870000	0.469721000
6	7.223103000	-1.220651000	-0.771565000
1	7.439435000	-0.666266000	-1.693914000
1	7.389134000	-2.278051000	-1.014612000
6	8.210327000	-0.770972000	0.304954000
1	8.083753000	0.306774000	0.471813000
1	9.230980000	-0.901253000	-0.078111000
6	8.096559000	-1.493745000	1.647560000
1	8.823985000	-1.051770000	2.338741000
1	7.111722000	-1.303047000	2.090831000
6	8.335298000	-2.996385000	1.565945000
1	7.575416000	-3.497144000	0.958144000
1	8.313170000	-3.454339000	2.559240000
1	9.311857000	-3.215617000	1.120046000
6	1.384081000	2.678347000	-0.221671000
1	1.511600000	3.461999000	-1.362520000
1	1.133452000	3.100897000	-2.312709000
6	2.122032000	4.706383000	-1.259390000
1	2.225364000	5.327462000	-2.142194000
6	2.596595000	5.151661000	-0.029584000
1	3.071469000	6.123897000	0.046180000
6	2.466006000	4.354186000	1.103088000
1	2.837639000	4.700736000	2.060983000
6	1.858482000	3.107436000	1.012445000
1	1.747150000	2.473511000	1.885412000
7	-2.839310000	1.074444000	0.252032000
7	-0.654710000	-0.245656000	-0.326963000
7	0.548370000	-0.777524000	-0.626333000
7	0.764746000	1.389906000	-0.322922000
8	-3.341615000	-1.028162000	-2.981555000
8	-1.785597000	-4.046168000	-0.316546000
8	-5.461349000	-1.972848000	0.665607000
17	-1.955705000	-1.054667000	2.405516000
75	-2.599682000	-1.109036000	-0.022402000

Table S31. Cartesian coordinates of complex **Mono-Re-Phe** in S_1 (in dichloromethane).

6	-2.997538000	-0.755742000	-1.895557000
6	-2.179591000	-2.943046000	-0.298786000
6	-4.431857000	-1.699006000	0.267732000
6	-4.005690000	1.670989000	0.650997000
1	-4.876422000	1.032331000	0.749153000
6	-4.111042000	3.023473000	0.851342000
1	-5.069917000	3.453336000	1.110417000
6	-2.946690000	3.826907000	0.710343000
1	-2.995954000	4.899820000	0.855302000
6	-1.759344000	3.227561000	0.388141000
1	-0.858201000	3.817143000	0.274414000
6	-1.699072000	1.829271000	0.199166000
6	-0.560534000	1.063659000	-0.120274000
6	1.388297000	0.166001000	-0.607351000
6	2.843738000	0.065805000	-0.887525000
1	3.385152000	0.509042000	-0.043462000
1	3.077302000	0.698474000	-1.754041000
6	3.314653000	-1.361015000	-1.143776000
1	3.116973000	-1.973226000	-0.256455000
1	2.715049000	-1.791387000	-1.952061000
6	4.793948000	-1.446695000	-1.509762000
1	4.984554000	-0.838118000	-2.404398000
1	5.017085000	-2.482015000	-1.795767000
6	5.753483000	-1.029518000	-0.399808000
1	5.601306000	0.027071000	-0.142709000
1	5.516653000	-1.602016000	0.506413000
6	7.215957000	-1.235190000	-0.779602000
1	7.411065000	-0.714795000	-1.726190000
1	7.389122000	-2.299513000	-0.984689000
6	8.216507000	-0.734621000	0.261608000
1	8.079949000	0.347068000	0.390721000
1	9.231868000	-0.867501000	-0.134482000
6	8.134968000	-1.408145000	1.631915000
1	8.868450000	-0.931999000	2.293379000
1	7.155505000	-1.212938000	2.084993000
6	8.391399000	-2.909784000	1.601868000
1	7.627738000	-3.441986000	1.026381000
1	8.392063000	-3.330691000	2.611686000
1	9.362945000	-3.133630000	1.147374000
6	1.393767000	2.643190000	-0.235321000
6	1.547210000	3.409896000	-1.385395000
1	1.176619000	3.036462000	-2.333963000
6	2.170459000	4.649478000	-1.298049000
1	2.293239000	5.253018000	-2.190752000
6	2.632233000	5.113404000	-0.070303000
1	3.116883000	6.081752000	-0.005468000
6	2.475050000	4.338018000	1.074479000
1	2.836169000	4.698524000	2.031500000
6	1.855004000	3.096493000	0.996184000
1	1.722857000	2.480793000	1.879381000
7	-2.854440000	1.046355000	0.332975000
7	-0.674549000	-0.268848000	-0.279816000
7	0.533597000	-0.814278000	-0.585238000
7	0.760432000	1.367034000	-0.321305000
8	-3.238061000	-0.564763000	-2.993746000
8	-1.933967000	-4.045417000	-0.476320000
8	-5.494653000	-2.094951000	0.409608000
17	-2.141830000	-1.239944000	2.346455000
75	-2.600113000	-1.065222000	-0.008630000

Table S32. Cartesian coordinates of complex **Mono-Re-Phe** in T_1 (in dichloromethane).

6	2.878784000	-0.854071000	1.927342000
6	2.033275000	-2.922600000	0.257093000
6	4.427203000	-1.692986000	-0.181386000
6	4.001413000	1.645140000	-0.660651000
1	4.866749000	0.998639000	-0.755499000
6	4.120466000	3.001246000	-0.871473000
1	5.083577000	3.419096000	-1.135133000
6	2.967409000	3.816238000	-0.734502000
1	3.030216000	4.887871000	-0.886488000
6	1.773856000	3.235603000	-0.410162000
1	0.877827000	3.833701000	-0.301051000
6	1.701873000	1.832317000	-0.213673000
6	0.567410000	1.080339000	0.096833000
6	-1.380974000	0.168769000	0.582220000
6	-2.835029000	0.074383000	0.858861000
1	-3.370486000	0.503649000	0.003318000
1	-3.068149000	0.728987000	1.709309000
6	-3.310792000	-1.345215000	1.143664000
1	-3.110167000	-1.976879000	0.270956000
1	-2.716754000	-1.758935000	1.964584000
6	-4.792317000	-1.417933000	1.503264000
1	-4.985869000	-0.789664000	2.383482000
1	-5.019769000	-2.446171000	1.810329000
6	-5.744166000	-1.022216000	0.378972000
1	-5.588340000	0.028465000	0.100529000
1	-5.503340000	-1.614221000	-0.513520000
6	-2.209259000	-1.216782000	0.754553000
1	-7.408527000	-0.676767000	1.689195000
1	-7.385958000	-2.276330000	0.980227000
6	-8.202603000	-0.735296000	-0.302415000
1	-8.063444000	0.343417000	-0.452016000
1	-9.220518000	-0.858728000	0.090122000
6	-8.113910000	-1.435921000	-1.658600000
1	-8.842702000	-0.971923000	-2.333724000
1	-7.131472000	-1.251088000	-2.109592000
6	-8.372789000	-2.936310000	-1.600338000
1	-7.613500000	-3.458027000	-1.009659000
1	-8.367846000	-3.377186000	-2.601576000
1	-9.347453000	-3.149725000	-1.147516000
6	-1.386823000	2.653638000	0.219311000
6	-1.533838000	3.418087000	1.371905000
1	-1.158135000	3.043020000	2.317818000
6	-2.157844000	4.657593000	1.290092000
1	-2.275955000	5.259459000	2.184526000
6	-2.626496000	5.123465000	0.065678000
1	-3.111854000	6.091736000	0.005317000
6	-2.475396000	4.350449000	-1.081505000
1	-2.841875000	4.712679000	-2.035812000
6	-1.854580000	3.108993000	-1.009107000
1	-1.727248000	2.495115000	-1.894293000
7	2.850400000	1.039085000	-0.335250000
7	0.679776000	-0.280484000	0.248079000
7	-0.534689000	-0.815318000	0.557961000
7	-0.752338000	1.377615000	0.299262000
8	3.081480000	-0.725186000	3.043915000
8	1.708284000	-4.013058000	0.394447000
8	5.501535000	-2.063781000	-0.278859000
17	2.338551000	-1.251403000	-2.405333000
75	2.551519000	-1.077573000	0.020461000

Table S33. Cartesian coordinates of complex **Bi-Re-metaPhe** in S_0 (in dichloromethane).

6	5.227982000	1.091383000	2.503147000	6	-4.688471000	-3.748588000	-0.097037000
6	7.034014000	-0.497088000	1.302699000	1	-5.584984000	-4.107397000	0.392377000
6	7.340693000	2.173749000	1.229205000	6	-3.796805000	-4.632432000	-0.685934000
6	4.688945000	3.748553000	-0.096975000	1	-4.000008000	-5.695507000	-0.654344000
1	5.585557000	4.107260000	0.392334000	6	-2.664734000	-4.126251000	-1.304640000
6	3.797291000	4.632500000	-0.685735000	1	-1.947360000	-4.786649000	-1.778026000
1	4.000609000	5.695553000	-0.654158000	6	-2.458300000	-2.754051000	-1.312444000
6	2.665072000	4.126447000	-1.304277000	1	-1.585096000	-2.333101000	-1.791287000
1	1.947691000	4.786929000	-1.777532000	6	-3.393478000	-1.931524000	-0.699522000
6	2.458498000	2.754268000	-1.312085000	6	-3.316349000	-0.483120000	-0.609322000
1	1.585164000	2.333423000	-1.790783000	6	-2.864332000	1.646667000	-0.635434000
6	3.393690000	1.931632000	-0.699329000	6	-2.154001000	2.924675000	-0.893936000
6	3.316429000	0.483234000	-0.609154000	1	-1.971701000	3.009558000	-1.972400000
6	2.864221000	-1.646509000	-0.635317000	1	-1.163105000	2.871213000	-0.425276000
6	2.153767000	-2.924447000	-0.893829000	6	-2.904761000	4.150304000	-0.389310000
1	1.971483000	-3.009323000	-1.972299000	1	-3.887219000	4.198927000	-0.871385000
6	2.904363000	-4.150153000	-0.389154000	1	-3.092387000	4.045398000	0.684690000
6	2.132369000	-5.435957000	-0.655461000	6	-2.132863000	5.436191000	-0.655490000
1	1.939722000	-5.529909000	-1.732691000	1	-1.940147000	5.530221000	-1.732701000
1	1.147838000	-5.376258000	-0.171934000	1	-1.148363000	5.376563000	-0.171893000
6	2.859361000	-6.681038000	-0.163784000	6	-2.860019000	6.681172000	-0.163799000
1	3.841832000	-6.742782000	-0.650696000	1	-3.842487000	6.742800000	-0.650734000
1	3.057690000	-6.583453000	0.912010000	1	-3.058362000	6.583541000	0.911987000
6	2.088562000	-7.970305000	-0.418759000	6	-2.089384000	7.970545000	-0.418735000
1	1.106645000	-7.907866000	0.070131000	1	-1.107444000	7.908206000	0.070122000
1	1.887539000	-8.065738000	-1.494629000	1	-1.888406000	8.066051000	-1.494608000
6	2.813676000	-9.218118000	0.069106000	6	-2.814640000	9.218246000	0.069205000
1	3.016668000	-9.122875000	1.144680000	1	-3.017603000	9.122924000	1.144778000
1	3.795140000	-9.282375000	-0.420511000	1	-3.796120000	9.282408000	-0.420392000
6	2.042921000	-10.508407000	-0.182712000	6	-2.044046000	10.508641000	-0.182562000
1	1.062818000	-10.443545000	0.307159000	1	-1.063923000	10.443871000	0.307282000
1	1.839923000	-10.602513000	-1.257283000	1	-1.841084000	10.602827000	-1.257133000
6	2.776626000	-11.749064000	0.307859000	6	-2.777889000	11.749184000	0.308091000
1	3.746073000	-11.856448000	-0.190276000	1	-3.747354000	11.856487000	-0.190028000
1	2.201415000	-12.659462000	0.115051000	1	-2.202784000	12.659659000	0.115333000
1	2.963747000	-11.695949000	1.385663000	1	-2.964994000	11.695982000	1.385894000
6	1.176028000	-0.193598000	-1.755418000	6	-1.175966000	0.193932000	-1.755494000
6	1.188436000	-0.201111000	-3.145377000	6	-1.188240000	0.201712000	-3.145451000
1	2.121209000	-0.358405000	-3.675249000	1	-2.120964000	0.359099000	-3.675384000
6	0.000131000	0.000370000	-3.836624000	7	-4.501906000	-2.426198000	-0.096299000
1	0.000182000	0.000475000	-4.920115000	7	-4.272605000	0.178208000	0.005566000
6	-0.000020000	0.000103000	-1.042686000	7	-4.002226000	1.500216000	-0.004151000
1	-0.000053000	0.000016000	0.041371000	7	-2.391531000	0.418730000	-1.037529000
17	6.750377000	0.835848000	-1.622993000	6	-5.227529000	-1.091350000	2.503119000
7	4.502245000	2.426182000	-0.096239000	6	-7.033914000	0.496795000	1.302787000
7	4.272630000	-0.178195000	0.005710000	6	-7.340247000	-2.174084000	1.229457000
7	4.002127000	-1.500177000	-0.004027000	17	-6.750394000	-0.836274000	-1.622861000
7	2.391529000	-0.418522000	-1.037383000	8	-4.804380000	-1.170597000	3.576120000
8	4.804974000	1.170759000	3.576194000	8	-7.680501000	1.391827000	1.627514000
8	7.680529000	-1.392181000	1.627401000	8	-8.181482000	-2.908054000	1.514240000
8	8.182054000	2.907619000	1.513874000	75	-5.934823000	-0.965219000	0.748543000
75	5.935058000	0.965047000	0.748500000	1	1.162864000	-2.870870000	-0.425190000
				1	3.091861000	-4.045295000	0.684886000
				1	3.886879000	-4.198852000	-0.871101000

Table S34. Cartesian coordinates of complex **Bi-Re-metaPhe** in S₁ (in dichloromethane).

6	5.155624000	1.135887000	2.493554000	6	-4.833712000	-3.751092000	-0.249932000
6	6.998815000	-0.424073000	1.312541000	1	-5.759897000	-4.100530000	0.192253000
6	7.263293000	2.251361000	1.240552000	6	-3.957224000	-4.640728000	-0.817428000
6	4.602918000	3.783077000	-0.117940000	1	-4.194100000	-5.696633000	-0.823799000
1	5.489968000	4.156462000	0.377794000	6	-2.754222000	-4.142395000	-1.385262000
6	3.703877000	4.651846000	-0.717858000	1	-2.037304000	-4.817317000	-1.838434000
1	3.891504000	5.717854000	-0.688405000	6	-2.509581000	-2.796560000	-1.353879000
6	2.584858000	4.127125000	-1.345024000	1	-1.599207000	-2.396596000	-1.782018000
1	1.862519000	4.775443000	-1.827524000	6	-3.444956000	-1.918624000	-0.761344000
6	2.398150000	2.752139000	-1.349668000	6	-3.346938000	-0.518486000	-0.652587000
1	1.536232000	2.315622000	-1.835133000	6	-2.890467000	1.638857000	-0.641176000
6	3.339409000	1.945454000	-0.724909000	6	-2.157176000	2.908132000	-0.881673000
6	3.282302000	0.496500000	-0.631541000	1	-1.960160000	2.999805000	-1.957593000
6	2.860730000	-1.638408000	-0.657968000	1	-1.171064000	2.837588000	-0.404218000
6	2.169591000	-2.926193000	-0.919888000	6	-2.890607000	4.143792000	-0.377511000
1	2.019064000	-3.025895000	-2.002020000	1	-3.868224000	4.211290000	-0.867407000
6	2.916514000	-4.138617000	-0.379187000	1	-3.090154000	4.036166000	0.694254000
6	2.165886000	-5.435063000	-0.654901000	6	-2.096984000	5.419519000	-0.628752000
1	2.006738000	-5.541791000	-1.736365000	1	-1.892990000	5.516766000	-1.703703000
1	1.166588000	-5.380755000	-0.202195000	1	-1.117605000	5.342125000	-0.137189000
6	2.890525000	-6.667423000	-0.128912000	6	-2.808475000	6.673439000	-0.136807000
1	3.887951000	-6.723433000	-0.585252000	1	-3.786638000	6.751755000	-0.630172000
1	3.055130000	-6.557339000	0.951391000	1	-3.015895000	6.574374000	0.937215000
6	2.141307000	-7.967317000	-0.394102000	6	-2.017550000	7.952611000	-0.380836000
1	1.144593000	-7.910808000	0.064544000	1	-1.039992000	7.874067000	0.114451000
1	1.973525000	-8.074985000	-1.474485000	1	-1.807641000	8.049526000	-1.454892000
6	2.864635000	-9.202578000	0.127215000	6	-2.727899000	9.208862000	0.107129000
1	3.034616000	-9.095006000	1.207362000	1	-2.939264000	9.112502000	1.181017000
1	3.860839000	-9.260928000	-0.332507000	1	-3.705179000	9.288886000	-0.388566000
6	2.115289000	-10.503443000	-0.134635000	6	-1.937433000	10.489098000	-0.134686000
1	1.120580000	-10.444626000	0.325638000	1	-0.961661000	10.408723000	0.361486000
1	1.944940000	-10.609686000	-1.213728000	1	-1.725854000	10.584198000	-1.207513000
6	2.847313000	-11.731498000	0.389072000	6	-2.656938000	11.738208000	0.355490000
1	3.832013000	-11.833046000	-0.079516000	1	-3.621370000	11.861008000	-0.148799000
1	2.287613000	-12.649848000	0.188386000	1	-2.067715000	12.641130000	0.169950000
1	3.002261000	-11.666286000	1.471323000	1	-2.852128000	11.683874000	1.431812000
6	1.152716000	-0.209137000	-1.780048000	6	-1.203915000	0.177082000	-1.770687000
6	1.160061000	-0.240589000	-3.169345000	6	-1.217480000	0.156412000	-3.161637000
1	2.090850000	-0.403704000	-3.700958000	1	-2.153349000	0.301818000	-3.689623000
6	-0.033106000	-0.054544000	-3.856883000	7	-4.627076000	-2.420797000	-0.201193000
1	-0.038571000	-0.072995000	-4.940370000	7	-4.325543000	0.176851000	-0.042917000
6	-0.020707000	-0.006335000	-1.065358000	7	-4.032707000	1.504669000	-0.036746000
1	-0.015422000	0.008064000	0.018666000	7	-2.411798000	0.403665000	-1.053640000
17	6.724711000	0.903443000	-1.616433000	6	-5.022952000	-1.215539000	2.375335000
7	4.435313000	2.458127000	-0.113922000	6	-7.035592000	0.498328000	1.371803000
7	4.245144000	-0.150062000	-0.010757000	6	-7.405447000	-2.106050000	1.290654000
7	3.993669000	-1.475764000	-0.020675000	17	-6.950689000	-0.777062000	-1.502402000
7	2.372828000	-0.418190000	-1.063349000	8	-4.481295000	-1.378535000	3.365215000
8	4.720725000	1.209189000	3.562389000	8	-7.671315000	1.351882000	1.788074000
8	7.656431000	-1.308449000	1.644460000	8	-8.265362000	-2.754811000	1.672444000
8	8.089808000	2.998909000	1.533533000	75	-5.947156000	-0.957153000	0.673339000
75	5.882336000	1.020028000	0.746416000	1	1.164799000	-2.875750000	-0.481654000
				1	3.070230000	-4.020468000	0.698921000
				1	3.913724000	-4.182651000	-0.830457000

Table S35. Cartesian coordinates of complex **Bi-Re-*meta*Phe** in T₁ (in dichloromethane).

6	5.179297000	-1.076977000	-2.499423000	6	-4.816495000	3.720863000	0.203473000
6	7.000129000	0.511375000	-1.321584000	1	-5.738961000	4.061726000	-0.253171000
6	7.302223000	-2.159981000	-1.243586000	6	-3.954236000	4.623852000	0.785918000
6	4.662579000	-3.725945000	0.116119000	1	-4.203035000	5.677241000	0.787396000
1	5.554639000	-4.087800000	-0.379165000	6	-2.757012000	4.140662000	1.371642000
6	3.775280000	-4.606192000	0.716779000	1	-2.055128000	4.825937000	1.833590000
1	3.977310000	-5.669590000	0.688467000	6	-2.496747000	2.799419000	1.351317000
6	2.649065000	-4.096016000	1.343027000	1	-1.591161000	2.407721000	1.796839000
1	1.935368000	-4.753558000	1.825898000	6	-3.421012000	1.909380000	0.745452000
6	2.443836000	-2.723664000	1.346273000	6	-3.323000000	0.519888000	0.654184000
1	1.575785000	-2.298628000	1.830935000	6	-2.889577000	-1.647345000	0.660905000
6	3.374354000	-1.904888000	0.721154000	6	-2.162633000	-2.913638000	0.922344000
6	3.297721000	-0.456912000	0.626046000	1	-1.991909000	-2.998651000	2.003573000
6	2.847496000	1.672326000	0.649537000	1	-1.164281000	-2.837874000	0.471260000
6	2.139580000	2.951262000	0.909969000	6	-2.878224000	-4.153325000	0.403194000
1	1.971848000	3.041988000	1.990315000	1	-3.867296000	-4.223720000	0.868813000
6	2.882156000	4.174671000	0.388293000	1	-3.050763000	-4.049238000	-0.673527000
6	2.113661000	5.461592000	0.659323000	6	-2.085208000	-5.424517000	0.678396000
1	1.936432000	5.560636000	1.738711000	1	-1.907717000	-5.517470000	1.758358000
1	1.122239000	5.399323000	0.190605000	1	-1.094346000	-5.344193000	0.210956000
6	2.833365000	6.704368000	0.151371000	6	-2.779071000	-6.682846000	0.172768000
1	3.822804000	6.768486000	0.623743000	1	-3.768355000	-6.764426000	0.642810000
1	3.016175000	6.601800000	-0.926739000	1	-2.961084000	-6.587465000	-0.906154000
6	2.066238000	7.994834000	0.411346000	6	-1.988173000	-7.957559000	0.439156000
1	1.077424000	7.930075000	-0.063050000	1	-0.999713000	-7.875880000	-0.033451000
1	1.880573000	8.095191000	1.489509000	1	-1.802995000	-8.050358000	1.518098000
6	2.784287000	9.240355000	-0.092562000	6	-2.681210000	-9.218480000	-0.061487000
1	2.972087000	9.140091000	-1.170457000	1	-2.868546000	-9.125912000	-1.140150000
1	3.772586000	9.306941000	0.382835000	1	-3.669086000	-9.302036000	0.412099000
6	2.017115000	10.531842000	0.164027000	6	-1.890175000	-10.494152000	0.201671000
1	1.030265000	10.464735000	-0.311772000	1	-0.903824000	-10.410232000	-0.272505000
1	1.829118000	10.630885000	1.240875000	1	-1.702510000	-10.585409000	1.279268000
6	2.743871000	11.770214000	-0.342434000	6	-2.592282000	-11.748067000	-0.301288000
1	3.720125000	11.879915000	0.141731000	1	-3.567276000	-11.874333000	0.181363000
1	2.171341000	12.681536000	-0.145959000	1	-2.002994000	-12.647564000	-0.100002000
1	2.916084000	11.712048000	-1.422474000	1	-2.763288000	-11.697492000	-1.381895000
6	1.162505000	0.222245000	1.779949000	6	-1.191328000	-0.180935000	1.781862000
6	1.178105000	0.240219000	3.169586000	6	-1.196464000	-0.174151000	3.173017000
1	2.110967000	0.405585000	3.696907000	1	-2.127894000	-0.330674000	3.705649000
6	-0.009067000	0.038261000	3.862774000	7	-4.593666000	2.399624000	0.157624000
1	-0.007856000	0.046339000	4.946391000	7	-4.321559000	-0.190282000	0.036554000
6	-0.013760000	0.017594000	1.070713000	7	-4.023873000	-1.519914000	0.046089000
1	-0.014979000	0.012546000	-0.013418000	7	-2.402391000	-0.406960000	1.069802000
17	6.744238000	-0.813325000	1.610255000	6	-4.944553000	1.033989000	-2.433741000
7	4.477102000	-2.403384000	0.110746000	6	-6.922801000	-0.608749000	-1.341922000
7	4.250716000	0.201552000	0.002652000	6	-7.290076000	2.087215000	-1.462753000
7	3.981419000	1.523745000	0.010688000	17	-7.070794000	0.952336000	1.396225000
7	2.376733000	0.446292000	1.057968000	8	-4.403178000	1.120886000	-3.435003000
8	4.745667000	-1.158739000	-3.568140000	8	-7.531205000	-1.513347000	-1.694179000
8	7.645260000	1.404193000	-1.655344000	8	-8.102068000	2.754758000	-1.904632000
8	8.139186000	-2.896530000	-1.534684000	75	-5.880848000	0.897956000	-0.728811000
75	5.903997000	-0.947065000	-0.752402000	1	1.142058000	2.893905000	0.456121000
				1	3.054180000	4.064551000	-0.687859000
				1	3.871596000	4.226312000	0.855640000

Table S36. Cartesian coordinates of complex **Bi-Re-paraPhe** in S_0 (in dichloromethane).

6	-6.907705000	1.416246000	-1.913533000
6	-7.975012000	0.027765000	0.125792000
6	-8.031433000	2.716964000	0.162671000
6	-4.978760000	4.082907000	-0.126767000
1	-5.975258000	4.505904000	-0.137522000
6	-3.858143000	4.899720000	-0.127793000
1	-3.981749000	5.975319000	-0.139619000
6	-2.603069000	4.311925000	-0.112867000
1	-1.704982000	4.918766000	-0.112690000
6	-2.507784000	2.927617000	-0.099417000
1	-1.541073000	2.443305000	-0.089738000
6	-3.674211000	2.175092000	-0.098953000
6	-3.744761000	0.723608000	-0.099482000
6	-3.476512000	-1.436800000	-0.118096000
6	-2.816346000	-2.766940000	-0.119581000
1	-2.128535000	-2.814451000	0.733695000
6	-3.797847000	-3.930903000	-0.068506000
6	-3.082744000	-5.275790000	-0.069682000
1	-2.401230000	-5.327176000	0.790155000
1	-2.452245000	-5.353004000	-0.965726000
6	-4.039859000	-6.460039000	-0.024501000
1	-4.672564000	-6.380495000	0.869673000
1	-4.720298000	-6.408743000	-0.885059000
6	-3.331602000	-7.809016000	-0.021869000
1	-2.697454000	-7.887145000	-0.915615000
1	-2.651379000	-7.859347000	0.839402000
6	-4.285755000	-8.995818000	0.022026000
1	-4.965950000	-8.946848000	-0.839412000
1	-4.920993000	-8.918037000	0.915094000
6	-3.579193000	-10.346036000	0.026139000
1	-2.944770000	-10.422999000	-0.866246000
1	-2.899881000	-10.394106000	0.886951000
6	-4.541810000	-11.524866000	0.070240000
1	-5.166025000	-11.490601000	0.969509000
1	-4.008641000	-12.480167000	0.072188000
1	-5.211469000	-11.519556000	-0.796379000
17	-6.191014000	1.407246000	2.434073000
7	-4.901718000	2.749667000	-0.113201000
7	-4.920157000	0.133578000	-0.125478000
7	-4.765633000	-1.206643000	-0.138610000
7	-2.789517000	-0.245134000	-0.093707000
8	-7.070528000	1.429139000	-3.058110000
8	-8.753240000	-0.814549000	0.223323000
8	-8.852998000	3.515531000	0.283989000
75	-6.654756000	1.400291000	-0.034684000
6	4.979605000	-4.082948000	0.125363000
1	5.976166000	-4.505779000	0.136546000
6	3.859125000	-4.899948000	0.126287000
1	3.982899000	-5.975525000	0.138457000
6	2.603954000	-4.312373000	0.110796000
1	1.705975000	-4.919374000	0.110524000
6	2.508425000	-2.928088000	0.096922000

1	1.541633000	-2.443948000	0.086785000
6	3.674730000	-2.175368000	0.096592000
6	3.745030000	-0.723863000	0.096635000
6	3.476391000	1.436503000	0.113841000
6	2.815930000	2.766491000	0.113998000
1	2.182075000	2.840755000	1.006603000
1	2.133114000	2.815409000	-0.743233000
6	3.797383000	3.930801000	0.070672000
1	4.472721000	3.869477000	0.930837000
1	4.425748000	3.843346000	-0.822313000
6	3.081865000	5.275469000	0.070308000
1	2.446369000	5.350877000	0.962972000
1	2.405118000	5.328180000	-0.793205000
6	4.038804000	6.460120000	0.032551000
1	4.714421000	6.407584000	0.896827000
1	4.676544000	6.382346000	-0.858194000
6	3.330061000	7.808838000	0.028273000
1	2.654736000	7.860432000	-0.836770000
1	2.690795000	7.885140000	0.918525000
6	4.283969000	8.996090000	-0.008079000
1	4.924344000	8.920130000	-0.897628000
1	4.959241000	8.945885000	0.857154000
6	3.576883000	10.346028000	-0.013876000
1	2.902491000	10.395327000	-0.878478000
1	2.937328000	10.421169000	0.874994000
6	4.539241000	11.525326000	-0.050405000
1	5.203908000	11.518800000	0.820042000
1	4.005689000	12.480410000	-0.053773000
1	5.168634000	11.492871000	-0.946125000
7	4.902327000	-2.749723000	0.111378000
7	4.920316000	-0.133616000	0.122792000
7	4.765541000	1.206598000	0.135078000
7	2.789618000	0.244694000	0.089875000
17	6.192225000	-1.407755000	-2.435915000
6	7.975250000	-0.027351000	-0.127425000
6	8.032089000	-2.716595000	-0.163624000
6	6.907436000	-1.415551000	1.911937000
8	8.753366000	0.815065000	-0.224945000
8	8.853804000	-3.515068000	-0.284513000
75	6.655154000	-1.400061000	0.033000000
1	-2.187769000	-2.843007000	-1.015783000
1	-4.478040000	-3.871012000	-0.924927000
1	-4.421111000	-3.841568000	0.827873000
6	1.366918000	0.108017000	0.044244000
6	0.734657000	0.021421000	-1.190648000
6	0.647770000	0.091206000	1.233389000
6	-0.647645000	-0.091925000	-1.237180000
6	-0.734530000	-0.022113000	1.186856000
6	-1.366794000	-0.108682000	-0.048046000
1	1.318600000	0.040047000	-2.103605000
1	1.164070000	0.160578000	2.183883000
1	-1.318475000	-0.040710000	2.099814000
1	-1.163950000	-0.161265000	-2.187672000
8	7.069766000	-1.428193000	3.056589000

Table S37. Cartesian coordinates of complex **Bi-Re-paraPhe** in S_1 (in dichloromethane).

6	-6.884471000	1.378457000	-2.079107000	1	1.544145000	-2.488599000	-0.022714000
6	-7.966842000	0.040143000	-0.014493000	6	3.678831000	-2.154832000	-0.113502000
6	-8.015872000	2.729567000	-0.039970000	6	3.743142000	-0.750433000	-0.037959000
6	-4.958463000	4.080726000	-0.343208000	6	3.500484000	1.436720000	0.100454000
1	-5.953804000	4.505906000	-0.367445000	6	2.834215000	2.762182000	0.179029000
6	-3.835727000	4.894349000	-0.358793000	1	2.235977000	2.802766000	1.098498000
1	-3.956381000	5.969731000	-0.395497000	1	2.114827000	2.838268000	-0.646590000
6	-2.582290000	4.303593000	-0.326605000	6	3.803645000	3.935944000	0.137522000
1	-1.682529000	4.907880000	-0.337798000	1	4.514223000	3.850173000	0.966820000
6	-2.490666000	2.919788000	-0.281078000	1	4.396501000	3.884566000	-0.782351000
1	-1.525653000	2.432414000	-0.257670000	6	3.082032000	5.275301000	0.212894000
6	-3.659210000	2.170427000	-0.266534000	1	2.482966000	5.316102000	1.132654000
6	-3.733400000	0.719475000	-0.233039000	1	2.369920000	5.352933000	-0.619872000
6	-3.469790000	-1.440330000	-0.201176000	6	4.029388000	6.467711000	0.176607000
6	-2.813080000	-2.771860000	-0.169827000	1	4.739368000	6.391748000	1.011183000
1	-2.095416000	-2.786062000	0.659510000	1	4.631725000	6.423802000	-0.740810000
6	-3.795515000	-3.928513000	-0.036304000	6	3.313718000	7.811056000	0.244786000
6	-3.085748000	-5.275817000	-0.004005000	1	2.603811000	7.885968000	-0.590364000
1	-2.373758000	-5.293149000	0.832119000	1	2.710251000	7.854047000	1.161856000
1	-2.488296000	-5.395740000	-0.917759000	6	4.258536000	9.005587000	0.209012000
6	-4.045700000	-6.451271000	0.128022000	1	4.862867000	8.963064000	-0.707609000
1	-4.646040000	-6.327726000	1.039397000	1	4.968556000	8.932070000	1.044275000
1	-4.756002000	-6.434571000	-0.709500000	6	3.544248000	10.350085000	0.275829000
6	-3.344257000	-7.803226000	0.166942000	1	2.834967000	10.422600000	-0.558699000
1	-2.742951000	-7.926129000	-0.744265000	1	2.940935000	10.391979000	1.191803000
1	-2.633836000	-7.818726000	1.004815000	6	4.497601000	11.536667000	0.238836000
6	-4.302298000	-8.980329000	0.299188000	1	5.197159000	11.506656000	1.081002000
1	-5.012184000	-8.966622000	-0.539291000	1	3.958946000	12.487610000	0.288214000
1	-4.905276000	-8.856976000	1.209349000	1	5.090197000	11.537638000	-0.682227000
6	-3.603177000	-10.333746000	0.341442000	7	4.945095000	-2.747881000	-0.201746000
1	-3.000845000	-10.456307000	-0.567913000	7	4.940302000	-0.134122000	-0.020619000
1	-2.894346000	-10.346607000	1.179382000	7	4.780082000	1.212964000	0.069526000
6	-4.569964000	-11.502540000	0.473809000	7	2.797294000	0.242317000	0.033772000
1	-5.162065000	-11.422225000	1.391685000	17	6.418778000	-1.296374000	-2.550761000
1	-4.042235000	-12.460471000	0.501683000	6	8.008749000	-0.025842000	-0.150728000
1	-5.269584000	-11.532645000	-0.368298000	6	8.112585000	-2.650968000	-0.299702000
17	-6.192426000	1.468309000	2.271635000	6	6.651472000	-1.576761000	1.786762000
7	-4.885027000	2.747910000	-0.298815000	8	8.823361000	0.775574000	-0.138701000
7	-4.910443000	0.132031000	-0.251536000	8	9.002784000	-3.364217000	-0.369514000
7	-4.758837000	-1.208394000	-0.233245000	75	6.621554000	-1.391931000	-0.158122000
7	-2.780404000	-0.250390000	-0.200293000	1	-2.216671000	-2.887587000	-1.083680000
8	-7.041312000	1.365587000	-3.224590000	1	-4.504500000	-3.902097000	-0.870739000
8	-8.748188000	-0.797474000	0.098116000	1	-4.387605000	-3.798197000	0.876185000
8	-8.836008000	3.532977000	0.057995000	6	1.381592000	0.112368000	-0.025471000
75	-6.641916000	1.405057000	-0.199125000	6	0.760460000	-0.051186000	-1.259905000
6	5.009059000	-4.090598000	-0.289442000	6	0.639837000	0.163234000	1.149965000
1	6.005848000	-4.511198000	-0.359661000	6	-0.620731000	-0.167629000	-1.320870000
6	3.908582000	-4.909578000	-0.296939000	6	-0.742147000	0.047802000	1.092338000
1	4.038132000	-5.981012000	-0.376395000	6	-1.357432000	-0.113396000	-0.143239000
6	2.620645000	-4.319266000	-0.195105000	1	1.356881000	-0.086333000	-2.164402000
1	1.730068000	-4.937046000	-0.186065000	1	1.142575000	0.282572000	2.102765000
6	2.516204000	-2.958002000	-0.105164000	1	-1.338818000	0.081181000	1.996790000
				1	-1.123860000	-0.290428000	-2.273140000
				8	6.664208000	-1.696826000	2.920447000

Table S38. Cartesian coordinates of complex **Bi-Re-*para*Phe** in T₁ (in dichloromethane).

6	6.768816000	1.222682000	2.236369000	1	-1.557153000	-2.609338000	-0.162684000
6	7.958805000	0.160895000	0.072971000	6	-3.673448000	-2.225655000	0.115713000
6	7.940460000	2.828446000	0.416763000	6	-3.734241000	-0.841219000	-0.058860000
6	4.839312000	4.072254000	0.755051000	6	-3.522751000	1.328997000	-0.422722000
1	5.821926000	4.513592000	0.863760000	6	-2.870625000	2.639227000	-0.665755000
6	3.695990000	4.853769000	0.824843000	1	-2.366969000	2.606144000	-1.640526000
1	3.787698000	5.919815000	0.990743000	1	-2.070795000	2.768586000	0.075134000
6	2.459887000	4.243870000	0.679441000	6	-3.831323000	3.819991000	-0.617253000
1	1.545072000	4.823117000	0.728822000	1	-4.623193000	3.674683000	-1.359868000
6	2.405418000	2.873355000	0.469399000	1	-4.325659000	3.845783000	0.360001000
1	1.454557000	2.371310000	0.354589000	6	-3.121252000	5.143075000	-0.873059000
6	3.592811000	2.156583000	0.409756000	1	-2.620419000	5.105961000	-1.849835000
6	3.704881000	0.721672000	0.209540000	1	-2.327118000	5.281122000	-0.126791000
6	3.496715000	-1.424270000	-0.082991000	6	-4.061002000	6.341401000	-0.834986000
6	2.873730000	-2.755643000	-0.293065000	1	-4.851965000	6.204990000	-1.584704000
1	2.238993000	-2.704483000	-1.186463000	1	-4.566984000	6.374188000	0.139316000
6	3.888007000	-3.883739000	-0.430930000	6	-3.357060000	7.669950000	-1.081465000
6	3.213151000	-5.234313000	-0.632100000	1	-2.567679000	7.806538000	-0.329640000
1	2.574717000	-5.194394000	-1.524886000	1	-2.847931000	7.635321000	-2.054382000
1	2.543722000	-5.437284000	0.214645000	6	-4.295168000	8.869825000	-1.048146000
6	4.206675000	-6.380332000	-0.774218000	1	-4.805620000	8.904754000	-0.075812000
1	4.876146000	-6.176282000	-1.620625000	1	-5.084371000	8.734572000	-1.800511000
1	4.846043000	-6.417726000	0.118025000	6	-3.592659000	10.199809000	-1.292965000
6	3.541398000	-7.736362000	-0.973903000	1	-2.804536000	10.334240000	-0.540929000
1	2.870722000	-7.939108000	-0.127687000	1	-3.082777000	10.164049000	-2.264291000
1	2.902244000	-7.698595000	-1.866655000	6	-4.539214000	11.391873000	-1.257832000
6	4.533435000	-8.883970000	-1.114527000	1	-5.318203000	11.299306000	-2.022115000
1	5.172966000	-8.922317000	-0.221941000	1	-4.009155000	12.332176000	-1.435991000
1	5.204807000	-8.681792000	-1.960434000	1	-5.038309000	11.470405000	-0.286096000
6	3.870922000	-10.241677000	-1.314494000	7	-4.931723000	-2.787323000	0.355197000
1	3.200354000	-10.442909000	-0.469150000	7	-4.953514000	-0.210855000	-0.038344000
1	3.232267000	-10.202610000	-2.206309000	7	-4.793867000	1.119697000	-0.279118000
6	4.871515000	-11.380852000	-1.453684000	7	-2.802980000	0.138932000	-0.291222000
1	5.533556000	-11.221333000	-2.311458000	17	-6.313831000	-1.303016000	2.732252000
1	4.369556000	-12.342490000	-1.595773000	6	-7.888207000	0.040244000	0.348593000
1	5.501587000	-11.463211000	-0.561636000	6	-8.081967000	-2.667598000	0.606999000
17	6.230684000	1.813778000	-2.096705000	6	-6.820686000	-1.641909000	-1.605908000
7	4.801729000	2.752517000	0.553350000	8	-8.643498000	0.901355000	0.371595000
7	4.895065000	0.161248000	0.200764000	8	-8.952005000	-3.388116000	0.761343000
7	4.777865000	-1.170794000	0.021307000	75	-6.591113000	-1.389969000	0.314017000
7	2.778019000	-0.257419000	0.029962000	1	2.194805000	-2.957835000	0.544829000
8	6.883488000	1.077134000	3.377654000	1	4.520785000	-3.914736000	0.462649000
8	8.764348000	-0.641467000	-0.106270000	1	4.554697000	-3.671776000	-1.273889000
8	8.743818000	3.653966000	0.446772000	6	-1.388777000	0.030390000	-0.213650000
75	6.594535000	1.467124000	0.364541000	6	-0.789775000	-0.242759000	1.014057000
6	-5.002970000	-4.107821000	0.571142000	6	-0.620780000	0.210387000	-1.359966000
1	-5.993302000	-4.503246000	0.767269000	6	0.590896000	-0.338110000	1.096105000
6	-3.909896000	-4.947379000	0.551752000	6	0.762141000	0.123632000	-1.278486000
1	-4.043032000	-6.004775000	0.740446000	6	1.354024000	-0.147193000	-0.050873000
6	-2.636051000	-4.395890000	0.272146000	1	-1.403267000	-0.375824000	1.898005000
1	-1.759677000	-5.032638000	0.224993000	1	-1.102095000	0.403811000	-2.311556000
6	-2.520516000	-3.050686000	0.058108000	1	1.376993000	0.258955000	-2.161076000
				1	1.074735000	-0.545092000	2.043886000
				8	-6.962370000	-1.797242000	-2.727885000